Distribution Agreement

In presenting this thesis or dissertation as a partial fulfillment of the requirements for an advanced degree from Emory University, I hereby grant to Emory University and its agents the non-exclusive license to archive, make accessible, and display my thesis or dissertation in whole or in part in all forms of media, now or hereafter known, including display on the world wide web. I understand that I may select some access restrictions as part of the online submission of this thesis or dissertation. I retain all ownership rights to the copyright of the thesis or dissertation. I also retain the right to use in future works (such as articles or books) all or part of this thesis or dissertation.

Signature:

_____ _____

Christine E Larkins Date

The Roles of Arl13b in Cilia, Cell Signaling, and Embryonic Development

By

Christine E Larkins
Doctor of Philosophy

Graduate Division of Biological and Biomedical Sciences
Biochemistry Cell and Developmental Biology

_____
Tamara Caspary
Advisor

_____
Ping Chen
Committee Member

_____
Victor Faundez
Committee Member

_____
Richard Kahn
Committee Member

_____
Maureen Powers
Committee Member

_____
Winfield Sale
Committee Member

Accepted:

_____
Lisa A. Tedesco, Ph.D.
Dean of the James T. Laney School of Graduate Studies

_____
Date

The Roles of Arl13b in Cilia, Cell Signaling, and Embryonic Development

By

Christine E Larkins

B.S., College of Charleston, 2005

Advisor: Tamara Caspary

An abstract of

A dissertation submitted to the Faculty of the

James T. Laney School of Graduate Studies of Emory University

in partial fulfillment of the requirements for the degree of

Doctor of Philosophy

in Biochemistry Cell and Developmental Biology

2010

Abstract

The Roles of Arl13b in Cilia, Cell Signaling, and Embryonic Development

By Christine E Larkins

Cilia are antennae-like projections that are found on the apical surface of most vertebrate cells. They were discovered almost a century ago, but their significance in multiple cellular events is only beginning to be understood. Cilia were initially recognized for their roles in creating motility, however, more recently it was found that non-motile primary cilia are required for various cell signaling events such as signaling pathway integrity, mechanosensation, and even light detection in photoreceptor cells.

Mutations in ciliary proteins can lead to a variety of human syndromes called ciliopathies. Left-right axis defects are common symptoms in ciliopathies because axis establishment in the embryo requires both motile and primary cilia, but the functions of primary cilia in the process are less understood. Other common symptoms, such as polydactyly, result from defects in the Sonic Hedgehog (Shh) signaling pathway. Almost all components of the Shh signaling pathway localize to the cilium which is required for pathway integrity. However, it is not clear how Shh signaling proteins interact within the cilium or why cilia are required for pathway integrity. Taken together, a better understanding of cilia protein function and their roles in embryonic development and signaling events is required for grasping the etiology of ciliopathies.

This dissertation focuses on understanding the function of the cilia protein Arl13b, which is mutated in the ciliopathy Joubert Syndrome. Loss of Arl13b leads to shortened cilia with a defect in cilia ultrastructure, although the precise function of Arl13b in cilia is not clear. Mouse mutants lacking Arl13b, *Arl13b*^{hennin}, have both left-right axis and Shh signaling defects. This dissertation examines the defects in establishing the left-right axis in *Arl13b*^{hennin} mutant embryos and investigates the function of Arl13b in ciliogenesis and Shh signaling. Through examining these processes I have found that Arl13b is important for maintaining proper levels of ciliary components, which is important for both Shh signaling and cilia structure, and I have shown that Arl13b may have additional roles outside of the cilium that are required for left-right axis establishment.

The Roles of Arl13b in Cilia, Cell Signaling, and Embryonic Development

By

Christine E Larkins

B.S., College of Charleston, 2005

Advisor: Tamara Caspary

A dissertation submitted to the Faculty of the

James T. Laney School of Graduate Studies of Emory University

in partial fulfillment of the requirements for the degree of

Doctor of Philosophy

in Biochemistry Cell and Developmental Biology

2010

TABLE OF CONTENTS

CHAPTER 1

CILIA, SIGNALING, AND EMBRYONIC DEVELOPMENT

1.1 The Significance of Cilia

Cilia, also called flagella, are long thin structures that project off the surface of cells and can be found in a wide range of organisms, from algae to humans, with their basic structure being conserved. They are historically known for their roles in motility, for example cilia propel the biflagellate green algae *Chlamydomonas reinhardti*, or beat on the vertebrate respiratory epithelium to move mucous out of airways. However, work in the past decade has emphasized a role for cilia in sensing environmental stimuli (Singla and Reiter, 2006; Eggenschwiler and Anderson, 2007; Berbari et al., 2009).

While much of our understanding of ciliogenesis and cilia structure and has come from work in *Chlamydomonas reinhardti* and the nematode *Caenorhabditis elegans*, the requirement of cilia for cell signaling events has been enhanced through studies in vertebrates (Veland et al., 2009). Studies in mammals have revealed the localization of Sonic Hedgehog (Shh) and Platelet-Derived Growth Factor (PDGF) pathway components to the cilium itself and cilia structure is required for Shh signaling pathway integrity (Huangfu et al., 2003; Schneider et al., 2005; Rohatgi et al., 2007). The primary cilium is also important for light detection in photoreceptors cells (Insinna and Besharse, 2008), and in the kidney, cilia act as mechanosensors, bending in response to fluid flow which opens mechanosensitive ion channels (Praetorius and Spring, 2001; Praetorius and Spring, 2003). The importance of cilia in cell signaling is highlighted in the fact that almost all vertebrate cells possess a cilium (Wheatley et al., 1996) (http://www.bowserlab.org /primarycilia/cilialist.html).

In humans, mutations that affect the structure and function of cilia lead to a class of diseases called ciliopathies (Bisgrove and Yost, 2006; Tobin and Beales, 2009). These

diseases present a wide array of symptoms due to the multiple functions and ubiquitous nature of the cilium, such as *situs inversus*, polydactyly, retinal degeneration, and cystic kidneys. The incidence of ciliopathies range from 1 in 1,000 to 1 in 150,000 depending on the disorder (Tobin and Beales, 2009). Examples of ciliopathies are Polycystic Kidney Disease, Primary Ciliary Dyskinesia, Bardet-Biedl Syndrome, Joubert Syndrome, and Meckel-Gruber Syndrome, and each of these diseases often results from a mutation in a single cilia protein. There are almost 1,000 proteins that have been found in cilia so far, and many of them have unknown function, making it important to understand the roles of cilia proteins (Gherman et al., 2006).

This dissertation focuses on using mouse and mammalian tissue culture as models to understand the function of cilia protein Arl13b, which is mutated in Joubert Syndrome (Cantagrel et al., 2008). In this introduction, I will describe cilia structure and how they are built. I will focus on what is known about the targeting of proteins to cilia, and area that is not well understand and may involve Arl13b. Then I will discuss how cilia are required for left-right axis specification and Shh signaling, processes which are disrupted in the mutants that lack Arl13b, the *Arl13b*$^{hennin\ (hnn)}$ mutants. Finally, I will describe the cilia defects in the *Arl13b*^{hnn} mutants and depict what is currently known about the function of Arl13b in cilia.

1.2 Cilia Structure, Building Cilia, and Intraflagellar Transport

The structural backbone of the cilium is the microtubule axoneme, which consists of a ring of nine outer doublet microtubules (Figure 1.2). The doublets consists of a circular A-tubule and a B-tubule that connects to the A-tubule (Figure 1.1). Motile cilia

have an additional central pair of microtubules and other associated proteins that are required for generating motility, such as radial spokes and axonemal dyneins, that are usually not found in primary cilia (Figure 1.1) (Satir and Christensen, 2007). The axoneme extends from the basal body, which is derived from the mother centriole of the cell and consists of nine outer triplet microtubules (Sorokin, 1962; Vorobjev and Chentsov Yu, 1982; Satir and Christensen, 2006). The transition zone is the region where the axoneme and basal body meet and consists of two parts: a pore like structure created from an array of fibers projecting from the distal end of the basal body to the base of the cilia membrane that may act to regulate protein entry to the cilium (Figure 1.2) (Anderson, 1972; Deane et al., 2001), and a ciliary membrane diffusion barrier which prevents free diffusion of membrane proteins in and out of the cilium creating the unique protein and lipid composition of the cilia membrane (Vieira et al., 2006; Janich and Corbeil, 2007; Hu et al., 2010).

The presence of cilia on cells is dependent on the cell cycle. When a cell enters quiescence, a cilium grows on the cell surface and is shed soon after the cell enters mitosis (Rieder et al., 1979; Tucker et al., 1979). In order for most cilia to form, the mother centriole must dock at the plasma membrane, which occurs initially through a vesicle associating with the distal end of the mother centriole (Sorokin, 1962; Veland et al., 2009). The axoneme begins to grow beneath the vesicle, and then the vesicle fuses with the plasma membrane (Sorokin, 1962; Dawe et al., 2007). What initiates axoneme growth from the basal body and later disassembly is not clear, but centrosomal proteins and proteins that regulate the cell cycle are likely involved (Pugacheva et al., 2007; Spektor et al., 2007).

The process of elongation and maintenance of the axoneme is better understood. This requires intraflagellar transport (IFT), which was first discovered when particles were observed moving up and down *Chlamydomonas* flagella using live imaging and differential interference contrast (DIC) microscopy (Kozminski et al., 1993). IFT is the movement of ciliary components into the cilium and turnover products out of the cilium through interactions with IFT protein complexes and the motors Kinesin-II, Kif17, and Dynein-2 (Figure 2) (Rosenbaum and Witman, 2002; Pedersen et al., 2008). IFT is conserved among ciliated organisms and consists of almost 20 IFT complex proteins that can be broken down into complexes A and B (Cole and Snell, 2009). Complex B IFT proteins and Kinesin-II move in the anterograde direction to transport proteins towards the cilia tip, while complex A proteins along with Dynein-2 are required for retrograde transport of proteins out of the cilium (Rosenbaum and Witman, 2002). Kif17 is a homodimeric kinesin that is also involved in anterograde IFT. In *C. elegans,* Kif17 coordinates with Kinesin-II to direct the proximal movement of IFT proteins toward the cilium tip, and Kif17 alone directs distal anterograde IFT (Snow et al., 2004). In mammals Kif17 is required for the trafficking of cyclic nucleotide gated (CNG) channels to cilia of olfactory neurons (Jenkins et al., 2006) as well as photoreceptor development (Insinna et al., 2008; Insinna et al., 2009).

The requirement of IFT in building the cilium is highlighted in studies of IFT mutants. For example, mutants that lack the anterograde motor Kinesin-II are unable to form cilia (Marszalek et al., 1999; Matsuura et al., 2002), and loss of the retrograde motor Dynein-2 function leads to cilia that are shortened with bulges at their tips, due to proteins being trapped in the cilium after they are transported there by anterograde IFT

(Pazour et al., 1999; Signor et al., 1999; Huangfu and Anderson, 2005; Ocbina and Anderson, 2008; Merrill et al., 2009). Similarly, loss of a single anterograde complex B IFT protein causes severely shortened or absent cilia and loss of a single retrograde complex A protein usually leads to shortened bulged cilia (Huangfu et al., 2003; Pedersen et al., 2008). Because axonemal proteins are constantly being turned over, IFT is also required for maintaining cilia length. For example, inducing loss of Kinesin-II function using a temperature sensitive *Chlamydomonas* mutant leads to a gradual loss of fully formed flagella (Kozminski et al., 1995), and *Chlamydomonas* mutants expressing a partially active Kinesin-II have shortened cilia (Marshall and Rosenbaum, 2001) due to inefficient IFT.

1.3 Targeting, Transport, and Entry to the Cilium

Many of the proteins that are found in cilia are unique to cilia. For example, the transmembrane cilia protein Polycystin-2 is not found in the surrounding plasma membrane (Pazour et al., 2002). Therefore, protein localization to the cilium must be regulated. In order for a protein to localize to the cilium, the protein must be sorted, targeted, and transported to the cilium, and then the protein must be able to pass through the transition zone to gain entry into the cilium (Leroux, 2007; Rohatgi and Snell, 2010; Seeley and Nachury, 2010). This process is not very well understood, although recent work regarding cilia targeting and entry has been found through studies of cilia membrane proteins and will be the focus of the discussion that follows.

Sorting at the Golgi

Initially, membrane proteins must pass through the Golgi on their way to the cilium. The sorting and transport of cilia membrane proteins from the Golgi is not clear, but may involve the complex B protein IFT20, which is the only IFT protein that has been localized to the Golgi (Baker et al., 2003; Follit et al., 2006). Knock-down of IFT20 in retinal pigment epithelium (RPE) cells leads to fewer cilia, and the cilia membrane protein Polycystin-2 is reduced in those cells that have cilia (Follit et al., 2006). However, a direct interaction between IFT20 and Polycystin-2 was not found, therefore IFT20 regulation of Polycystin-2 targeting to cilia may be indirect (Follit et al., 2006). A second protein linked to sorting of cilia membrane proteins is the clathrin adaptor protein AP-1. Loss of the AP-1 subunit μ1 in *C. elegans* causes the odorant receptor ODR-10 to localize to the plasma membrane instead of the cilium, indicating a defect in targeting to the cilium (Dwyer et al., 2001). Clearly, other proteins involved in sorting must be identified.

The recognition of proteins destined to the cilium may occur through a cilia targeting sequence (CTS), or through interactions with proteins that have a CTS (Rosenbaum and Witman, 2002). However, few CTSs have been found. One of these is a VxPx motif in the cilia membrane proteins Polycystin-2, CNGB1b, and Rhodopsin (Deretic et al., 2005; Geng et al., 2006; Jenkins et al., 2006; Mazelova et al., 2009). The VxPx motif in Rhodopsin interacts with Arf4, a Golgi associated Arf family GTPase, which may function to regulate sorting of Rhodopsin and other cilia proteins into vesicles destined to the cilium (Mazelova et al., 2009). A second motif, Ax[S/A]xQ was found in several different cilia localized G-protein coupled receptors (GPCR) such as Somatostatin receptor-3 (SSTR3) (Berbari et al., 2008). Putting this sequence in non-ciliary GPCRs

caused them to localize to cilia, however, loss of this sequence from SSTR3 did not prevent its cilia localization, indicating a second domain capable of targeting SSTR3 (Berbari et al., 2008). Taken together, sorting and targeting of cilia proteins is a complex process that likely requires interactions with proteins in the Golgi that have yet to be identified.

Transport to the Cilium

After cilia membrane proteins are sorted into vesicles, there are at least two possible routes for delivery to the cilium. The first is that these vesicles are transported directly to the cilium. This model is supported by live imaging of IFT20 moving between the Golgi and cilium in RPE cells (Follit et al., 2006). Additionally, studies in photoreceptors showed direct transport of the GPCR Opsin from the Golgi to the connecting cilium (Papermaster et al., 1985; Bhowmick et al., 2009).

There is also data to support a second method of transport where membrane proteins may first be targeted to the plasma membrane and then are transported laterally to the cilia membrane. This is supported by a study of the transmembrane Shh signaling protein Smoothened (Smo), which localizes to the cilium in response to the Shh ligand (Corbit et al., 2005). One study showed that Smo enters the cilium from a plasma membrane pool independent of dynamin mediated endocytosis (Milenkovic et al., 2009), however, a second study found that Smo entry is from an intracellular pool (Wang et al., 2009), suggesting that both lateral transport from the plasma membrane and direct transport from the Golgi may be involved. In either scenario, because a membrane diffusion barrier exists at the base of the cilium (Hu et al., 2010), transport into the cilium must occur through an active process, perhaps through interactions with IFT proteins. In

fact, Smo co-localizes with IFT88 outside of the cilium in Shh treated cells (Wang et al., 2009), and knockdown of Kif3a, a subunit of Kinesin-II, results in loss of Smo to ciliated cells (Kovacs et al., 2008). Because there is data that supports two methods of transport to the cilium, it is possible that different cilia membrane proteins rely on different mechanisms for localization depending on whether they are constitutively localized to cilia, such as IFT20 or Opsin, or whether their localization is signal dependent, such as Smo (Rohatgi and Snell, 2010).

Exocytosis of Cilia Targeted Vesicles

Some IFT proteins share sequence homology to the vesicle coat proteins COPI and clathrin (Jekely and Arendt, 2006), and IFT proteins have been associated with exocytosis in non-ciliated cells (Finetti et al., 2009), raising the possibility that ciliogenesis is a specialized form of exocytosis. Vesicles can be seen accumulating at the basal body region and fusing at the base of the cilium (Webber and Lee, 1975), which is also where IFT proteins and other cilia membrane proteins accumulate (Rosenbaum and Witman, 2002). It has been suggested that both soluble and insoluble cilia proteins may require vesicle association for cilia entry (Baldari and Rosenbaum, 2010).

Proteins involved in fusion of vesicles at their target membranes, such as the exocyst complex, are also implicated in ciliogenesis. The exocyst complex is an octomeric protein complex that was first identified in yeast as being necessary for secretion and is conserved in mammalian cells being necessary for many exocytic events (Novick et al., 1980; TerBush et al., 1996; Grindstaff et al., 1998; Oztan et al., 2007). The exocyst functions to regulate fusion of vesicles at target membranes (Prigent et al., 2003; Zhang et al., 2004). The exocyst complex proteins, Sec10, Sec8, and Sec6 have been

found in cilia or at the base of cilia, and Sec10 has been shown to be required for ciliogenesis in MDCK cells (Rogers et al., 2004; Zuo et al., 2009; Babbey et al., 2010).

Rab GTPases that interact with the exocyst have also been linked to ciliogenesis, such as Rab10, Rab8, and Rab11 (Nachury et al., 2007; Babbey et al., 2010; Knodler et al., 2010). Rab8 loss of function in hTERT-RPE cells leads to reduced and shortened cilia, while expression of a constitutively active form causes an increase in cilia length (Nachury et al., 2007), identical to the phenotypes observed in Sec10 knock-down and overexpressing MDCK cells (Zuo et al., 2009). Similarly, loss of Rab11 function causes shortened cilia (Knodler et al., 2010). These data support a model where the exocyst complex and associated GTPases may regulate vesicle targeting and fusion at the periciliary membrane.

Passage Through the Transition Zone

The final step for ciliary entry is passage through the transition zone. The fibers projecting from the distal end of the basal body have been suggested to act similarly to the nuclear pore in restricting protein entry into the cilium (Rosenbaum and Witman, 2002). This is supported by recent studies showing that Importin-β1 and Importin-β2 are localized to the cilium and are needed for ciliary entry of the transmembrane protein Crumbs3 and the soluble homodimeric motor Kif17 (Fan et al., 2007; Dishinger et al., 2010). The cilia motor Kif17 contains a KRKK sequence in its C-terminus that interacts with Importin-β2 and is necessary for cilia localization (Dishinger et al., 2010). Interestingly, the authors found that this sequence can also act as a nuclear localization sequence (NLS) in the isolated C-terminal half of Kif17 (Dishinger et al., 2010). Therefore, the KRKK sequence is necessary for cilia localization, but it is not sufficient,

indicating that other interactions are required for the localization of Kif17 to the cilium instead of the nucleus. Dishinger *et al* proposed that interactions with cargoes or membranes may be responsible for the ciliary entry of Kif17. It is intriguing to speculate that passage of all ciliary proteins through the transition zone occurs through either direct or indirect interactions with Importin-β.

1.4 Cilia in Left-Right Axis Specification

One of the most common symptoms of ciliopathies is defective left-right (LR) axis specification, which occurs at a rate of 1 in 10,000 in the general population (Tobin and Beales, 2009). These are most often manifested as *situs inversus* (a complete reversal of organ laterality), because this defect is the least detrimental to organ function, but can also arise as heterotaxia (individual organs having reversed orientation independent of other organs), or isomerism (mirroring of an organ that normally has a distinct left and right side) (Raya and Belmonte, 2006). The LR axis is determined during early embryonic development with both the mechanical and sensory function of cilia being required, however the precise mechanism for cilia establishing the LR axis is still unclear (Shiratori and Hamada, 2006).

Three body axes must be specified for development of vertebrate embryos. The anterior-posterior (AP) axis is the first to be established followed by dorsal-ventral (DV). The final axis to be specified is the LR axis, which occurs just prior to and is required for directed visceral organ development. It has been suggested that left-right axis establishment occurs through the orientation of a chiral molecule or structure along the AP and DV axis of the embryo causing a LR asymmetric event that leads to molecular

asymmetry (Brown and Wolpert, 1990). In many different vertebrate embryos, cilia are that chiral structure that generates LR asymmetry (Peeters and Devriendt, 2006; Shiratori and Hamada, 2006; Basu and Brueckner, 2008; Hirokawa et al., 2009).

In the mouse embryo, at embryonic day (e)7.5 a structure called the node forms on the ventral side of the embryo. The node is a teardrop shaped valley of ciliated epithelial cells, and these cilia are oriented in the extra-embryonic space and tilted towards the posterior side of the embryo (Nonaka et al., 2005). The node cilia rotate in a clockwise direction, creating a leftward flow of extraembryonic fluid (Figure 1.3) (Basu and Brueckner, 2008; Hirokawa et al., 2009). It is not clear how the leftward flow, termed nodal flow, establishes the left side of the embryo, but two models have been proposed (Shiratori and Hamada, 2006; Hirokawa et al., 2009). One model suggests that nodal flow establishes the left side of the embryo by causing immotile cilia at the left side of the node to bend, which opens mechanosensitive calcium channels (McGrath et al., 2003). In support of this, there are immotile cilia at the node periphery and all node cilia contain the mechanosensitive calcium channel, Polycystin-2 (McGrath et al., 2003). Additionally, an intracellular calcium flux can be seen at the left side of the node, which is dependent on cilia motility and Polycystin-2 (McGrath et al., 2003). The second model suggests that secreted ligands are carried by nodal flow to the left side of the node to induce signaling. This is supported by a study that found vesicles, termed nodal vesicular particles, that contain Shh and Retinoic Acid are carried by nodal flow to the left side of the node where they induce the calcium flux (Tanaka et al., 2005). However, this study is controversial as more recently it was shown that Shh signaling is not required in the node for LR axis establishment (Tsiairis and McMahon, 2009). It therefore remains a possibility that a

combination of the two models may be required for establishing the LR axis, however more studies are required to tease apart these possibilities (McGrath et al., 2003; Tanaka et al., 2005).

Nodal flow is required for the enriched expression of *Nodal* at the left side of the node, and studies have shown that reversal of fluid flow is sufficient to reverse the LR axis (Nonaka et al., 2002). Nodal is a TGF-β secreted ligand that is expressed symmetrically in the crown cells on the left and right sides of the node prior to nodal flow. After nodal flow induces *Nodal* enrichment at the left side of the node, Nodal signaling enhances its expression at the left node periphery, and the Nodal ligand then diffuses to the left lateral plate mesoderm (LPM) to induce its expression there (Figure 1.3) (Collignon et al., 1996; Lowe et al., 1996; Oki et al., 2007). In the LPM, *Nodal* also induces the expression of its inhibitors *Lefty1* and *Lefty2* in the midline and LPM, respectively (Yamamoto et al., 2003). Lefty1 and Lefty2 are also secreted TGF-β signaling proteins and function by binding to the Nodal ligand and/or to its receptor to inhibit signaling. Lefty1 and -2 are capable of diffusing over longer distances than Nodal, allowing them to prevent the diffusion of Nodal to the right LPM (Meno et al., 1998; Meno et al., 2001; Nakamura et al., 2006). The process of a diffusible ligand inducing its own expression as well as that of its more readily diffusible inhibitors leads to a model called self-enhancement lateral inhibition (SELI), whereby an initially small difference in signaling in separate regions of the embryo can be converted into a more robust one through self-enhancement of the signal and long range inhibition (Nakamura et al., 2006). Indeed, the initially small difference in *Nodal* expression in the node becomes robust in the left LPM. *Nodal* expression persists in the LPM for only about six hours of

development, but this allows Nodal to induce the expression of *Pitx2*, the transcription factor that regulates asymmetric organ development (Ryan et al., 1998; Campione et al., 1999; Lin et al., 1999; Liu et al., 2001).

Defects in cilia structure and/or motility lead to an inability to properly specify the LR axis. One example is the LR axis defects that occur in Kartagener's Syndrome (Sutherland and Ware, 2009). Kartagener's Syndrome patients lack functional axonemal dyneins, thereby creating cilia that are immotile (Afzelius, 1976). Immotile cilia are unable to create nodal flow and the result is reversal of organ asymmetry in half of patients with Kartagener's Syndrome (Peeters and Devriendt, 2006). Mouse embryos with immotile cilia, such as the *left-right dynein* (*Lrd*) mutant, have randomized *Nodal* expression in the LPM such that expression is reversed 25% of the time, bilateral 25%, normal 25%, or absent 25% of the time (Lowe et al., 1996; Supp et al., 1997). Bilateral or absent Nodal in the LPM leads to isomerism, meaning that an organ with a distinct left and right side will have two left or two right sides. While this phenotype is easily seen in the mouse embryos, this phenotype is rarely seen in humans because it is detrimental to organ function causing embryonic lethality.

In contrast to mutants with immotile cilia, mouse mutants that lack cilia, such as *IFT172* or *Kif3a* null embryos, have bilateral expression of *Nodal* and its target *Pitx2* in almost all embryos examined (Marszalek et al., 1999; Huangfu et al., 2003). Because there would be a loss of fluid flow in mutants that lack cilia, as what is seen in *Lrd*-/- mutants, one may expect to see the same randomized pattern of *Nodal* expression. However, cilia are required for signaling in the midline which is required for *Lefty1* expression; therefore *Lefty1* expression is lost in mutants lacking cilia (Nakamura et al.,

2006). Loss of the Nodal inhibitor in the midline would allow Nodal to diffuse to the opposing LPM and induce its own expression there even if it was initially expressed in either the left or right LPM alone. In addition, loss of *Lefty1* in the midline would allow for an increase in Nodal signaling activity in the LPM, which is likely the reason that mutants lacking cilia do not show a class of embryos with no LPM expression of *Nodal* as what is seen in immotile cilia mutants (Nakamura et al., 2006). In support of this model, $Lrd^{-/-}$; $Lefty1^{-/-}$ mutants show a pattern of expression similar to mutants lacking cilia (Nakamura et al., 2006).

Many studies of cilia and their roles in LR axis establishment have been from mutants that lack cilia or have immotile cilia. These studies have heightened our understanding of the requirement of nodal flow in LR axis establishment, but neglect to tease apart other roles cilia may have in establishing the LR axis. Chapter three of this dissertation focuses on characterizing the left-right axis defects in the $Arl13b^{hnn}$ mutant, which has shortened cilia and a pattern of *Nodal* expression that is not seen in other mutants with cilia defects.

1.5 Shh Signaling and Cilia

Defects in Sonic Hedgehog (Shh) signaling contribute to many of the symptoms found in ciliopathies, such as polydactyly and holoprosencephaly. In mammals, the Shh signaling pathway depends on cilia for proper signaling to occur, while in *Drosophila* Shh signaling does not require cilia and takes place in non-ciliated cells (Han et al., 2003; Sarpal et al., 2003). How various Shh signaling components are utilized also differs between the *Drosophila* and mammalian Shh signaling pathways, suggesting that cilia

have co-evolved with the Shh pathway perhaps as a way to deal with the complexities of patterning the mammalian embryo (Wong and Reiter, 2008). With the initial discovery that cilia mutations affect Shh signaling in mammals came great advancements in our understanding of the Shh signaling pathway (Huangfu et al., 2003; Garcia-Garcia et al., 2005). We now know that almost all components of the Shh pathway are dynamically localized to cilia, but precisely why they are localized there and how they interact in the cilium is not known (Corbit et al., 2005; Rohatgi et al., 2007; Chen et al., 2009; Wen et al., 2010).

The Shh signaling pathway is potentiated through the Gli transcription factors. There are three Gli proteins in vertebrates, Gli1, Gli2, and Gli3, and all three localize to cilia, although Gli1 does not require cilia localization for function (Haycraft et al., 2005). Gli2 and Gli3 contain an N-terminal repressor domain and a C-terminal activation domain that flank a zinc finger DNA binding domain (Sasaki et al., 1999). Gli1 does not contain a repressor domain and therefore only acts as a transcriptional activator. Although Gli2 and Gli3 contain activator and repressor domains, Gli2 is the primary activator while Gli3 primarily acts as a repressor (Wong and Reiter, 2008). In the absence of Shh ligand, Gli2 and Gli3 are localized to the tips of cilia where Gli3 is modified for cleavage creating Gli repressor (GliR) (Haycraft et al., 2005). GliR then translocates to the nucleus to inhibit Shh target genes while Gli2 is usually degraded completely (Figure 1.4) (Wang et al., 2000). In the presence of the Shh ligand, Gli2 and Gli3 are enriched in the tips of cilia, and the cleavage and degradation of Gli2 and Gli3 are inhibited allowing the formation of Gli activator (GliA) (Figure 1.4) (Pan et al., 2006; Chen et al., 2009; Wen et al., 2010). Mutants that lack cilia fail to activate the Glis although there is an

abundance of full length Gli protein (Haycraft et al., 2005; Huangfu and Anderson, 2005; Liu et al., 2005). Thus, an unknown modification must occur in the cilium that is required to activate the full-length proteins. Nonetheless, the readout of Shh signaling is found in the ratio of GliA and GliR, such that varying concentrations of Shh ligand will lead to differing GliA/GliR ratios, causing specific transcriptional programs to occur in the responding cells (Stamataki et al., 2005).

Upstream of the Gli proteins, Shh signaling is carried out by components that dynamically localize to the cilium. The twelve-transmembrane protein Patched (Ptch1) is localized to the cilium, and in the presence of Shh ligand, Shh binds Ptch1 inhibiting its function and causing Ptch1 to move out of the cilium (Rohatgi et al., 2007). Although the mechanism is unclear, repression of Ptch1 activity activates the seven-transmembrane protein Smoothened (Smo) causing it to enter the cilium (Corbit et al., 2005; Rohatgi et al., 2007). Localization of Smo to the cilium is required for pathway activation as disruption of Smo trafficking to cilia results in lack of Shh pathway activation even in the presence of Shh ligand (Kovacs et al., 2008). Again through an unknown mechanism, Smo activation inhibits the formation of GliR and the Glis become activated. Suppressor of Fused (Sufu), is a negative regulator of the Shh signaling pathway that functions by binding the Gli proteins to inhibit their function. Sufu is also localized to the tips of cilia, although it was discovered that Sufu localization is not required for function (Chen et al., 2009; Jia et al., 2009; Humke et al., 2010). Because it is not clear how the Shh signaling components are interacting or why many of the components require cilia for function, it is important to examine Shh signaling defects in cilia protein mutants.

In the embryonic neural tube, Shh signaling specifies ventral cell types in a concentration dependent manner (Ericson et al., 1997). Shh ligand is produced in the notochord and diffuses to the ventral neural tube where it induces specification of the floor plate (Echelard et al., 1993). The floor plate also produces Shh and the diffusion of Shh from the floor plate results in a steep gradient of Shh signaling activity in the ventral neural tube such that the highest levels of activity are in the floor plate and levels are quickly reduced as you move dorsally (Wong and Reiter, 2008). The Shh activity gradient leads to specification of the ventral neuronal cell types, the motor neurons and four classes of interneurons, such that each cell type is specified depending on the GliA/GliR ratio in the responding cells which results from the amount and duration of Shh signaling activity the cell receives (Ericson et al., 1997; Stamataki et al., 2005).

Mouse mutants lacking anterograde IFT do not form cilia and have neural tube patterning defects (Marszalek et al., 1999; Huangfu et al., 2003; Huangfu and Anderson, 2005; Liu et al., 2005; Houde et al., 2006). Because these mutants are unable create GliA, there is a loss of the most ventral cell types in the neural tube. Although there is a loss of GliA function, there is a reduction in GliR levels allowing these mutant embryos to specify some of the most dorsal ventral neuronal precursors, such as V2 precursors (Huangfu et al., 2003). This is in contrast to *Shh* null embryos, which lack V2 precursors because of their uninhibited ability to create GliR (Chiang et al., 1996; Meyer and Roelink, 2003).

Loss of retrograde IFT leads to phenotypes similar to what is found in anterograde mutants: there is a complete loss of the most ventral neuronal precursors in the caudal neural tube (Huangfu and Anderson, 2005; May et al., 2005). Interestingly, reduced rates

of retrograde IFT, such as what is found in the *THM1* mutant, a homolog of the complex A protein IFT139, leads to expanded ventral cell types in the neural tube, indicating an expansion of Shh activity (Tran et al., 2008). It is unclear how reduced retrograde IFT leads to expansion of Shh signaling activity while complete loss of retrograde IFT causes reduced Shh signaling. Further analysis of cilia mutants and how they affect Shh signaling will be important for understanding the requirement of cilia in mammalian Shh signaling. Chapter four of this dissertation will examine Shh signaling in the *Arl13b*^{hnn} mutant, which has shortened cilia and a unique pattern of Shh signaling activity in the neural tube.

1.6 Arl13b Function in Cilia and Shh signaling

The cilia protein Arl13b [ADP ribosylation factor (Arf)-like 13b] is a member of the Arf family of GTPases and was first identified in a forward genetic screen in mouse looking for recessive mutations that cause neural tube defects (Garcia-Garcia et al., 2005). The *Arl13b*$^{hennin\ (hnn)}$ mutant has a point mutation in the splice acceptor site of exon two that results in loss of Arl13b protein, and mutant embryos have shortened cilia and a defect in the axoneme where the B-tubule does not connect to the A-tubule (Figure 1.5) (Caspary et al., 2007). The *Arl13b*^{hnn} mutants display phenotypes associated with defects in cilia and Shh signaling, such as polydactyly, spina bifida, exencephaly, left-right axis defects, and they die at e13.5 (Caspary et al., 2007). Since its identification in mouse, causative mutations in *Arl13b* have been found in the ciliopathy Joubert Syndrome (Cantagrel et al., 2008).

There are almost 30 mammalian members of the Arf family of GTPases, many of which have unknown function, but some of the best studied Arf proteins function to regulate vesicle traffic by recruiting proteins to sites of vesicle budding (Kahn et al., 2005; D'Souza-Schorey and Chavrier, 2006). Arl13b is an unusual member of the Arf family of small GTPases for two reasons. First, almost all other Arf family members consist only of their Arf domain, while Arl13b has a long (217 amino acid) C-terminal domain that contains coiled-coil motifs in addition to its N-terminal Arf domain (Caspary et al., 2007). Second, Arl13b can bind GTP but may not have the ability to hydrolyze GTP based on its protein sequence. Arf family members contain guanine nucleotide binding motifs in their Arf domain that allows GTP binding, but the amino acid that is required for GTP hydrolysis is not conserved in Arl13b (Caspary et al., 2007). Arf family GTPases act as molecular switches, with GTP binding making them active, and hydrolysis making them inactive; therefore, Arl13b may be a constitutively active protein or may hydrolyze GTP through an unknown mechanism.

Arl13b is one of three Arf family proteins that have been localized to the cilium. Arl3 localizes to cilia, although its function there is not clear. Arl3 has been linked to regulation of microtubule acetylation in the cell body, and as the ciliary axoneme is highly acetylated, Arl3 may play a role in regulating axoneme dynamics (Zhou et al., 2006). In mice, loss of Arl3 does not cause any obvious defects in cilia structure although overexpression of dominant active Arl3 leads to truncated cilia in *Leishmania donovani* (Cuvillier et al., 2000; Schrick et al., 2006). Interestingly, Arl3 was shown to interact genetically with the *Arl13b* ortholog *Arl13* in *C. elegans* and these results indicated that Arl3 and Arl13b may have inverse functions in cilia (Li et al., 2010). The Arf family

member Arl6 was shown to regulate the ciliary trafficking complex, the BBSsome (Jin et al., 2010), and expression of wild-type Arl6 causes shorter and fewer cilia in hTERT-RPE cells, while expression of dominant negative Arl6 resulted in increased ciliogenesis and longer cilia (Wiens et al., 2010). This is in contrast to the *Arl13b*^{hnn} mutant, which has shortened cilia in the embryonic node (Caspary et al., 2007). Few studies have examined the requirement for Arl13b in ciliogenesis, but a study in *C. elegans* showed that *Arl13* functions to stabilize anterograde IFT proteins and that loss of *Arl13* leads to shortened sensory cilia (Cevik et al., 2010). However, the structure of *C. elegans Arl13* and vertebrate Arl13b are not identical and it is therefore important to examine Arl13b function in vertebrate cells. Studies thus far examining Arl13b in vertebrate cilia have focused on Arl13b localization and protein domain function, keeping the mechanism of Arl13b action in cilia indefinable (Hori et al., 2008; Duldulao et al., 2009; Cevik et al., 2010). In chapter four of this dissertation I will closely examine the role of Arl13b in mammalian ciliogenesis and show results that suggest Arl13b may function to regulate the trafficking of proteins to cilia.

Cilia are required for Shh signaling, and many of the phenotypes in *Arl13b*^{hnn} mutants are reflective of Shh signaling defects, specifically exencephaly, spina bifida, and polydactyly. In the neural tube of *Arl13b*^{hnn} mutants, there is a cilia dependent expansion of Shh signaling activity such that the highest levels of Shh activity are not reached and the gradient is lost (Caspary et al., 2007). This intermediate level of Shh activity in *Arl13b*^{hnn} mutants corresponds to the level that is required for specification of motor neuron precursors (pMNs). Thus, there is an expansion of pMN cells and motor neurons (MNs) in the *Arl13b*^{hnn} neural tube (Caspary et al., 2007). This phenotype is

dramatically different from mutants that lack cilia, which are unable to activate the Shh signaling pathway and only specify the most dorsal interneurons (Huangfu et al., 2003; Liu et al., 2005; Houde et al., 2006). Genetic studies in the *Arl13b*^{hnn} mutant showed that the expansion of Shh signaling activity is ligand independent, similar to other cilia mutants, but that GliA is disrupted while GliR formation is unaffected, a phenotype not seen in other cilia mutants (Caspary et al., 2007; Wong and Reiter, 2008). Chapter four of this dissertation focuses on understanding how the *Arl13b*^{hnn} mutation affects Shh signaling at the level of pathway component localization to the cilium.

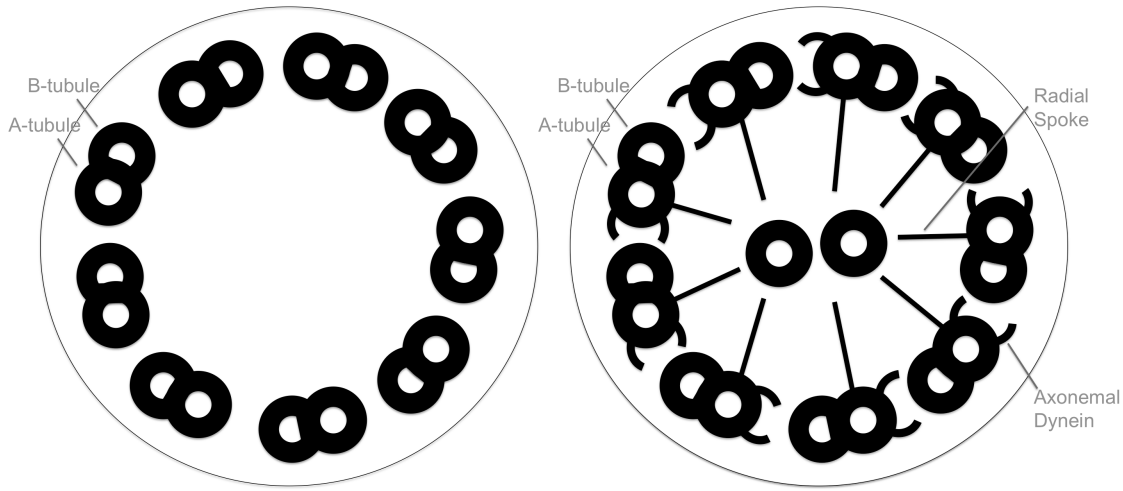

Figure 1.1. Primary vs. motile cilia. Primary and motile cilia contain nine outer doublet microtubules. Motile cilia have a central pair of microtubules and other structures important for generating motility: the radial spokes and axonemal dyneins, which are both anchored to the A-tubule.

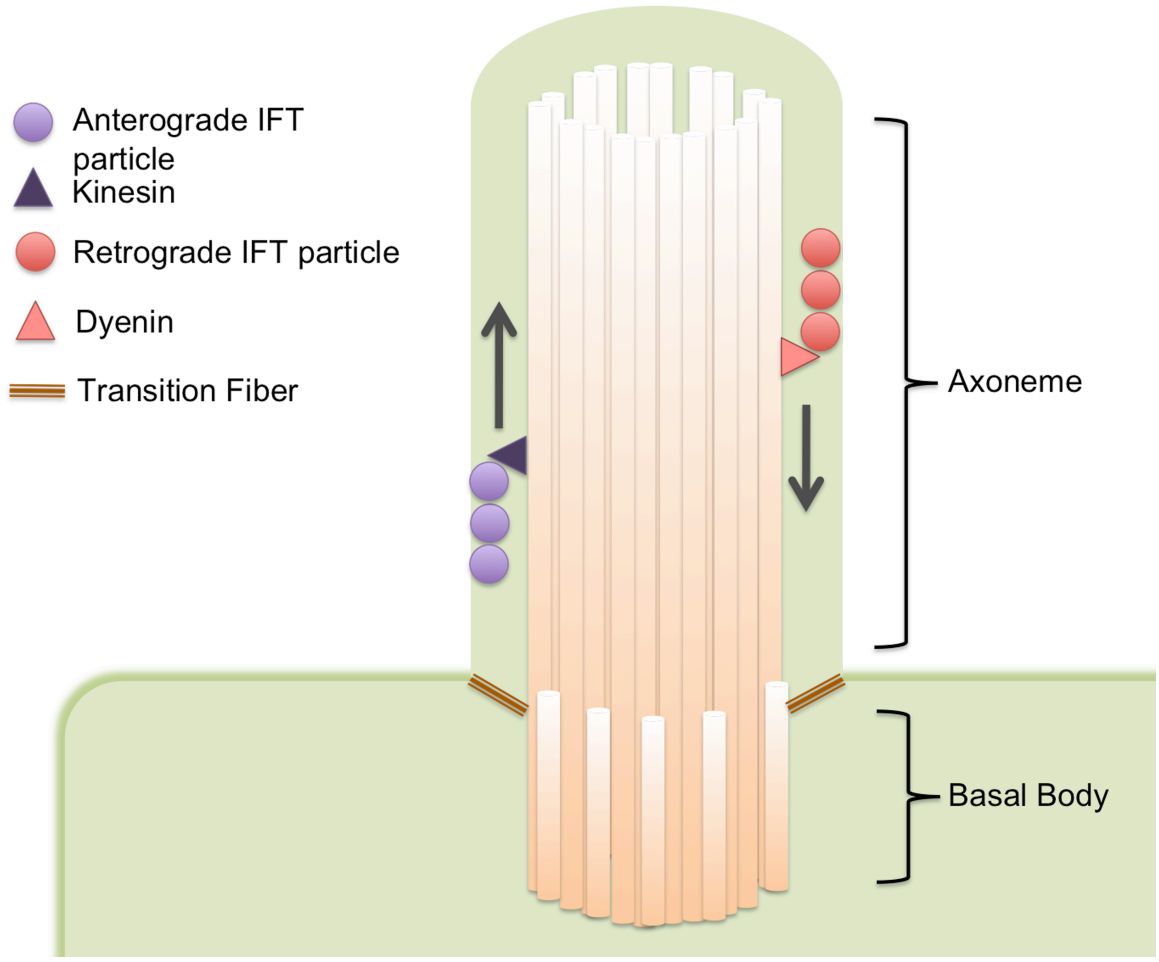

Figure 1.2. Cilia structure and IFT. The cilium contains nine outer doublet microtubules that are continuous with the triplet microtubules of the basal body. Transition fibers are found between the distal end of the basal body and the base of the cilia membrane. IFT particle proteins carried by kinesin and dynein move along the axoneme toward the tip and base of the cilium, respectively.

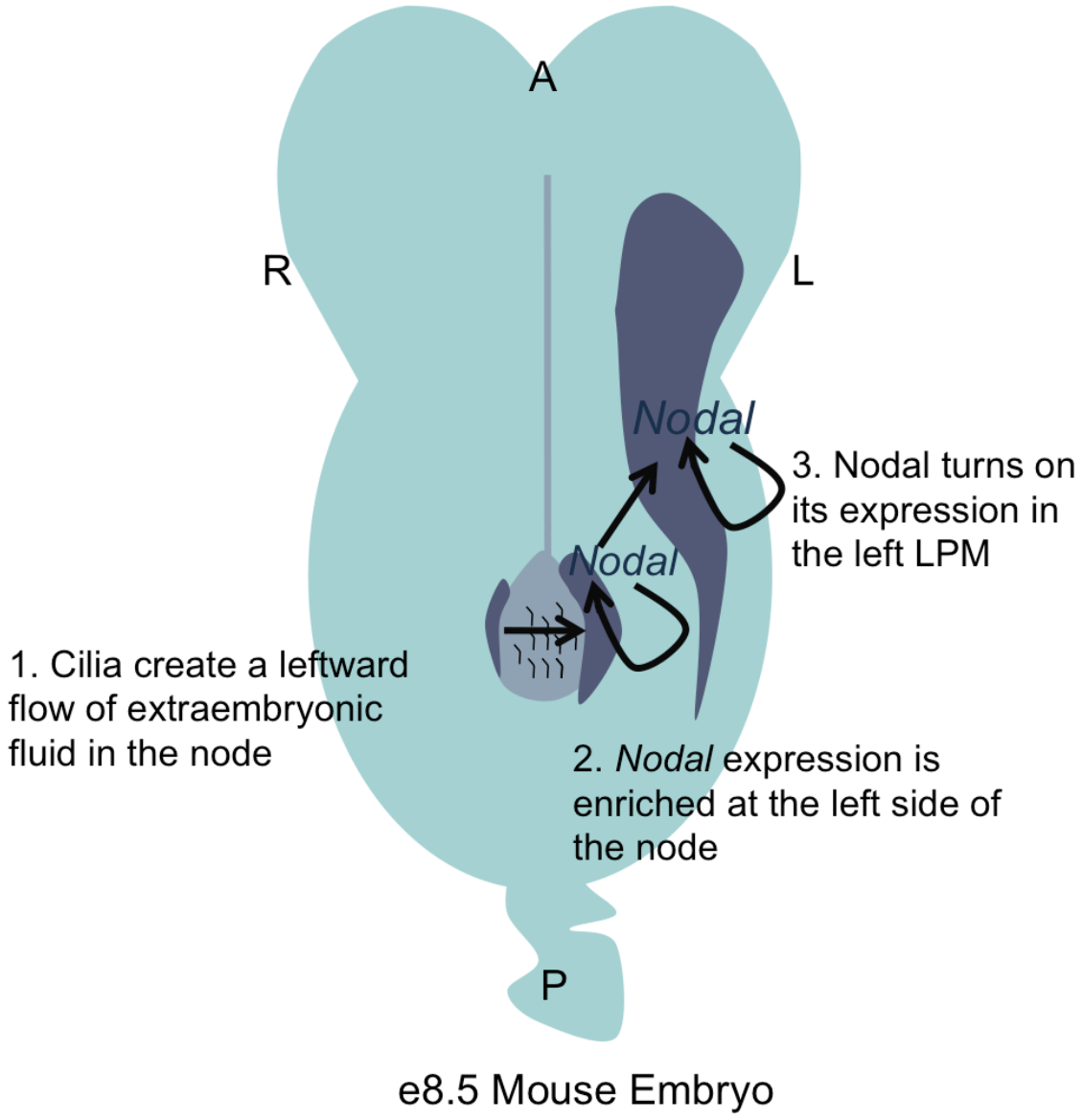

Figure 1.3. A summary of LR axis specification in mouse. 1) Cilia in the node rotate to create a leftward flow of extraembryonic fluid. 2) *Nodal* expression is enriched at the left side of the node, and Nodal enhances and maintains its expression in the node. 3) Nodal from the node induces its expression in the LPM and autoregulates its expression there.

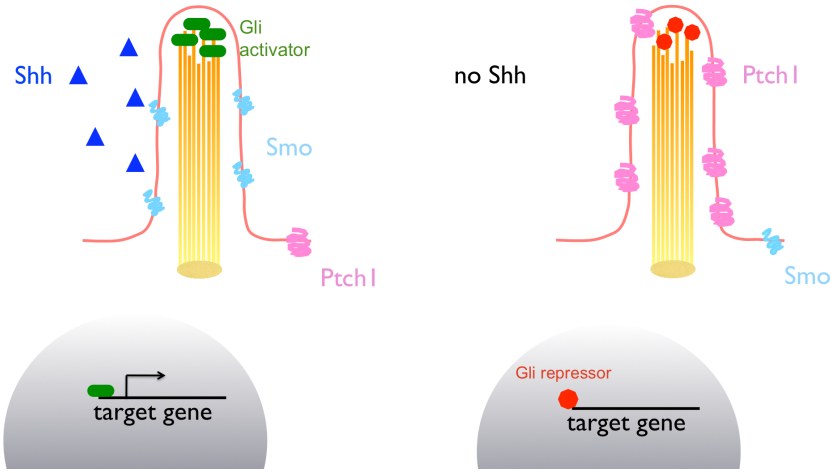

Figure 1.4. Shh signaling and cilia. In the presence of Shh ligand, Ptch1 is removed from the cilium while Smo and the Glis are enriched in cilia. The Glis are converted to GliA and can enter the nucleus to activate transcription of Shh target genes. In the absence of ligand, Ptch1 is enriched in cilia, and the Gli proteins are converted to GliR in the cilium. GliR can then enter the nucleus to repress Shh target genes.

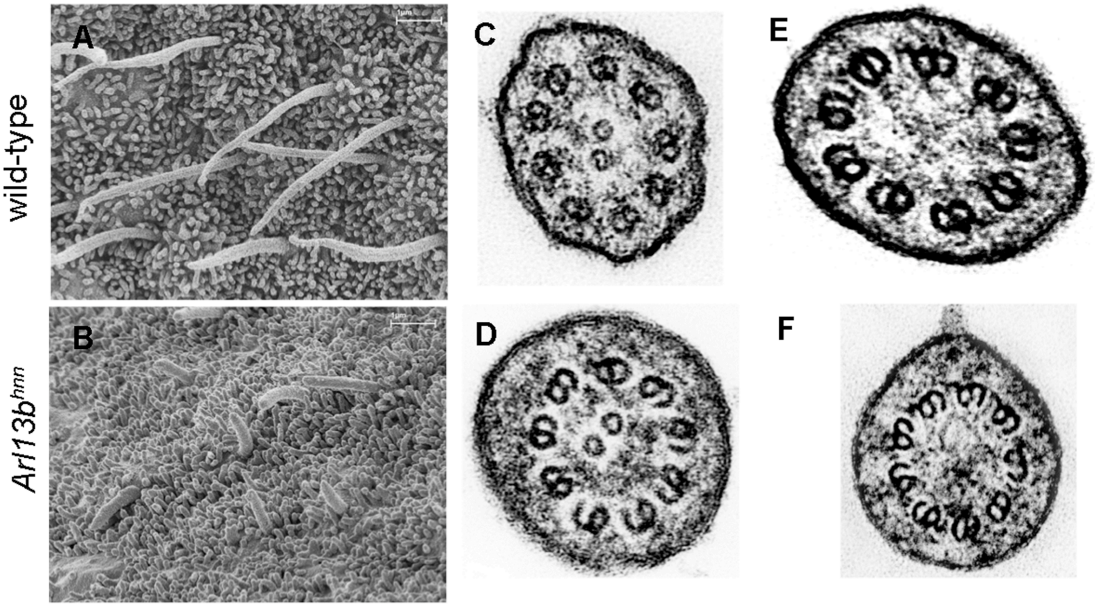

Figure 1.5. Cilia structure is disrupted in *Arl13b*^{hnn} embryos. A-B) scanning electron micrograph of cilia in the node of wild-type and *Arl13b*^{hnn} mutant embryos. C-F) transmission electron micrograph of cross sections from motile and immotile cilia. There is a disconnect at the inner junction of the A- and B-tubule in *Arl13b*^{hnn} mutant cilia.

CHAPTER 2

MATERIALS AND METHODS

Mouse Strains and Genotyping

All strains were bred at least ten generations on the C3H background. Alleles used were: *Arl13b*^{hnn}, *IFT172*^{wim}, *BATgal*, *Patched-lacZ*, and *Nodal*^{lacZ} (Collignon et al., 1996; Goodrich et al., 1997; Maretto et al., 2003; Huangfu and Anderson, 2005; Caspary et al., 2007). The *Arl13b*^{hnn} and *IFT172*^{wim} mutations were introduced in the Black6 background, therefore genotyping primers amplify short tandem repeats that differ between C3H and Black6 DNA and flank the mutation. Ear punch DNA was digested overnight with Proteinase-K (Sun et al.) at 55°C. The DNA was then diluted 1:20 in water, and PCR was performed for genotyping using the following primers (5' to 3') and conditions:

Arl13b^{hnn}: 94°C for 20sec, 55°C for 30sec, 72°C for 45sec, repeated fifty-five times

hnn147 Forward: AATGCCTCAAGTGCCTCTTT

hnn147 Reverse: GGGACTCATCTTTGGGAACA

hnn174 Forward: TGTGGGTGGCATATGTAGGA

hnn174 Reverse: GCTAGCTATTTTCTGTTGCTGGA

IFT172^{wim}: 94°C for 20sec, 55°C for 30sec, 72°C for 45sec, repeated fifty-five times

d5MIT148 Forward: GCTGCAAAGAAGAGAGAGGG

d5MIT148 Reverse: CCTCTGGCCAGCATGATATA

Shh201 Forward: TTGTCCTCTGGCTTCCAACTGG

Shh201 Reverse: CTTCAACCCTCTCCTTTCATTGC

BATgal: 94°C for 30sec, 50°C for 30sec, 72°C for 30sec, repeated 40 times

BATgal PCR requires AmpliTaq Gold (Low et al.)

Forward: CGGTGATGGTGCTGCGTTGGA

Reverse: ACCACCGCACGATAGAGATTC

Nodal^{lacZ}: 94°C for 30sec, 53°C for 45sec, 72°C for 1min, repeated 37 times

Nodal PCR requires AmpliTaq Gold (Low et al.)

Wild-type *Nodal* allele Forward: ATGTGGACGTGACCGGACAGAACT

Wild-type *Nodal* allele Reverse: CTGGATGTAGGCATGGTTGGTAGGAT

Nodal^{lacZ} Forward: GTCGTTTTACAACGTCGTGACT

Nodal^{lacZ} Reverse: GATGGGCGCATCGTAACCGTGC

In situ Hybridization

Timed matings of heterozygous mice were performed and embryos were harvested at e7.5 or e8.5 in phosphate buffered saline (PBS) with 0.4% bovine serum albumin (BSA). All extraembryonic tissue was removed. *In situ* hybridization was performed following standard protocol with the following adjustments: 1) Day 1 of *in situ* hybridization was performed on ice except for Proteinase-K (Sun et al.) Treatment which was done at room temperature; 2) PK treatment for e8.5 embryos was done for 8 minutes and e7.5 embryos were treated for 6 minutes; 3) the RNA probe prehybridization and hybridization steps were performed at 70°C; 4) the amount of RNA probe added was varied (between 4ul and 10ul) depending on the strength of signal from the probe, and this was determined after each probe was made. The probes used and their sources were

as follows: *Nodal* from Elizabeth Robertson, *Gdf1* was from Nancy Wall, *Shh* and *Foxa2* probes were from Andy McMahon, *NotchI* was from Janet Rossant, *Lefty1* and *Lefty2* probes were from Hiroshi Hamada, *Pitx2* was from Axel Schweickart, and *Dll1* probe was obtained from Radhika Atit.

Genotyping of the embryos was performed after *in situ* hybridization. Embryos were transferred to 200ul tubes to perform PK treatment. A forcep was used to transfer the embryo to the 200ul tube so that very little liquid was transferred with the embryo so as not to dilute the PK solution. An extra 2-3 ul of PK was added per embryo, because they are difficult to digest. PK and genotyping were then carried out as described above.

Whole Mount β-galactosidase Assay

Embryos homozygous for *Arl13b*^{hnn} and carrying either the *BATgal*, *Patched-lacZ,* or *Nodal-lacZ* reporter alleles were harvested at e8.5, and fixed in 4% PFA with 0.2% glutaraldehyde for 15 minutes (Goodrich et al., 1997; Maretto et al., 2003). Embryos were washed in rinse buffer (0.1M phosphate buffer, 2mM $MgCl_2$, 0.01% sodium deoxycholate, 0.02% NP-40) three times for 15 minutes each and then treated with 1mg/mL X-gal in 5mM potassium ferricyanide and 5mM potassium ferrocyanide in the dark at room temperature overnight.

Organ Analysis

For organ analysis, timed matings were done and embryos were harvested at e12.5. Organs were removed from the body cavity to allow imaging of the lungs. Images were taken with a Leica MZFLIII and Q capture software.

Mouse Embryonic Fibroblasts

e12.5 embryos were harvested in PBS 0.4% BSA. The head and visceral organs were removed and then the body cavity was transferred to clean PBS. The embryo was then transferred to a 1ml syringe with an 18G needle. Under a sterile hood, the embryo was passed through the needle about 5 times in 1ml of DMEM (high glucose, 10% FBS, with penicillin and streptomycin). The 1ml of media containing embryonic cells was then transferred to a gelatinized plate containing 10ml of DMEM (high glucose, 10% FBS, with penicillin and streptomycin). After the cells reached confluence, they were split 1:5. Cells were not used beyond passage 4.

TritonX-100 Treatment and Immunofluorescence

All cells were grown on poly-lysine coated coverslips except for MEFs, which were grown on gelatinized coverslips. For membrane removal prior to fixation, cells on coverslips were treated with 60ul of 0.1% Triton X-100 in PBS (without calcium or magnesium) for 1min. The cells were then fixed by adding 60ul of 4% PFA in PBS to the coverslips for 10min. Untreated cells were immediately fixed in 4% PFA for 10 minutes. After fixing, all cells were transferred to dishes containing wash solution (1% heat inactivated goat serum, 0.1% Triton X-100, 1X PBS) for 10 minutes. The cells were then incubated with primary antibody overnight at 4°C. After washing three times for 20 min

each, the cells were incubated in secondary antibody (Invitrogen Alexa fluors, 1:200) and Hoechst (Acros 33258, 1:3000) for 1 hour at room temperature. The cells were again washed three times for 20 min each and mounted in Prolong Gold Antifade Reagent (Invitrogen, P36934) Primary antibodies were used at the following dilutions: Arl13b 505, 1:1500; IFT88, 1:500 (Brad Yoder); GFP rabbit polyclonal, 1:500 (Millipore, AB 3080); GFP mouse monoclonal 1:500, (Chemicon, MAB 3580); Gli2, 1:2000 (Jonathan Eggenschwiler); Gli3C and Gli3N, 2ug/ml (Suzie Scales) (Wen et al., 2010); Sufu, 1:25 (Santa Cruz, SC-10933); Smo, 1:100 (Santa Cruz, SC-6366); acetylated α-tubulin, 1:2500 (Sigma, T-6793); and γ-tubulin, 1:1000 (Sigma, T-6557).

Fluorescence Recovery after Photobleaching

IMCD3 cells were transduced with 10ul of a viral construct expressing Arl13b-GFP, which was generated by the Emory University Viral Core. All cells were grown to confluence. SSTR3-GFP cells were from Greg Pazour and IFT88-YFP cells were from Brad Yoder. FRAP was performed on a Zeiss LSM510 META confocal using 63x objective with optical zoom. Five scans at 3% power were taken prior to bleaching, and cilia were then photobleached using the 488nm laser with 25 iterations at 50% power. Images were again scanned at 3% laser power after bleaching. For determination of movement in the cilium, an image was scanned at 500ms intervals at scan speed of 983.04ms. For determination of turnover in the entire cilium, an image was scanned at 5s intervals at the same scan speed. Fluorescence intensity measurements had background subtracted and the bleached region was normalized to the entire cilium (for determination of movement within the cilium) or to an unbleached region in the same field (for

determination of turnover in the cilium) using the following formula as described previously (Griffis et al., 2002): $(Un_0/Un)*(Bl/Bl_0) = I_{norm}$ where I_{norm} is the normalized fluorescence intensity of the bleached region, Bl is the intensity of the bleached region at time t, Un is the intensity of the entire cilium or an unbleached region at time t, Bl_0 is the average intensity of the bleached region prior to photobleaching, and Un_0 is the average intensity of the entire cilium or unbleached region intensity prior to photobleaching.

Shh Stimulation and Luciferase Assay

Conditioned media was generated as previously described (Taipale et al., 2000). In summary, 293 EcR Shh cells (ATCC, CRL-2782) were grown to confluence in a 10cm dish. The standard culture medium (ATCC DMEM, 10% FBS, Zeocin, G418) was removed, and a final concentration of 1uM Muristerone-A (MurA, Invitrogen) was added to the cells in 2% serum DMEM. After 24 hours, the conditioned media was collected and fresh 2% serum DMEM supplemented with MurA was again added to the cells. A collection was taken again after 24 hours, and that media was combined with the media from the first collection.

For the luciferase assay, MEFs were plated in a gelatinized 24 well plate (200,000 cells/well) in DMEM (high glucose, 10% FBS, penicillin and streptomycin). The following day, cells were transfected with 750ng of 8xGli Firefly luciferase (Sasaki et al., 1997) and 50ng Renilla luciferase using Lipofectamine 2000. After transfection, cells were serum starved in DMEM High Glucose with 0% serum. After 24 hours of serum starving, conditioned media diluted 1:4 was added to the cells. Untreated control cells were given 0.5% serum media at this point. After 24 hours of treatment, the cells were

harvested, and a dual luciferase assay was performed following manufacturers instructions (Promega, E1910).

For immunofluorescence of MEFs treated with Shh conditioned media, cells were plated at 800,000 cells per well of a 6 well plate containing gelatinized coverslips. The next day, cells were serum starved for 24 hours and treated with conditioned media as described for the luciferase assay. After 24 hours of Shh stimulation, the cells were harvested for immunofluorescence.

Arl13b Knockdown Virus

The knock down viral construct was generated using Sigma's Mission custom viral vector synthesis. The vector, clone ID, and targeting sequence were pLKO.1-puro-CMV-TagRFP, TRCN0000100504, and CCTGTCAGAAAGGTGACACTT, respectively. The targeting sequence recognizes the coding region of Arl13b starting at nucleotide 349 of the mRNA.

IMCD3 cells were transduced in a 12 well plate with the knock down construct at a multiplication of infectivity of 5. After transduction, cells were treated with puromycin at 2ug/ml for 3 days. After treatment, cells were passaged to a 6 well plate for immunofluorescence or to be harvested for Western blotting.

Gel filtration

All procedures were carried out on ice or at 4°C. Six confluent 10-cm dishes of WT or hnn MEF were lysed using 500 ul of Ne2 extraction buffer (250mM sucrose, 10 mM Hepes pH7.9, 450 mM NaCl, 2mM MgCl2, 2mM CaCl2, 1% sodium cholate, 1

tablet/10 ml of protease inhibitor EDTA free, 1U/ml DNAse). The extraction was carried out for 15 minutes on ice. The lysates were spun at 13,000 rpm for 10 minutes at 4°C. The proteins in supernatants were then resolved on a Superdex 200 gel filtration column at a flow rate of 0.5 ml/min in Ne2 buffer. Molecular weight markers were resolved in parallel runs for comparison. Aliquots from the gel filtration fractions were subjected to Western blot and IP for analysis.

Western Blot

50ul samples of the gel filtration fractions or 15ug of cell lysates were loaded into a 10% SDS-PAGE and transferred to an Amersham Bioscience nitrocellulose membrane. The membranes were subjected to Western Blot analysis with antibodies against Arl13b (1:500), Sec-8 (1:2000), or IFT88 (1:1000), followed by immunodetection using Amersham Bioscience ECL detection kit.

Immunoprecipitation

200ul of the gel filtration fractions were subjected to immunoprecipitation of Sec8. The samples were first pre-cleared using 50ul of Roche 50% protein G agarose beads for 2 hours on a rotator at 4°C. The samples were spun for 5 min at 13,000rpm. The supernatants were incubated with Sec8 antibody (1:100) overnight on a rotator at 4°C. The following day, the beads were re-introduced for 2 hours. The samples were spun for 5min and the beads were washed twice with Ne2 extraction buffer (described above). The proteins were eluted from the beads using 15ul of 4X protein loading dye containing 2-betamercaptoethanol and subjected to Western blot analysis.

Arl13b constructs and overexpression in MEFs

Arl13b was cloned using the Gateway system (Invitrogen). Full length Arl13b (coding for amino acid 1-427 without stop codon), the N-terminal domain (coding for amino acid 1-212 of Arl13b), and the C-terminal domain (coding for amino acid 210-427 of Arl13b) were cloned into pENTR/SD/D-TOPO (Invitrogen, K242020). The inserts were recombined into the pcDNA-DEST47 (C-terminal GFP tag, Invitrogen, 12281010) and pcDNA-DEST40 (N-terminal GFP tag, Invitrogen, 12274015) using Gateway LR clonase (Invitrogen, 11791-019) following manufacturer's instructions.

350,000 cells per well were seeded in a pre-gelatinized 6-well plate containing coverslips in DMEM (High Glucose, 10% FBS, penicillin, streptomycin). After 24 hours, the cells were transfected following manufacturer's recommendations using Lipofectamine 2000 (Invitrogen) complexed with the Arl13b expression plasmids (described above). After the cells were incubated with the complexes, the media was changed to serum free DMEM High Glucose for 24 hrs. The cells were then fixed using 4% PFA and were subjected to immunofluorescence. Cilia were measured using LSM Image Examiner software.

Arl13b-GFP expression virus

The L13 lentiviral mammalian expression vector was obtained from the Emory University Viral Vector Core. The Arl13b-GFP insert was generated by PCR from the pcDNA-DEST47 plasmid containing full length Arl13b using the following primers (5' to 3'): forward- GCTAGCTCAAACAAGTTTGTACAAAAAAGC, reverse-

GGATCCATTCTAGATCGAACCACTTTG. The primers introduced a 5' NheI site and a 3' BamHI site that were used to insert Arl13b-GFP into L13.

CHAPTER 3

THE CILIA PROTEIN ARL13B IS REQUIRED FOR EFFICIENT NODAL SIGNALING ACTIVITY DURING LEFT-RIGHT AXIS SPECIFICATION IN MOUSE

3.1 Summary

Specification of the left-right axis is a process that requires cilia. The first known left-right asymmetric event to occur in the mouse embryo is a leftward fluid flow, termed nodal flow that is created by rotating cilia on the node surface. This flow generates asymmetric expression of *Nodal*, which establishes the left side of the embryo. Because of the important role cilia play in generating the left-right axis, mutations in cilia genes often lead to left-right axis defects. However, exactly how fluid flow establishes the left side of the embryo is not clear, and it is not known exactly what other roles cilia and/or cilia proteins play in specifying the left-right axis. Here we show that the cilia protein Arl13b is required for left-right axis specification, but that mutants lacking Arl13b display a unique pattern of Nodal expression. We show that Arl13b is required for efficient Nodal signaling activity in the node and lateral plate mesoderm, making Arl13b the first known ciliary gene to have a role in Nodal signaling activity.

3.2 Introduction

The vertebrate body plan is established during embryo development through the specification of the three axes: anterior-posterior, dorsal-ventral, and left-right (LR). In vertebrates, the LR axis is the final axis to be specified just prior to visceral development, and its specification is necessary for asymmetric organs such as the heart, lungs, and stomach to develop and function properly (Peeters and Devriendt, 2006; Shiratori and Hamada, 2006). Work in the last 15 years has provided tremendous advances in our understanding of how the LR axis is established, but many steps along the way from the initial breaking of bilateral symmetry to the development of asymmetric organs remain

elusive (Bisgrove et al., 2003; Tabin, 2005; Speder et al., 2007; Raya and Izpisua Belmonte, 2008; Vandenberg and Levin, 2009).

In mouse, the first known LR asymmetric event is the leftward flow of extraembryonic fluid in an organizing center called the node. This fluid flow, called nodal flow, is created by the rotation of motile cilia on the surface of the node and is necessary for establishing the LR axis (Nonaka et al., 1998; Okada et al., 1999; Nonaka et al., 2002). A similar mechanism has been found in rabbit, zebrafish, frogs, and is thought to occur in humans (Bisgrove et al., 2003; Essner et al., 2005; Feistel and Blum, 2006; Schweickert et al., 2007; Okabe et al., 2008). It is unclear what signals are being transmitted by nodal flow, but the result is the enriched expression of the TGF-β signaling protein Nodal at the left node periphery (Collignon et al., 1996; Lowe et al., 1996). Nodal autoregulates its expression allowing maintenance and amplification of *Nodal* in the left node periphery. *Nodal* enrichment in the node then allows Nodal to induce its expression in the left lateral plate mesoderm (LPM) (Oki et al., 2007). In the LPM, *Nodal* induces expression of *Pitx2*, the transcription factor that guides asymmetric organ development (Ryan et al., 1998; Campione et al., 1999; Lin et al., 1999; Liu et al., 2001). The requirement for Nodal and Pitx2 in LR axis development is very well conserved, also being needed for left-right axis establishment in urochordates and even mollusks (Yoshida and Saiga, 2008; Grande and Patel, 2009).

Besides turning on its own expression, Nodal induces the expression of its inhibitors *Lefty1* and *Lefty2*, also TGF-β proteins, in the lateral plate mesoderm as well as the midline. Both *Lefty1* and *Lefty2* act to inhibit Nodal signaling by binding to the Nodal receptor and Nodal itself (Sakuma et al., 2002; Chen and Shen, 2004). *Lefty1* has its

highest expression in the midline, while *Lefty2* is highest in the left LPM. Because *Nodal* can diffuse over very long distances to induce its own expression, *Lefty1* acts as a midline barrier preventing *Nodal* from inducing its own expression in the right LPM (Meno et al., 1998; Meno et al., 2001). The high expression of *Lefty2* in the left LPM, limits the amount of time *Nodal* is expressed there, and expression of both *Lefty1* and *Lefty2* create a situation in the LPM where the Nodal ligand must reach a concentration threshold in order to overcome inhibition by the Lefty proteins and induce robust expression of *Nodal* in the LPM (Nakamura et al., 2006).

There are several other signaling events that are necessary for the left-sided enrichment of *Nodal* in the node and its subsequent expression in the left LPM. Wnt signaling, specifically *Wnt3a,* induces Notch at the node and Notch signaling is required for *Nodal* to be enriched in the left node periphery (Krebs et al., 2003; Raya et al., 2003; Masa-aki Nakaya and Yamaguchi, 2005); *Cerl2* is an inhibitor of Nodal that likely amplifies *Nodal* enrichment in the node (Marques et al., 2004); and Shh signaling is needed to make the LPM competent for *Nodal* expression and to induce expression of *Gdf1* at the node periphery, which is needed for Nodal ligand diffusion to the left LPM (Zhang et al., 2001; Tanaka et al., 2007; Tsiairis and McMahon, 2009). The gene network for LR axis establishment involves many players, some of which are still unknown, that turn a localized leftward flow of extraembryonic fluid into a global LR asymmetry that can guide visceral organ development.

Here we describe the LR axis defects found in the *Arl13b*$^{hennin\ (hnn)}$ mouse mutant. *Arl13b*^{hnn} mutants lack the cilia protein Arl13b (Arf-like 13b) which leads to shortened cilia in the node with a defect in the axoneme manifested as a disconnect between the A-

tubule and B-tubule (Caspary, 2007). We show that the LR axis defects in the *Arl13b*^{hnn} mouse are due to a delayed randomized followed by late bilateral expression of *Nodal* in the LPM. Surprisingly, the LR axis defects are due in part to a genetic interaction between *Arl13b* and *Nodal* that suggests the levels of Nodal signaling in the node and LPM of these mutants are reduced. This is the only cilia mutant described so far to show this specific phenotype, and proposes a role for the cilia protein Arl13b in Nodal signaling activity.

3.3 Results

Arl13b^{hnn} *mutants display heterotaxia*

Arl13b^{hnn} mice display a variety of phenotypes including randomized heart looping, an indication of LR axis defects (Garcia-Garcia et al., 2005). To characterize the extent of the LR axis defects in *Arl13b*^{hnn} mutants, we examined the orientation of the heart, lungs, and stomach in embryonic day (e)12.5 embryos. In mice, the left lung has a single lobe while the right lung has four, so we determined the left versus right lung by the presence of lobes. We found that in *Arl13b*^{hnn} mutants the lungs most often showed left isomerism (44.4% of embryos) and normal orientation at a high rate (38.9%), although the right lung had smaller and fewer lobes (Figure 3.1 A-F, Table 1, and data not shown). The heart and stomach orientation were almost completely randomized and were not coordinated, for example, the heart may be on the left while the stomach is on the right (Figure 3.1 A-F, Table 3.1), indicating that there was not only a defect in the global specification of the LR axis, but individual organs were interpreting the LR axis distinctly, a defect known as heterotaxia. This defect is seen in several other mouse

mutants with LR defects as well as in human laterality disorders (Chen et al., 1998; Meno et al., 1998; Lin et al., 1999; Lowe et al., 2001; Peeters and Devriendt, 2006).

Nodal and *Pitx2* are misexpressed

To assess the molecular steps that establish the left-right axis, we performed *in situ* hybridizations for *Nodal* and for its target gene *Pitx2*. There is no morphological difference between wild-type and *Arl13b*^{hnn} mutants at e8.5, therefore all of our *in situ* hybridizations were genotyped post phenotypic analysis to prevent any bias in assessment of the expression patterns. In *Arl13b*^{hnn} mutants, we found that *Pitx2* was most often expressed bilaterally in the LPM and splanchnopleure of e8.5 and e9.5 embryos, respectively, although we saw normal left-sided expression and no expression at a high frequency (Figure 3.2, A, B, D). This pattern is consistent with the lung laterality in *Arl13b*^{hnn} mutants (Table 3.1).

We next examined *Nodal* expression in the LPM, as *Nodal* is responsible for initiating expression of *Pitx2*. Wild-type embryos have *Nodal* expression in the left LPM starting at the 2-3 somite stage, and it is extinguished by the 6-7 somite stage (Figure 3.3, A-D). In *Arl13b*^{hnn} , we found *Nodal* expression was delayed in the LPM until the 4-5 somite stage, at which point half of the embryos still did not show *Nodal* expression (Figure 3.3, E, F, H). Of those embryos with expression at the 4-5 somite stage, it was in the left LPM or bilateral, and at the 6-7 somite stage almost all embryos had bilateral LPM expression (Figure 3.3, F-H). Since Nodal is normally extinguished at the 6-7 somite stage (Figure 3.3, C, D), *Arl13b*^{hnn} mutants, not only have both spatial and temporal defects in *Nodal* expression.

The midline barrier in **Arl13b^{hnn}** *mutants is intact*

We wanted to examine the potential causes for the late bilateral *Nodal* expression in *Arl13b^{hnn}* mutants. Mutants showing bilateral *Nodal* expression often have defects in *Lefty1* expression in the midline (Masa-aki Nakaya and Yamaguchi, 2005; Nakamura et al., 2006). Our previous analysis of *Arl13b^{hnn}* showed that e9.5 mutants lack a floorplate in the caudal neural tube raising the possibility that bilateral *Nodal* expression in *Arl13b^{hnn}* could be due to a lack of floorplate specification and therefore loss of *Lefty1* expression (Caspary et al., 2007). However, we did see expression of the floor plate marker *Foxa2* as well as *Lefty1* in mutant embryos at e8.5 (Figure 3.4). Interestingly, *Lefty1* was not expressed in the midline at the 6-7 somite stage of our mutant embryos although *Nodal* expression persisted in the LPM at this stage (Figure 3.4, A-F, Figure 3.2, G, H), indicating the 6-7 somite stage bilateral expression of *Nodal* could be due to the loss of *Lefty1* in the midline. Because Nodal in the LPM induces *Lefty1* expression in the midline and Nodal persists in the LPM of our mutants at the 6-7 somite stage, the loss of *Lefty1* expression could be due to a gradual loss of floorplate integrity, which is supported by the weakened *Foxa2* expression we saw at 6-7 somite stage (Figure 3.4, I, J). While examining *Lefty1* expression, we also observed *Lefty2* expression and found it follows the same pattern as *Nodal* in the LPM (Figure 3.4, A-B, D-E, and data not shown, n=13).

Nodal *enrichment in the* **Arl13b^{hnn}** *node is reduced*

The enrichment of *Nodal* at the left side of the node allows Nodal ligand to activate its expression in the left LPM. We therefore analyzed *Nodal* enrichment in the node of *Arl13b*^{hnn} mutants. Surprisingly, we still saw enrichment of *Nodal* at the left side of the node at presomite stages in *Arl13b*^{hnn} mutants identical to what we saw in wild-type embryos (Figure 3.6, A, B). At later somite stages, we saw fewer *Arl13b*^{hnn} mutant embryos with *Nodal* enrichment, even though *Nodal* enrichment was very robust in wild-type (Figure 3.6, A, B), indicating an inability to maintain *Nodal* enrichment. 6-7 somite stage wild-type and mutant embryos had very low levels of *Nodal* in the node so enrichment at this stage was not determined.

We compared *Nodal* enrichment in *Arl13b*^{hnn} mutants to mutants that lack cilia, the *IFT172*^{wim} mutants, to see if they had similar defects in *Nodal* enrichment. Interestingly, we still saw enrichment of *Nodal* in *IFT172*^{wim} mutants although that enrichment was seen more often on the right side of the node than in wild-type and *Arl13b*^{hnn} mutant embryos (Figure 3.6, A-C). The *IFT172*^{wim} embryos most often showed *Nodal* enrichment at the 2-3 somite stage, and we saw very few embryos with enrichment at presomite and 4-5 somite stages (Figure 3.6, C). Seeing enrichment of *Nodal* in the node was surprising considering these mutants do not have a directed fluid flow in the node, and suggests that *Nodal* enrichment can occur without fluid flow, but that the enrichment is no longer directed to the left. Because our mutants showed a *Nodal* enrichment phenotype that was distinct from mutants with no cilia, this suggests that the inability to maintain *Nodal* enrichment in our mutants is not directly caused by a lack of fluid flow.

Wnt and Shh signaling pathways are sufficient for* Nodal *expression in* Arl13b^{hnn} *mutants

Several signaling pathways are active in the node and LPM that affect *Nodal* expression. In order to investigate the cause of the initial delay in *Nodal* expression, we examined these pathways. A *Wnt3a* null mutant shows a similar delay in *Nodal* expression followed by bilateral expression of *Nodal* in the LPM. *Wnt3a* is required for Notch signaling at the node, which in turn is needed for *Nodal* expression (Masa-aki Nakaya and Yamaguchi, 2005). There has also been a link between cilia and Wnt signaling (Germino, 2005; Simons et al., 2005; Corbit et al., 2007). Taken together, Wnt signaling was a likely candidate to be disrupted in our mutants. In order to examine canonical Wnt signaling activity in our mutant embryos we incorporated the BATgal reporter allele, which expresses the *lacZ* gene in response to Wnt signaling activity. We found no difference in Wnt signaling between wild-type and mutant embryos (Figure 3.5, A, B). Likewise, we saw no change in expression of *Dll1*, the *Wnt3a* target, or of *Notch1* and its target *Lfng* (Figure 5, C-H).

The Sonic Hedgehog (Shh) signaling pathway induces expression of *Gdf1* at the node periphery, which is required for *Nodal* diffusion to the LPM (Zhang et al., 2001; Tanaka et al., 2007). Shh signaling has also been found to be needed for *Nodal* expression in the LPM (Tsiairis and McMahon, 2009), and we know there are Shh signaling defects in *Arl13b^{hnn}* mutants at later stages (Caspary, 2007). However, we saw no change in *Shh* expression, and using *Patched-lacZ* to monitor Shh signaling activity, there was no difference between wild-type and mutant embryos. *Gdf1* expression was

also normal (Figure 3.5, I-N). Taken together, our data suggest that the Wnt and Shh signaling pathways are sufficient for Nodal expression in the node and LPM.

The Nodal *expression defect in* Arl13b^{hnn} *mutants is cilia dependent*

We next wanted to determine if the delayed *Nodal* expression in the *Arl13b^{hnn}* LPM was due to their shortened cilia. Shortened cilia should cause a defect in nodal flow, however other mutants with flow defects do not show such a severe delay in *Nodal* expression (Lowe et al., 1996), leading to our prediction that the delayed Nodal expression is due to a cilia independent function of Arl13b. We generated *Arl13b^{hnn}* mutants that lack cilia by crossing the *Arl13b^{hnn}* mutants to *IFT172^{wim}* mutants. The *Arl13b^{hnn};IFT172^{wim}* embryos showed bilateral expression of *Nodal* starting at the 2-3 somite stage similar to what is seen in *IFT172^{wim}* single mutants (Figure 3.3, E-P). This result indicates that the shortened cilia in our mutants do play a role in the *Nodal* expression phenotype we saw in the LPM. However, we did see that the expression of *Nodal* in the LPM of our double mutants was weaker than that in a single *IFT172^{wim}* mutant, indicating an intermediate phenotype (Figure 3.3, M-N). This suggests that a cilia dependent function of Arl13b is required for *Nodal* expression in the LPM, although it does not rule out the possibility of a cilia independent function.

There is a genetic interaction between Arl13b *and* Nodal

Because *Nodal* autoregulates its expression in both the node and LPM, a reduction in Nodal signaling activity could lead to a loss of maintaining *Nodal* expression in the node as well as a failure to induce expression in the LPM. Therefore, we

genetically reduced Nodal activity in our *Arl13b*^{hnn} mutants using the null *Nodal*^{lacZ} allele. If the levels of Nodal signaling are reduced in our mutants, we should see a more severe Nodal expression pattern in *Arl13b*^{hnn}; *Nodal*^{lacZ} mutants. Indeed, the *Arl13b*^{hnn}; *Nodal*$^{lacZ/+}$ embryos lacked *Nodal* expression in the LPM at all somite stages using either beta-galactosidase activity or *in situ* hybridizations as a readout (Figure 3.7, B, C, E, F). *Nodal* expression in the node was also faint in the *Arl13b*^{hnn}; *Nodal*$^{lacZ/+}$ mutants (Figure 3.7, F). This result suggests that in *Arl13b*^{hnn} mutants, Nodal signaling activity is reduced in both the node and LPM.

We confirmed the loss of *Nodal* expression in the *Arl13b*^{hnn}; *Nodal*$^{lacZ/+}$ LPM by examining *Pitx2* expression, and, as expected, *Pitx2* expression was lost in the LPM (Figure 3.2, C-E). These molecular patterns were reflected by the organ laterality in the *Arl13b*^{hnn}; *Nodal*$^{lacZ/+}$ mutants which showed right isomerism in the lungs, again with the lobes being smaller that wild-type, as well as a midline stomach (Figure 3.1, G-I, Table 3.1).

To determine if there is a reduction of Nodal signaling activity at earlier stages, we examined *Nodal* expression in *Arl13b*^{hnn};*Nodal*$^{lacZ/+}$ at e7.5 and saw that its expression using the beta-galactosidase assay was indistinguishable from wild-type (Figure 3.7, A, D). Similarly, at e12.5 in *Arl13b*^{hnn};*Nodal*$^{lacZ/+}$ mutants, there were no defects in mesoderm or endoderm derivatives, which are specified by Nodal in the pre-gastrulation embryo.

3.4 Discussion

Establishment of the LR axis in mouse development has been intensely studied for the last 15 years, and great advancements in our understanding of the process have been achieved, but there are still many steps that have yet to be understood. The *Arl13b*^{hnn} mutant provides a unique defect in *Nodal* expression that can be used to heighten our understanding of LR axis specification and Nodal signaling.

Organ laterality and the dose of Pitx2 *in* Arl13b^{hnn} *mutants*

In many different LR axis defective mutants and human syndromes, the visceral organs may have different lateralities even though a single global LR axis decision has been specified. The cause of this has been perplexing, but it has been suggested that individual organs may require different doses of Pitx2, either in the amount of Pitx2 the developing organ is presented with or the length of time the developing organ sees Pitx2 or both. The complex pattern of *Nodal* and *Pitx2* expression in *Arl13b*^{hnn} mutants supports this idea. Because the lungs follow almost exactly the *Pitx2* expression pattern we saw in our mutants, they may only require a small dose of Pitx2 for LR specification to occur. However, the heart and stomach obviously require more precise amounts of *Pitx2*, as they developed with a random orientation in our mutants and chose a left or right side independently of one another.

Arl13b is needed for efficient Nodal signaling

The genetic interaction we found between *Arl13b* and *Nodal*, suggests there is reduced Nodal signaling in the node and LPM of *Arl13b*^{hnn} mutants. When we reduced Nodal levels in *Arl13b*^{hnn} mutants by introducing the *Nodal*^{lacZ} allele, we saw a more

severe effect on *Nodal* expression in both the node and LPM of our mutants- *Nodal* expression was weakened in the node, and was completely lost in the LPM. There are several possibilities for how Arl13b is affecting Nodal signaling. First Arl13b may have a direct role in the Nodal signaling pathway or it could indirectly control Nodal activity through regulation of other signaling events, and second the function of Arl13b may be cilia dependent or independent or some combination of the two.

Because the cilia are shortened in *Arl13b*^{hnn} mutants, fluid flow is likely disrupted to some extent, however at the 4-5 stage in our mutants, *Nodal* and *Pitx2* expression in the LPM were most often bilateral or left sided. In contrast, the *Left-right dynein* (*Lrd*) mutant, which has structurally intact albeit immotile cilia, shows random expression of *Nodal* in the LPM such that 25% of the embryos have bilateral expression, 25% are in the right LPM, 25% left, and 25% lack expression in the LPM. Therefore, nodal flow may be sufficient in many of embryos to establish the left side even though the cilia length in *Arl13b*^{hnn} mutants is half that of wild-type embryos (Caspary et al., 2007).

We predict the delayed *Nodal* expression pattern we saw in *Arl13b*^{hnn} mutants is due to a cilia independent function of Arl13b, because other cilia mutants such as *Lrd, inversin, Dnhch2,* and *IFT172*^{wim} do not have neither severely delayed *Nodal* expression in the LPM nor a genetic interaction with *Nodal* (Okada et al., 1999; Huangfu et al., 2003; Huangfu and Anderson, 2005). However the shortened cilia in *Arl13b*^{hnn} mutants may contribute to the delayed expression, as *Lefty1* expression in the midline is dependent on cilia, and *Lefty1* is expressed in *Arl13b*^{hnn} mutants. Therefore, we would expect loss of cilia in *Arl13b*^{hnn} would cause loss of *Lefty1* expression in the midline and thereby permit increased Nodal signaling activity in LPM. Indeed, in our *Arl13b*^{hnn};

IFT172^{wim} mutants *Nodal* expression in the LPM was no longer delayed, however the expression in the LPM was less robust than that in an *IFT172*^{wim} mutant, suggesting that Nodal signaling levels were reduced in the double mutants although it was not as severe as in the *Arl13b*^{hnn} single mutants. This intermediate phenotype is consistent with a cilia independent function of Arl13b in generating efficient Nodal signaling activity. Nodal signaling has not been found to require cilia for function and depends heavily on endocytosis and recycling of its receptors at the plasma membrane (Constam, 2009). Some cilia proteins have functions outside of the cilium (Zhou et al., 2006; Finetti et al., 2009), and as Arl13b is a membrane associated GTPase (Cevik et al., 2010), Arl13b could play a role at the plasma membrane to regulate Nodal signaling through regulation of receptor localization or endocytosis of the pathway components. It will be important for future studies to determine if Arl13b has cilia independent roles, and how that may affect Nodal signaling.

If Nodal signaling is reduced in *Arl13b*^{hnn} mutants, we may expect to see other developmental defects that require Nodal signaling in addition to the LR axis defects. Nodal signaling is required for mesoderm, endoderm, and AP axis formation, all of which are intact in our mutants. However, studies have shown that LR axis specification is more sensitive to levels of Nodal signaling than other developmental processes (Lowe et al., 2001; Brennan et al., 2002; Norris et al., 2002), leading to our model that loss of Arl13b may lead to less efficient Nodal signaling activity, such that only LR axis specification is affected. Another possible model is that Arl13b is required at a step of Nodal signaling that is only utilized during LR axis specification. For example, the co-receptor for Nodal, *Cryptic*, is required for Nodal signaling activity and is only expressed during LR axis

establishment (Shen et al., 1997). Arl13b could therefore regulate its localization and/or function. Teasing apart these possibilities will require further examination of Arl13b function at the cellular level and determining precisely how Nodal signaling is affected in *Arl13b*^{hnn} mutants.

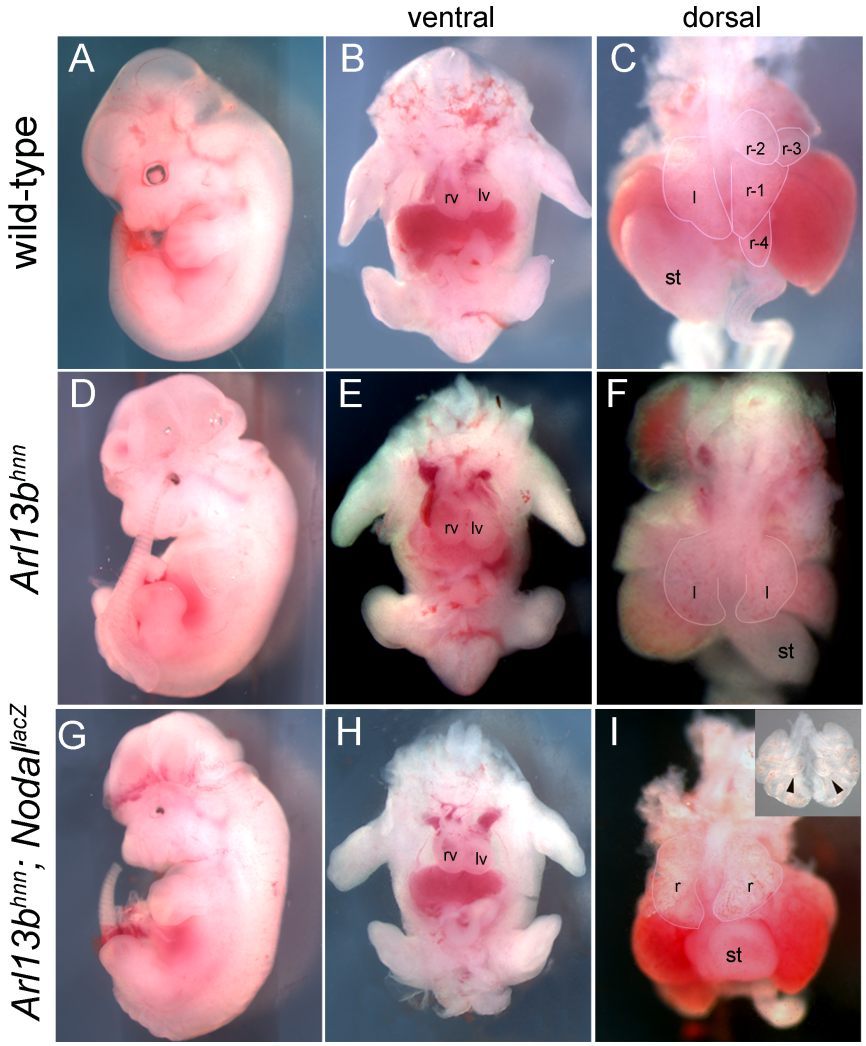
ventral
dorsal
wild-type
Arl13b^hnn
Arl13b^hnn; Nodal^lacZ
A
B
C
D
E
F
G
H
I
rv
lv
r-2
r-3
r-1
r-4
l
st
r

Figure 3.1. Organ laterality. A-C) Wild type e12.5 embryos. D-F) e12.5 *Arl13b*^{hnn} mutant embryos. G-I) e12.5 *Arl13b*^{hnn};*Nodal*$^{lacZ/+}$ embryos. B) A ventral view of the internal organs of the wild-type embryo shows normal placement of the heart with its apex towards the left. C) A dorsal view of the organs shows the left-right asymmetry of the lungs, where there is a single left lobe and 4 right lobes. The stomach is on the left side of the embryo. E) Ventral view of an *Arl13b*^{hnn} mutant with its heart apex toward the left. F) A dorsal view of the same embryo in D and E shows the stomach on the right as well as a single lobed left and right lung. H) *Arl13b*^{hnn};*Nodal*$^{lacZ/+}$ mutant shows the heart apex toward the left. I) There are small lobes on both the left and right lung with the stomach in the center of the embryo. Inset is a ventral view of the lungs with arrowheads pointing to the lobes. rv, right ventricle; lv, left ventricle; st, stomach; l, left; r, right.

Table 3.1. Organ Laterality

	heart			lungs					stomach			
	left	right	n=	normal	reversed	left isom.	right isom.	n=	right	left	center	n=
Wild type	100%	0%	6	100%	0%	0%	0%	6	100%	0%	0%	6
Arl13b^{hnn}	57.9%	42.1%	19	38.9%	6%	44.4%	11.1%	18	52.4%	42.9%	4.8%	21
Arl13b^{hnn}; *nodal*^{lacZ}	62.5%	37.5%	8	0%	0%	0%	100%	5	0%	12.5%	87.5%	8

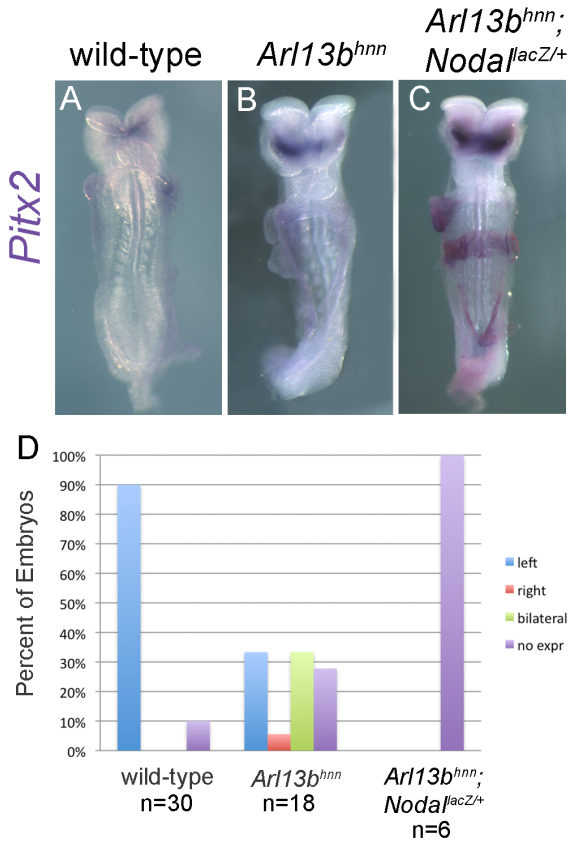

Figure 3.2. *Pitx2* expression is disrupted in *Arl13b*^{hnn} mutants. A-C) *Pitx2 in situ* hybridization in e8.5 embryos. A) Wild type *Pitx2* expression is in the left LPM. There non-specific staining in the extraembryonic tissue. B) *Arl13b*^{hnn} mutant embryo with bilateral *Pitx2* expression. C) *Arl13b*^{hnn};*Nodal*$^{lacZ/+}$ embryo with no expression in the LPM. D) Graph shows the number of embryos with each expression pattern of *Pitx2* in the LPM.

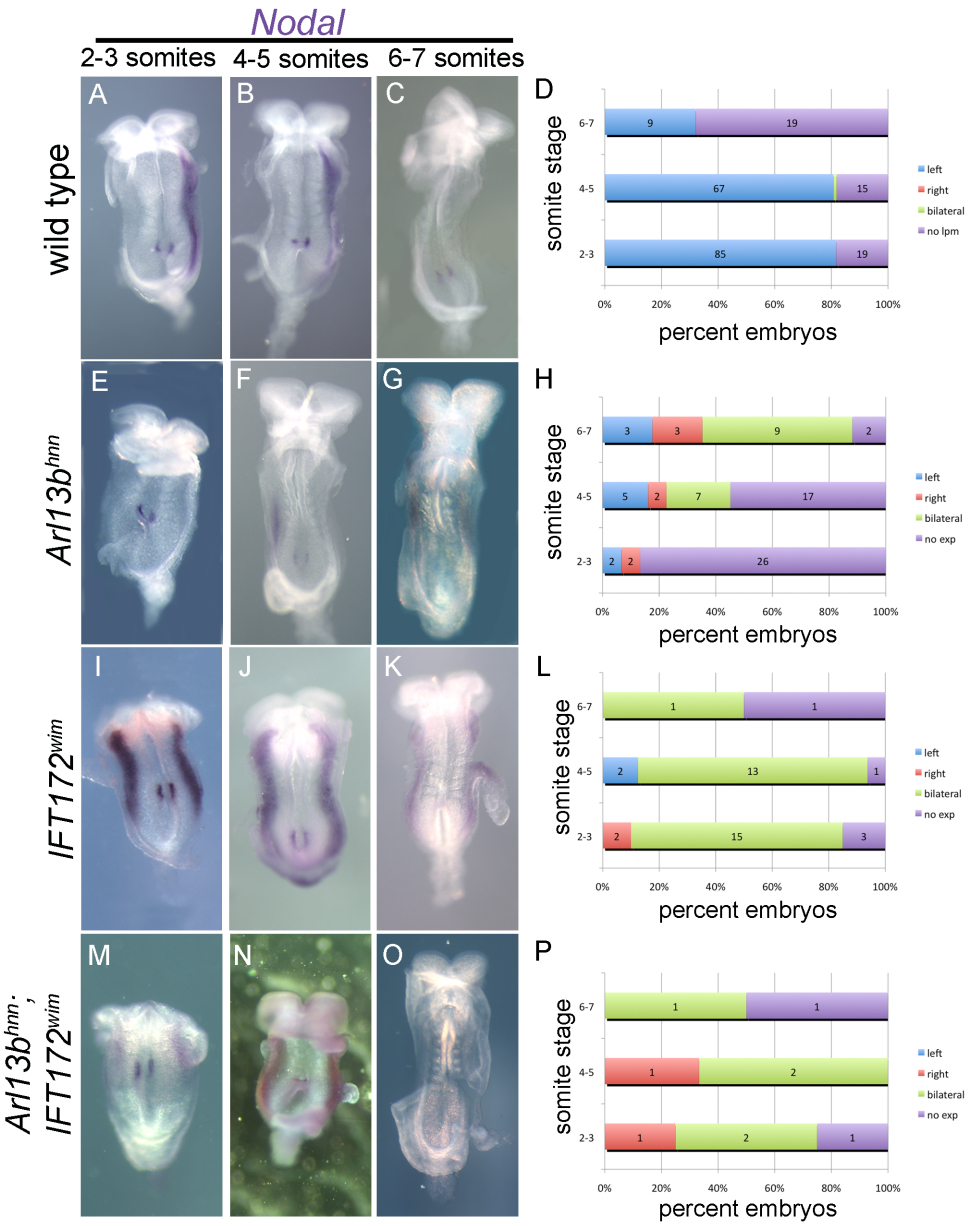
Nodal
2-3 somites
4-5 somites
6-7 somites
wild type
Arl13b^hnn
IFT172^wim
Arl13b^hnn; IFT172^wim
A
B
C
D
E
F
G
H
I
J
K
L
M
N
O
P
somite stage
6-7
4-5
2-3
percent embryos
0%
20%
40%
60%
80%
100%
left
right
bilateral
no lpm
no exp
9
19
67
15
85
19
3
3
9
2
5
2
7
17
2
2
26
1
1
2
13
1
2
15
3
1
1
1
2
1
2
1

Figure 3.3. *Nodal* expression is disrupted in *Arl13b*^{hnn} mutants. A-C, E-G, I-K, M-O) *in situ* hybridization for *Nodal*. A-C) Wild type embryos showing *Nodal* expression in the left LPM starting at the 2-3 somite stage (A) and being extinguished at the 6-7 somite stage (C). E-G) *Arl13b*^{hnn} mutant embryos showing no expression at the 2-3 somite stage (E), right sided expression at the 4-5 somite stage (F), and bilateral expression at the 6-7 somite stage (G). I-K) *IFT172*^{wim} mutants showing bilateral *Nodal* expression starting at the 2-3 somite stage. M-O) *Arl13b*^{hnn}; *IFT172*^{wim} mutants have bilateral expression of *Nodal* starting at the 2-3 somite stage (M). D, H, L, P) Graphs quantifying the number of embryos with each *Nodal* expression pattern at specific somite stages.

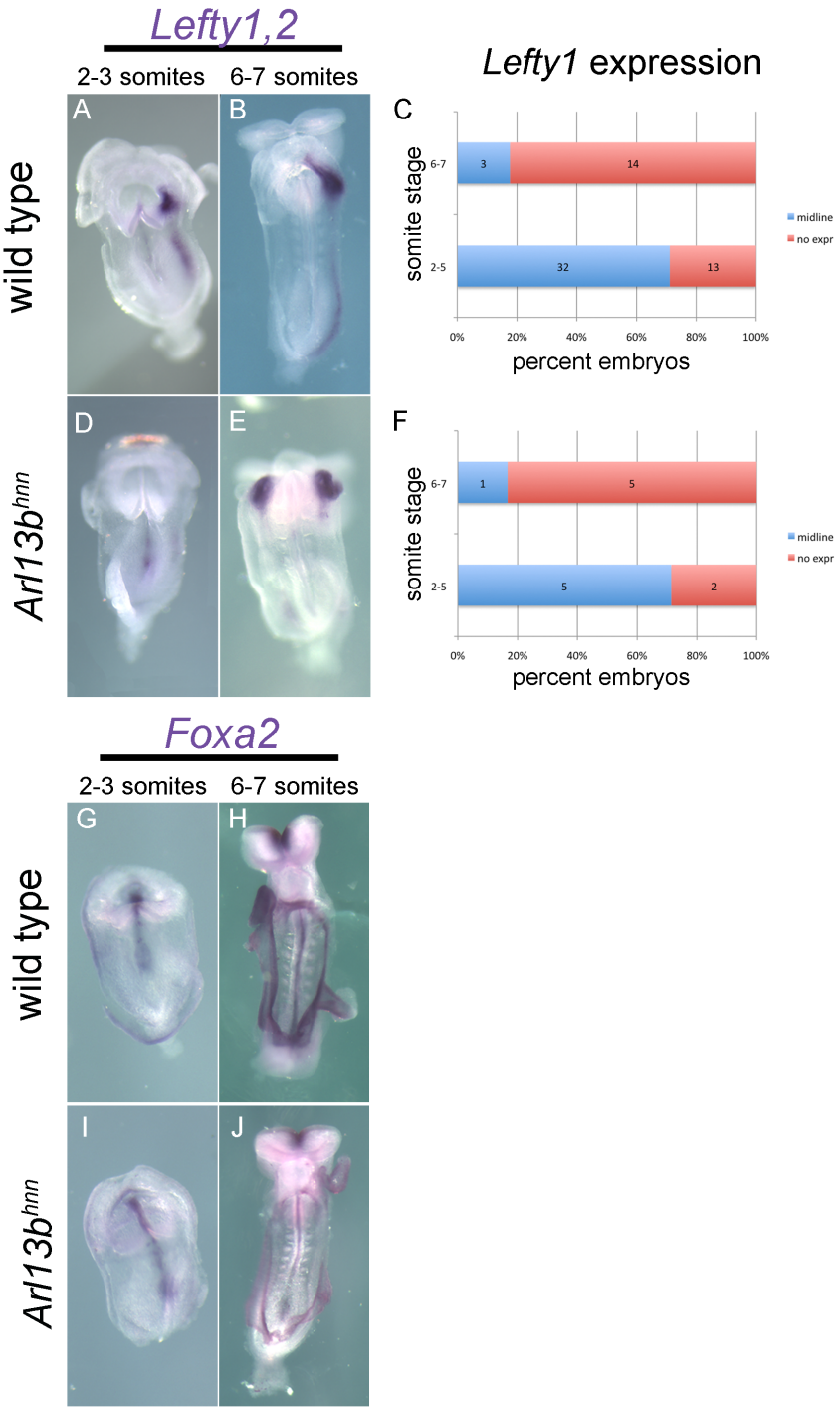
Lefty1,2
2-3 somites
6-7 somites
wild type
Arl13b^hnn
A
B
D
E
Lefty1 expression
C
somite stage
6-7
2-5
3
14
32
13
midline
no expr
0%
20%
40%
60%
80%
100%
percent embryos
F
1
5
5
2
Foxa2
G
H
I
J

Figure 3.4. Midline patterning is normal at early somite stages in *Arl13b*^{hnn} mutants. A-E) *Lefty1 and Lefty2 in situ* hybridization in wild-type (A, B) and *Arl13b*^{hnn} (D, E). The percent of embryos with expression of *Lefty1* in the midline is quantified in C and F. G-J) *foxa2 in situ* hybridization in wild type (G, H) and *Arl13b*^{hnn} mutants (I, J).

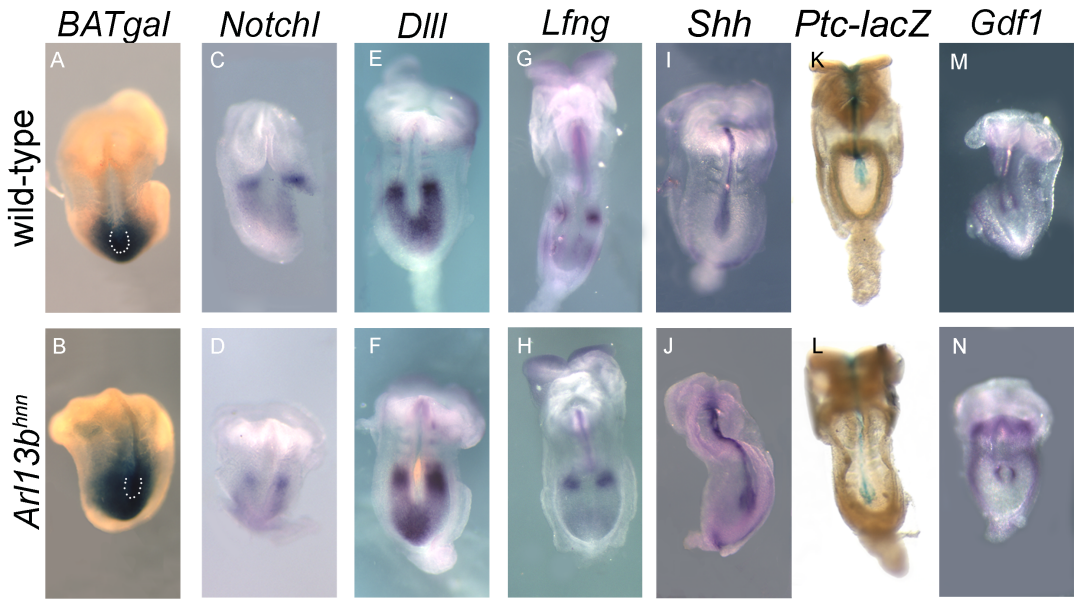

Figure 3.5. Wnt and Shh signaling are intact in *Arl13b*^{hnn} mutants. A-B) whole mount β-galactosidase assay shows no difference in Wnt signaling between wild-type (A) and *Arl13b*^{hnn} mutant (B) embryos. C-H) Whole mount *in situ* hybridization for *Notch1* (C-D) *Dll1* (E-F) and *Lfng* (G-H) shows that Notch signaling is intact in *Arl13b*^{hnn} mutants compared to wild type. I-J) Whole mount *in situ* hybridization for *Shh* is identical between wild type and *Arl13b*^{hnn} mutants. K-L) *Ptch1-lacZ* shows no change in Hedgehog response between wild type and *Arl13b*^{hnn} mutant embryos. M-N) the Shh signaling target *Gdf1* is expressed normally in *Arl13b*^{hnn} mutants.

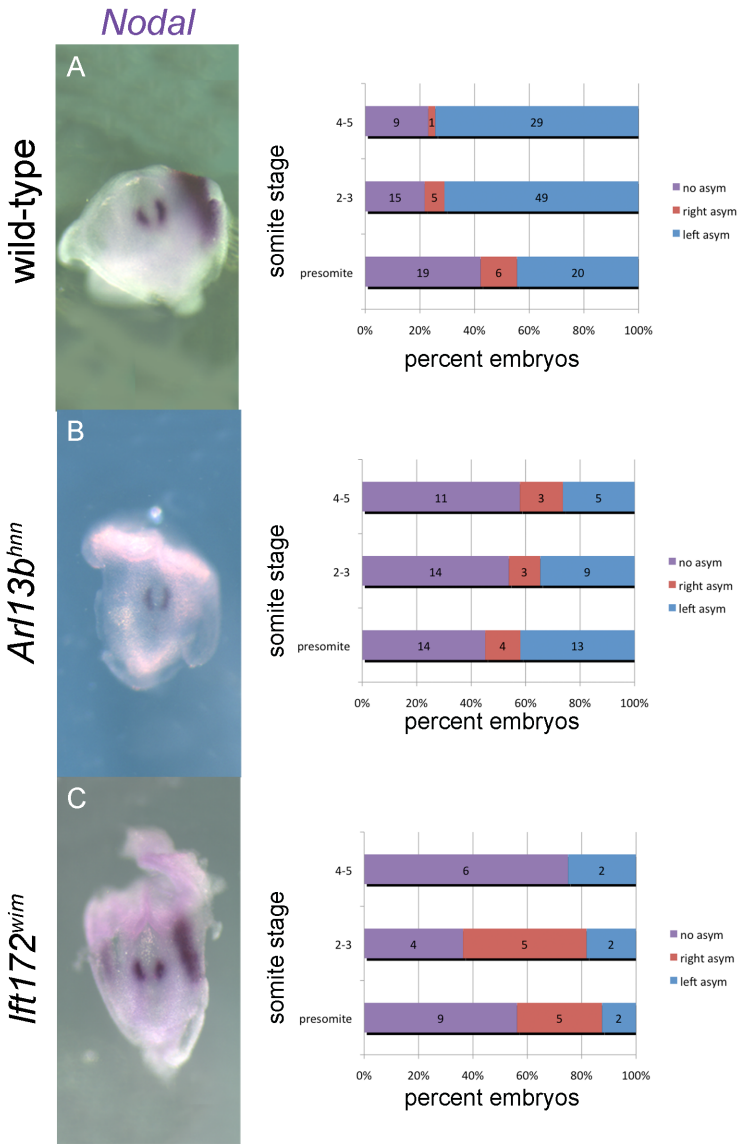

Figure 3.6. *Arl13b*^{hnn} embryos show *Nodal* enrichment defects in the node. A) 2-3 somite wild type embryo showing left-sided enrichment of *Nodal*. The graph shows percent of embryos with *Nodal* enrichment broken down by somite stage. B) 2-3 somite stage *Arl13b*^{hnn} mutant embryo without *Nodal* enrichment in the node. The graph shows *Nodal* is initially enriched at presomite stages. C) 2-3 somite stage *IFT172*^{wim} embryo showing right-sided enrichment of *Nodal*. Graph shows enrichment *IFT172*^{wim} mutant embryos.

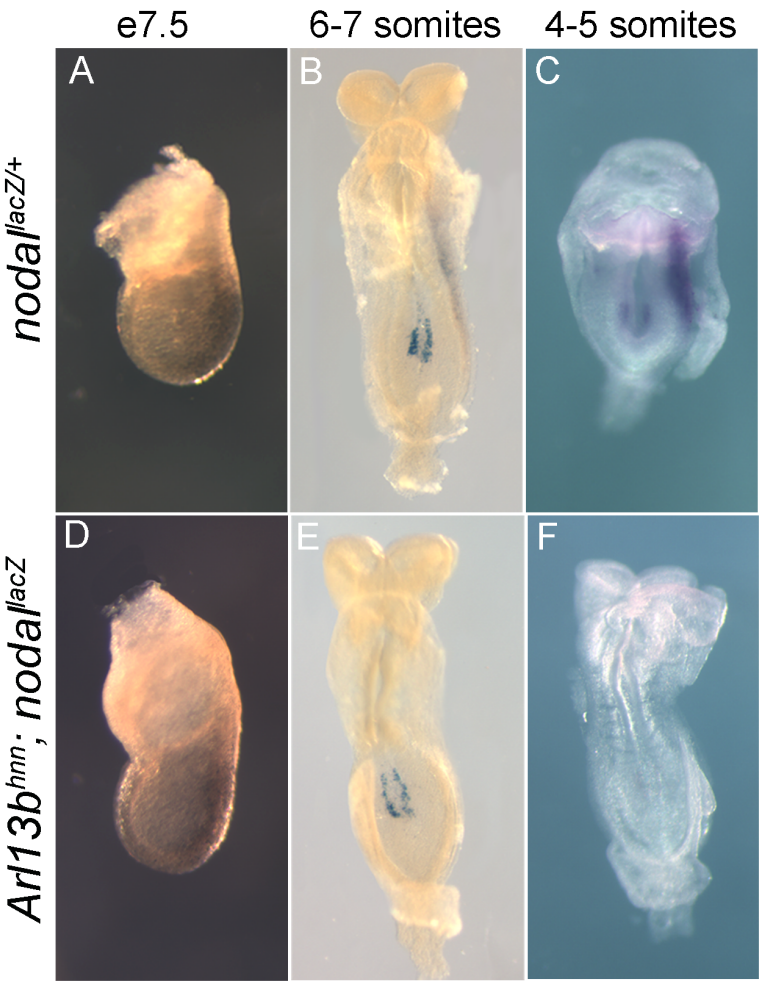
e7.5
6-7 somites
4-5 somites
A
B
C
D
E
F
nodal^lacZ/+
Arl13b^hnn; nodal^lacZ

Figure 3.7. There is a genetic interaction between *Arl13b* and *Nodal*. A-B) e7.5 whole mount β-galactosidase assay in wild-type (A) and *Arl13b*^{hnn} mutant (B) embryos with the *nodal-lacZ* allele. C-D) 6-7 somite stage embryos with whole mount β-galactosidase assay showing no expression in the LPM of *Arl13b*^{hnn} mutants (C) while there is expression in the left LPM of wild type (D). E-F) Whole mount *in situ* hybridization confirms the lack of *Nodal* expression in *Arl13b*^{hnn} mutant embryos with the *nodal-lacZ* allele (F) while expression is intact in wild type embryos (E).

CHAPTER 4

ARL13B REGULATES CILIOGENESIS AND THE DYNAMIC LOCALIZATION OF SHH SIGNALING PROTEINS

4.1 Summary

Arl13b is a cilia protein within the Arf family and Ras superfamily of GTPases that is required for cilia structure, but has poorly defined functions there. Previously, we showed that mice lacking Arl13b have short cilia and abnormal Sonic hedgehog (Shh) signaling. Components of the Shh signaling pathway localize dynamically to cilia in response to the Shh ligand and here we show these dynamics are disrupted in the absence of Arl13b. Significantly, we found Smo is enriched in Arl13b null cilia regardless of Shh pathway stimulation indicating Arl13b regulates the ciliary entry of Smo. Furthermore, our analysis defines a role for Arl13b in localizing Smo within the cilium. This could be linked to the role of Arl13b in ciliogenesis, since Arl13b controls cilia length and may be in a complex with the intraflagellar transport protein IFT88 and the exocyst complex protein Sec8.

4.2 Introduction

The regulation of protein delivery and movement within primary cilia is key to our understanding of how cilia are built and how their length is controlled, as well as how cell signaling pathways are regulated (Rosenbaum and Witman, 2002; Veland et al., 2009). All three of these processes are disrupted in the absence of Arl13b, a small GTPase that localizes to cilia. *Arl13b*$^{hennin\ (hnn)}$ mutant mouse embryos have cilia that are half the length of wild-type cilia and a specific defect in the axoneme, where the B-tubule of the outer doublet microtubules is not connected to the A-tubule (Caspary et al., 2007). In addition, these mutant embryos show a low level of expanded Shh activation in the neural tube (Caspary et al., 2007). In mammals, Arl13b is one of about 30 ADP-

ribosylation factor (ARF) proteins, best known for regulatory roles in membrane traffic (D'Souza-Schorey and Chavrier, 2006). Therefore, defining the molecular actions of Arl13b in cilia or ciliogenesis is predicted to shed light on the links between cilia formation and signaling, with possible links to membrane traffic.

Almost all components of the Shh signaling pathway are localized to the cilium, and their localization shifts in response to the Shh ligand (Corbit et al., 2005; Haycraft et al., 2005; Rohatgi et al., 2007; Chen et al., 2009; Wen et al., 2010). In the absence of ligand, the Gli transcription factors, Gli2 and Gli3, are localized to the tips of cilia and are processed to form a transcriptional repressor (GliR) (Haycraft et al., 2005; Huangfu and Anderson, 2005; Liu et al., 2005). This processing involves the phosphorylation and cleavage of the full-length Glis, with the N-terminal domain acting as the repressor and the C-terminal domain being degraded (Wang et al., 2000). The receptor for the Shh ligand, Patched (Ptch1), is also found in the cilia membrane, and in the absence of ligand represses pathway activation by inhibiting the downstream activator, Smoothened (Smo) (Rohatgi et al., 2007). When Shh ligand is present, Shh binds Ptch1, causing it to move out of the cilium, and this allows Smo to enter the cilium (Rohatgi et al., 2007). Smo localization to the cilium inhibits GliR formation and, via an unknown mechanism, the full-length Glis become Gli activators (GliAs)(McMahon et al., 2003). Suppressor of Fused (Sufu) is also localized to the tips of cilia, although recently Sufu was found to inhibit Shh signaling independently of the cilium by binding and sequestering the Glis in the cytoplasm (Chen et al., 2009; Jia et al., 2009; Humke et al., 2010).

Precisely how Shh signaling proteins are targeted and moved in and out of the cilium is not clear, but intraflagellar transport (IFT) is required (Huangfu et al., 2003;

Haycraft et al., 2005; Liu et al., 2005). IFT is the bidirectional movement of ciliary protein complexes, which is required to build and maintain the cilium (Kozminski et al., 1993; Rosenbaum and Witman, 2002; Pedersen et al., 2008). Anterograde IFT carries cargo toward the tip of the cilium, while retrograde transport carries turnover products out of the cilium; deletion of anterograde or retrograde IFT proteins results in distinct ciliary phenotypes, but in either case, both GliA and GliR are affected, resulting in disrupted Shh activity (Huangfu et al., 2003; Huangfu and Anderson, 2005; Liu et al., 2005; Houde et al., 2006) (May et al., 2005; Ocbina and Anderson, 2008; Tran et al., 2008; Cortellino et al., 2009).

Surprisingly, disruption of cilia structure does not always affect Shh signaling, as shown by Rfx3 mouse mutants, which have short cilia and normal Shh activity (Bonnafe et al., 2004). This underscores the ill-defined nature of the mechanisms by which a growing list of cilia/basal body protein mutants affect Shh signaling (Ferrante et al., 2006; Vierkotten et al., 2007; Norman et al., 2009; Patterson et al., 2009; Boehlke et al., 2010). *Arl13b*^{hnn} mutants are unusual, because in them the production or function of GliA only, and not GliR, is affected. In this study, we looked at these mutants to see what could link all these threads: a small regulatory GTPase, a specific anomaly in the ciliary ultrastructure, and the unique defect in Gli function. We show that Arl13b is instrumental to the localization of Shh signaling components and may be complexed with a component of the exocyst and IFT88, an interaction that could be critical to its regulation of ciliogenesis through trafficking of ciliary proteins.

4.3 Results

Defects in post-translational modifications of ciliary tubulin are consistent with defects in the architecture of* Arl13b^{hnn} *cilia

Arl13b^{hnn} is a null allele and the cilia in the mutant mouse embryos display an ultrastructural defect whereby the B-tubule of the microtubule-based outer doublets does not connect to the A-tubule (Caspary et al., 2007). Zebrafish and tetrahymena mutants with defects in tubulin glutamylation display a similar phenotype (Redeker et al., 2005; Pathak et al., 2007; Dave et al., 2009). To examine such post-translational modifications in the axoneme of *Arl13b*^{hnn} cilia, we derived primary mouse embryonic fibroblasts (MEFs) from e12.5 *Arl13b*^{hnn} and wild-type embryos. Using immunofluorescence, we examined tubulin glutamylation and measured the average fluorescence intensity in the entire cilium relative to cell body staining. We saw a significant reduction in staining in the *Arl13b*^{hnn} axoneme compared with wild-type (Figure 4.1, A-C). We then extended these analyses to another tubulin post-translational modification, acetylation. Although the functional significance of tubulin acetylation is less clear, the cilia axoneme is highly acetylated and could be a mark of stable microtubules (Perdiz et al., 2010). We found tubulin acetylation is also reduced to similar levels as glutamylation in *Arl13b*^{hnn} MEFs (Figure 4.1, A-C), indicating a more general defect in tubulin post-translational modifications in our mutants.

Arl13b regulates cilia length

To further investigate the role of Arl13b in ciliogenesis, we examined cilia in cultured wild-type and *Arl13b*^{hnn} MEFs. About 70% of wild-type MEFs were ciliated, whereas just under 20% of *Arl13b*^{hnn} MEFs had cilia (Figure 4.2, A). In contrast, all cells

of the *Arl13b*^{hnn} embryonic node are ciliated (Caspary et al., 2007). However, reminiscent of what we found in vivo, the *Arl13b*^{hnn} MEF cilia were shorter than wild-type cilia, suggesting that Arl13b controls ciliary length both in the embryo and in culture (Figure 4.2, C, D, M).

To unravel how Arl13b might regulate cilia length, we examined cilia in MEFs overexpressing untagged Arl13b or Arl13b-GFP. We found wild-type MEFs overexpressing untagged Arl13b or Arl13b-GFP had much longer cilia than untransfected cells, and both constructs rescued the cilia length defect in *Arl13b*^{hnn} MEFs (Figure 4.2, B, E-H, M). The rescued cilia were longer than wild-type, consistent with Arl13b protein levels being important. The cilia in wild-type or *Arl13b*^{hnn} MEFs overexpressing Arl13b-GFP were shorter than those expressing untagged Arl13b, indicating the C-terminal GFP tag impaired Arl13b's function consistent with previous observations with tagged versions of other Arf GTPases (Jian et al., 2010). In the few cases when Arl13b-GFP was restricted from the cilium and instead was evident throughout the cell body and nucleus, there was no change in ciliary length, suggesting Arl13b may need to be in the cilium to regulate ciliary length (Figure 4.2, M).

Of the 30 mammalian Arf family proteins, most are ~20-kD proteins consisting of the Arf domain only (D'Souza-Schorey and Chavrier, 2006). Arl13b is unusual in that it has an additional 24-kD novel C-terminus, much of which its non-vertebrate orthologues lack. We examined the localization and function of the Arf domain as well as the novel C-terminal domain by tagging each with GFP and expressing each in wild-type and *Arl13b*^{hnn} MEFs. Neither half of Arl13b could localize to cilia, as the full-length version did; we found the tagged Arf domain in diffuse puncta within the cell body and the

tagged C-terminal domain in the nucleus (Figure 4.2, I-L). Furthermore, neither half of Arl13b had any affect on cilia length in wild-type or *Arl13b*^{hnn} MEFs, consistent with our finding that full-length Arl13b-GFP regulated cilia length only when it was in cilia (Figure 4.2, M). Thus, only full-length Arl13b localizes to cilia to regulate cilia length.

Arl13b localizes to the cilia membrane

We previously demonstrated that Arl13b is expressed in cilia and does not overlap with the basal body in fibroblasts (Caspary et al., 2007). To define where in the cilium Arl13b localizes, we took advantage of the long cilia in the mouse kidney cell line IMCD3 and used immunofluorescence. As in the fibroblasts, Arl13b was visible along the entire length of the cilium but was not at the basal body (Figure 4.3, A, C). To determine whether Arl13b within the cilium associates with the membrane or the axoneme, we treated cells with the detergent TritonX-100 prior to fixation. We saw a loss of Arl13b staining in TritonX-100-treated cells, but acetylated α-tubulin staining remained intact, suggesting the majority of Arl13b is not associated with the axoneme (Figure 4.3, A-D). We also saw that the known cilia membrane protein SSTR3 fused with GFP (SSTR3-GFP) was lost upon pretreatment with detergent, consistent with Arl13b also being membrane associated (Figure 4.3, E, F). Curiously, we saw that Arl13b staining remained at the base and tip of the cilium after detergent treatment prior to fixation, which we did not observe with SSTR3-GFP, raising the possibility that some Arl13b is anchored to the axoneme or other machinery found at the base and tip of the cilium.

We next used fluorescence recovery after photobleaching (FRAP) to determine the dynamics of Arl13b movement within the cilium of IMCD3 cells. To do this, we generated a lentivirus capable of driving expression of Arl13b-GFP, and infected IMCD3 cells. When we photobleached the central region of the cilium, we saw rapid recovery of Arl13b-GFP fluorescence in the bleached region (Figure 4.4, A, C). We performed the parallel analysis with SSTR3-GFP (Figure 4.4, B, C) and found the same rates of recovery for Arl13b-GFP and SSTR3-GFP (Figure 4.4, C). To determine Arl13b turnover within the cilium, we photobleached Arl13b-GFP as well as SSTR3-GFP in the entire cilium and saw very little recovery of either protein over the course of the experiment, which we followed for 2 minutes 23 seconds (Figure 4.4, D, E, G). In contrast, in a parallel analysis photobleaching IFT88-EYFP expressing cells, we saw a faster rate of recovery (Figure 4.4, F, G), consistent with previous data showing IFT recovery in the cilium is faster than the recovery of cilia membrane proteins (Hu et al., 2010). Taken together, these data are consistent with Arl13b associating with the membrane of the cilium.

Arl13b is in a complex with IFT88 and Sec8

Our data suggest that Arl13b plays a role in the control of cilia length and that Arl13b may be acting at the cilia membrane. To investigate the underlying mechanism of Arl13b regulating cilia structure, we examined the quaternary structure of Arl13b and its associated proteins in detergent (1% cholate) extracts from wild-type and *Arl13b*^{hnn} MEFs using gel filtration chromatography. In wild-type MEFs, Arl13b peaked in fractions 8-12. Because IFT is important for cilia length regulation, and exocyst complex mutants have

similar cilia phenotypes as our mutants (Rosenbaum and Witman, 2002; Zuo et al., 2009), we examined fractions for IFT88 and the exocyst protein Sec8 to determine whether they interact with Arl13b. We found that IFT88 peaked in fractions 8-10, suggesting the possibility of a cocomplex with Arl13b. In contrast, Sec8 displayed peak fractions at a larger apparent molecular mass, which tailed into and through those fractions containing Arl13b and IFT88 (Figure 4.5, A). These data are consistent with Arl13b interacting with IFT88 and potentially the exocyst protein Sec8.

To test the model that Arl13b may be important to the overall stability of a complex containing Sec8 and/or IFT88, we repeated the gel filtration profile of the same proteins in detergent extracts from *Arl13b*^{hnn} MEFs. Interestingly, IFT88 and Sec8 each eluted in later fractions than those from wild-type extracts, corresponding to proteins with a smaller apparent molecular mass (Figure 4.5, B). Surprisingly, even the Sec8-containing fractions that did not cofractionate with Arl13b in wild-type MEFs shifted in the *Arl13b*^{hnn} MEFs, and IFT88 and Sec8 displayed more extensive coelution profiles than in the extracts from wild-type cells (Figure 4.5, B). Thus, the loss of Arl13b in *Arl13b*^{hnn} MEFs may result in the instability of complexes that contain IFT88 and/or Sec8.

To further test the model that Arl13b, IFT88, and Sec8 exist in a common protein complex, we performed immunoprecipitations. When we immunoprecipitated with Sec8 antibody in wild-type whole cells lysates and immunoblotted for IFT88 and Arl13b, we found both proteins co-precipitated (Figure 4.5, C). This was also true when we immunoprecipitated with Sec8 antibody and immunoblotted for IFT88 and Arl13b in fractionated wild-type extracts from the early, middle, and late fractions that contain all

three proteins (fractions 8, 10, and 12, respectively; Figure 4.5, A). When we performed the same immunoprecipitation on fractions obtained from *Arl13b*^{hnn} MEFs we found that Sec8 was still able to specifically precipitate IFT88, but we detected no Arl13b reflecting the fact that these were Arl13b null cells. Thus, data from immunoprecipitations are consistent with the model that IFT88 and Sec8 are present in a complex that can include Arl13b.

The identification of a protein complex that contains Arl13b, Sec8, and IFT88 was provocative, as IFT is the major transport machinery that builds cilia. To further investigate the relationship between IFT and Arl13b, we tested whether Arl13b regulates IFT in mammalian cells. We took advantage of an IMCD3 cell line that stably expressed IFT88-EYFP, enabling us to perform FRAP and measure the rate of IFT88-EYFP recovery. To deplete the cells of Arl13b, we used a lentivirus coexpressing Arl13b shRNA and RFP, enabling us to specifically identify knockdown cells. We proved the knockdown was efficient by Western blot, as we detected only 30% of the wild-type Arl13b levels in cells treated with the knockdown virus (Figure 4.6, A). Arl13b was not detected by immunofluorescence in 50% of RFP-positive cells, and the phenotype was similar to what we found in the Arl13b null MEFs: 50% fewer cilia, and those that were present were shortened (Figure 4.6, B, C, E). When we measured the rate of recovery of IFT88-EYFP at the ciliary tip, we saw no significant change between IMCD3 wild-type and Arl13b knockdown cells (Figure 4.6, H). Because the knockdown is sufficient to reflect the established Arl13b cilia phenotype, the simplest interpretation is that Arl13b does not regulate the rate IFT. Nevertheless, we cannot rule out such a function, since some Arl13b remains after knockdown.

Dynamic localization of Shh signaling proteins is disrupted in Arl13b^{hnn} MEFs

Arl13b functions in the cilium to regulate Shh signaling, because like *IFT172^{wim}* single mutant embryos that lack cilia completely, Arl13b mutants that also lack cilia (*Arl13b^{hnn} IFT172^{wim}* double mutant embryos) display no Shh response. However, in contrast to most cilia mutants in mouse, *Arl13b^{hnn}* single mutant embryos have a low level of ligand-independent Shh pathway activation in the neural tube, due to a specific disruption in GliA activity (Caspary et al., 2007). Since the goal of Shh signaling is to control the balance of GliA and GliR and this balance requires cilia, we investigated the localization of Shh components in the cilia of *Arl13b^{hnn}* mutant MEFs with and without Shh stimulation.

To monitor Shh activity in wild-type and *Arl13b^{hnn}* MEFs, we cotransfected a Firefly luciferase reporter construct with 8 Gli binding sites in its promoter (8xGli luciferase assay) with a Renilla luciferase expression construct to control for transfection efficiency (Sasaki et al., 1997). The levels of normalized luciferase activity in untreated wild-type and *Arl13b^{hnn}* MEFs were similar. Wild-type MEFs showed almost a 7-fold increase in normalized luciferase activity when treated with Shh-conditioned media, whereas *Arl13b^{hnn}* MEFs displayed only a 2-fold increase, indicating that *Arl13b^{hnn}* cells have a lowered response to the Shh ligand (Figure 4.7, A). This is similar to what we observed in vivo, where the pathways could not be activated to the highest levels in the absence of Arl13b.

To examine the dynamics of Shh components within cilia, we used antibodies against the endogenous proteins. Normally, Gli2 and Gli3 localize to the ciliary tip and

are further enriched there after Shh stimulation (Chen et al., 2009; Wen et al., 2010). Indeed, using antibodies that recognize full-length Gli2 (Gli2), full-length Gli3 and cleaved Gli3R (Gli3N), or only full-length Gli3 (Gli3C) to measure ciliary tip fluorescence intensity relative to cell body staining (Wen et al., 2010), we found full-length Gli2 and Gli3 were enriched in wild-type MEFs after treatment with Shh-conditioned media (Figure 4.7, B, D, F, N), but there was no significant change in Gli2 and Gli3 enrichment in *Arl13b*^{hnn} MEFs after Shh treatment (Figure 4.7, C, E, G, N). Similarly, we confirmed that Sufu, a mediator of Gli function, shows enrichment in the tips of cilia after Shh treatment in wild-type but not *Arl13b*^{hnn} MEFs (Figure 4.7 H, I, N).

Smo and Ptch1 localize along the length of the cilium in a complementary manner: Ptch1 in the absence of ligand and Smo upon pathway stimulation (Corbit et al., 2005; Rohatgi et al., 2007). As expected, we saw Ptch1 ciliary levels decrease and Smo ciliary levels increase after Shh stimulation in wild-type MEFs (Figure 4.7, J-N). We investigated how these dynamics changed in the absence of Arl13b and found Ptch1 staining did not significantly change in response to Shh stimulation in *Arl13b*^{hnn} MEFs (Figure 4.7, L-N). Consistent with our previous genetic data demonstrating constitutive Shh activity in the absence of Arl13b, we found Smo in *Arl13b*^{hnn} MEFS without Shh stimulation (Figure 4.7, J, K, N). This indicates that Arl13b plays a critical role in regulating the entry of Smo into cilia and that all the machinery necessary for the trafficking of Smo into cilia is intact in the absence of Arl13b. Upon Shh stimulation in *Arl13b*^{hnn} MEFS, we found Smo was further enriched. However, regardless of whether or not the cells were stimulated, we found Smo was not evenly distributed in cilia lacking Arl13b, in contrast to even Smo staining along the whole cilium in wild-type MEFs,

arguing that Arl13b regulates proper localization or targeting of Smo within the cilium (Figure 4.7, J, K). Smo staining was most often concentrated at the ciliary tip although we also found it concentrated at other positions along the cilium. In sum, these results demonstrate a fundamental defect in the trafficking of Shh signaling proteins in *Arl13b*^{hnn} MEFs.

4.4 Discussion

Our data show that Arl13b is essential for regulating Smo, the key activator of Shh signaling, into the cilium and for its proper targeting or localization once in the cilium. Additionally, our data show Arl13b plays an important role in ciliogenesis and the localization of ciliary proteins, potentially through regulation of a protein complex containing IFT88 and the exocyst component, Sec8. The fact that Arl13b is a GTPase within the Arf family is strongly suggestive of it playing a regulatory role in organelle biogenesis and function. Cell lines with disrupted Arl13b expression have reduced numbers of cilia, and those that are present are shorter. We identified two proteins that may exist in a complex with Arl13b: IFT88 and Sec8, which are each important for protein trafficking and ciliogenesis. The abnormal tubulin modifications we found in mutant cilia are consistent with the structural defect in the axoneme that may contribute to the short cilia. Additionally, we found the dynamics of Shh components were disrupted. Taken together, these data suggest that Arl13b regulates protein movement to or from cilia.

The Role of Arl13b in Ciliogenesis

We found that Arl13b is in a protein complex that may also contain Sec8 and IFT88. The exocyst is a hetero-octomeric complex best known for its function in targeting exocytic vesicles to the plasma membrane; it has recently been associated with ciliogenesis. Three of the exocyst proteins, Sec6, Sec8, and Sec10, have been localized to the cilium or to the base of the cilium (Rogers et al., 2004; Zuo et al., 2009; Babbey et al., 2010), and a recent study showed that the exocyst protein Sec10 has ciliogenesis defects similar to those we found for Arl13b: namely, overexpression of Sec10 resulted in longer cilia length, whereas knockdown caused reduced and shortened cilia (Zuo et al., 2009). Zou et al. found that IFT88 protein levels are reduced in Sec10 knockdown cells, an indication that IFT88 may complex with exocyst components. We showed the IFT88-Sec8 interaction occurs regardless of the presence of Arl13b, consistent with the formation of cilia, albeit short ones, in the absence of Arl13b.

Since the exocyst complex is regulated at the plasma membrane by interactions with GTPases (Wu et al., 2008; He and Guo, 2009), one possibility is that Arl13b targets the exocyst complex as well as associated proteins to cilia. This would be similar to the role of Arl6, which recruits coat complexes to the cilium (Jin et al., 2010). A similar function was proposed for Rab10, which localizes to the base of nascent cilia, as well as to the cilium itself (Babbey et al., 2010). Rab10 and Rab8 are mammalian homologues of yeast Sec4p, which is known to interact with exocyst components (Guo et al., 1999). Rab10 interacts with the exocyst complex in mammalian cells, and Rab8 regulates cilia length, consistent with the phenotypes in Sec10 and Arl13b mutant cells (Nachury et al., 2007; Babbey et al., 2010). Arl13b may coordinate with Rab8 and Rab10 to regulate the exocyst complex at the cilium. The question then becomes whether the interaction with

IFT88 is integral to the interaction of exocyst components or reflects a subsequent role of Arl13b within the cilium. Untangling these possibilities will require us to uncover other proteins that Arl13b interacts with and to characterize dynamic movement of the Arl13b-exocyst-IFT complex.

Our finding that Arl13b associates with the ciliary membrane with the same dynamics as the known cilia membrane protein SSTR3 is consistent with Arl13b associating with cell membranes through N-terminal palmitoyl anchors in 293T cells (Cevik et al., 2010). Furthermore, these dynamics fit with recent evidence that cilia membrane proteins have little turnover within the cilium (Hu et al., 2010). In light of our discovery that Arl13b cofractionates with IFT88, it is interesting that IFT proteins are tightly associated with the cilia membrane while being transported along the axoneme and that the Arl13b *Caenorhabditis elegans* orthologue ARL13 stabilizes IFT (Pigino et al., 2009; Cevik et al., 2010). We did not see a defect in IFT recovery using our FRAP method to examine IFT dynamics in *Arl13b* knockdown cells. It remains unclear whether this discrepancy is due to the remaining Arl13b protein in the knockdown or to subtle changes in IFT that may exist in our mutants being undetectable by this method, or due to the distinct biology of mammalian Arl13b, since *C. elegans* ARL13 lacks about a third of the novel C-terminal domain.

The ~24 kD C-terminal domain of Arl13b is critical to its function. The domain is vertebrate-specific, required for Arl13b to localize to cilia, and we found that tagging it with GFP reduces the ability of Arl13b to regulate cilia length. The fact that it localizes to the nucleus when GFP tagged is interesting given that it contains a basic sequence that may act as a nuclear localization signal. Recent data demonstrated a similar sequence in

the C-terminus of Kif17 mediates cilia localization and that a truncated Kif17 lacking its N-terminus also localizes to the nucleus (Dishinger et al., 2010). Interestingly, Importin-β has been localized to cilia and is required for cilia entry of some proteins (Fan et al., 2007; Dishinger et al., 2010), raising the possibility that Arl13b localizes to cilia through an Importin-β interaction domain in its C-terminus. As the N-terminus of Arl13b contains palmitoylation sites (Cevik et al., 2010), interactions with vesicles or periciliary membrane may be required for cilia versus nuclear localization.

While the reduction of both acetylation and glutamylation in *Arl13b*^{hnn} cilia is consistent with the architectural defect of the axoneme, we cannot say whether the modification defects we see are the result or the cause of a defect in protein trafficking to cilia. Interestingly, in *C. elegans,* the Arl13 mutant phenotype is rescued by loss of Arl3 function, and loss of Arl3 increases tubulin acetylation in HeLa cells (Zhou et al., 2006), indicating these two proteins may have inverse functions in regulation tubulin modifications. Additionally, IFT is needed to traffic proteins responsible for tubulin modification to cilia (Fan et al., 2010), so a defect in IFT could also result in reduced tubulin modifications. Determining other interactors of Arl13b will be important for teasing apart these possibilities.

The Role of Arl13b in Shh Signaling

The *Arl13b*^{hnn} mutant embryos display constitutive, low-level Shh activity regardless of the presence of Shh ligand (Caspary et al., 2007). However, using a luciferase assay in *Arl13b*^{hnn} MEFs, we saw pathway activation only when the cells were stimulated. This is likely explained by the 50% reduction of cilia in *Arl13b*^{hnn} MEFs

compared with wild-type, since we know that pathway activation in the absence of Arl13b depends on the presence of cilia. Therefore, to determine how Arl13b could be regulating Shh signaling in the embryo, we focused on ciliated *Arl13b*^{hnn} MEFs to examine localization of Shh signaling components.

Consistent with the constitutive Shh activity we previously found in *Arl13b*^{hnn} embryos, we found Gli2 and Gli3 were not enriched at the ciliary tip when we stimulated *Arl13b*^{hnn} MEFs with Shh conditioned media. Additionally, we found Smo in the cilia in the absence of Shh stimulation mimicking the ligand independent activation of Shh signaling we saw in the *Arl13b*^{hnn} neural tube. Despite Ptch1, Gli2 and Gli3 not shifting their localization in response to Shh stimulation in the *Arl13b*^{hnn} MEFs, there was not a complete block of Shh components moving in and out of cilia since Smo localized to cilia and was further enriched upon Shh stimulation. However, it is unlikely this additional Smo activates the pathway since the Gli proteins do not respond. These results suggest that the relative levels of Shh signaling proteins in cilia are important for activation and repression of the pathway, and studies of other cilia mutants support this model. For example, the Rab23 mutant mouse has excess activation of the Shh signaling pathway in the neural tube (Eggenschwiler et al., 2001), and Rab23 mutant cells were recently shown to have increased trafficking of Smo into the cilium (Boehlke et al., 2010). However, our analysis of Arl13b argues that Smo simply being present in cilia is not sufficient for the range of Shh response. The punta of Smo we see in the absence of Arl13b will likely provide the fundamental explanation for the inability of *Arl13b*^{hnn} embryos to reach high levels of Shh activation by defining the role of Arl13b in Smo localization within the cilium. Future studies are left to examine the mechanism of Shh signaling component

interaction in the cilium to better explain how relative levels of Shh signaling proteins in cilia regulate the pathway.

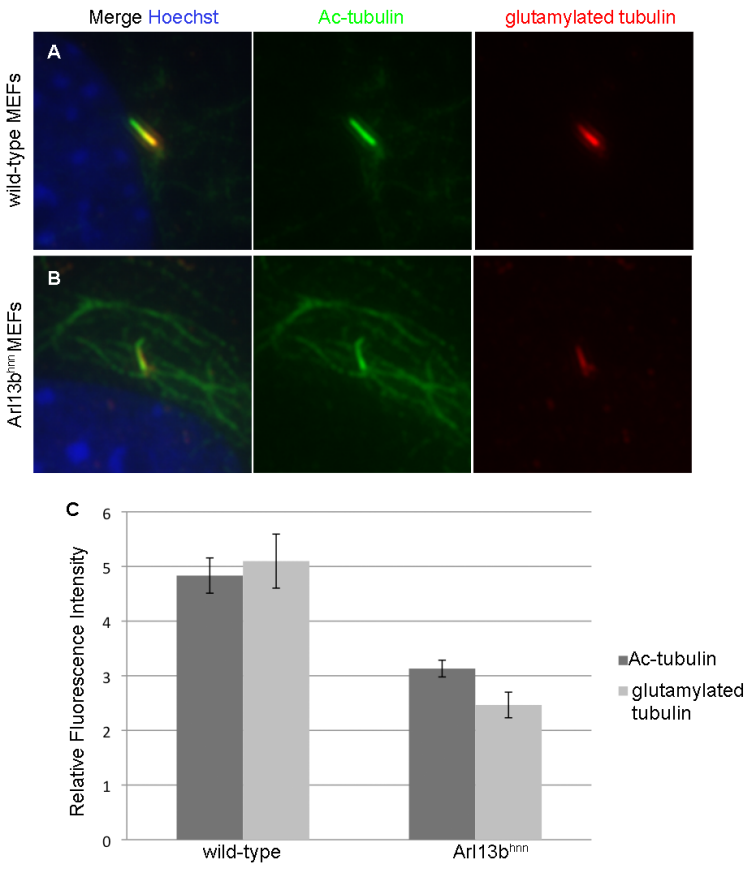

Figure 4.1. Tubulin modification defects exist in *Arl13b*^{hnn} mutant MEFs. A-B) Immunofluorescence for acetylated α-tubulin (Ac-tubulin, green) and glutamylated tubulin (red) in wild-type (A) and *Arl13b*^{hnn} (B) MEFs shows reduced staining in *Arl13b*^{hnn} MEFs. C) Quantification of Ac-tubulin and glutamylated tubulin fluorescence intensity relative to background. Error bars are ± the SEM. $p < 0.0001$ for both Ac-tubulin and glutamylated tubulin using student's t-test.

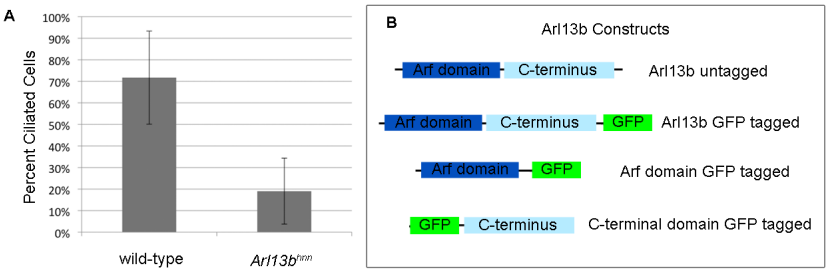
A
Percent Ciliated Cells
100%
90%
80%
70%
60%
50%
40%
30%
20%
10%
0%
wild-type
Arl13b hnn
B
Arl13b Constructs
Arf domain
C-terminus
Arl13b untagged
Arf domain
C-terminus
GFP
Arl13b GFP tagged
Arf domain
GFP
Arf domain GFP tagged
GFP
C-terminus
C-terminal domain GFP tagged

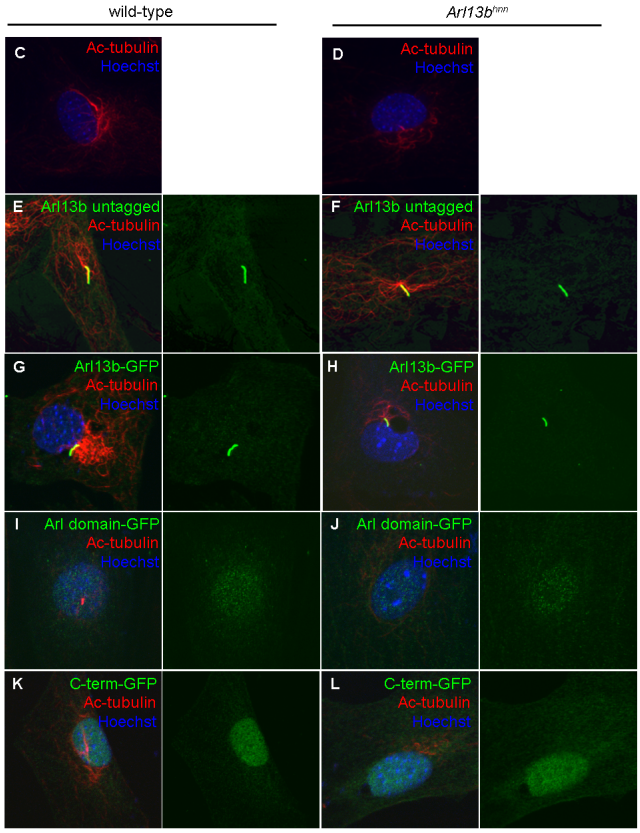
wild-type
Arl13b hnn
C Ac-tubulin Hoechst
D Ac-tubulin Hoechst
E Arl13b untagged Ac-tubulin Hoechst
F Arl13b untagged Ac-tubulin Hoechst
G Arl13b-GFP Ac-tubulin Hoechst
H Arl13b-GFP Ac-tubulin Hoechst
I Arl domain-GFP Ac-tubulin Hoechst
J Arl domain-GFP Ac-tubulin Hoechst
K C-term-GFP Ac-tubulin Hoechst
L C-term-GFP Ac-tubulin Hoechst

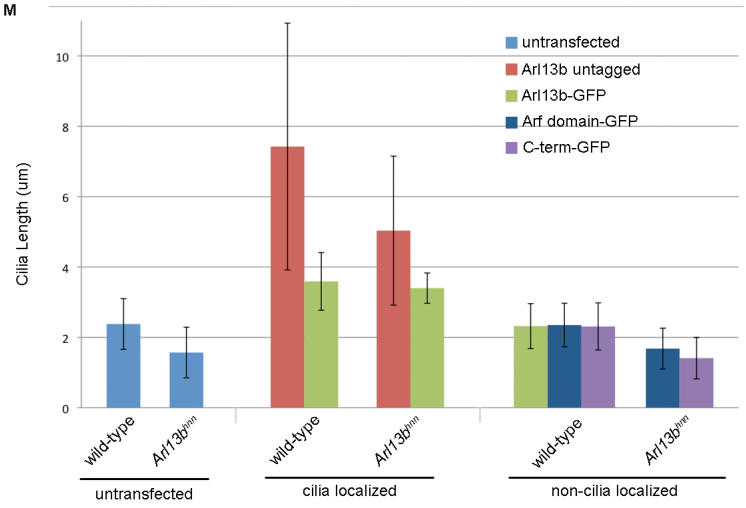
M
Cilia Length (um)
10
8
6
4
2
0
untransfected
Arl13b untagged
Arl13b-GFP
Arf domain-GFP
C-term-GFP
wild-type
Arl13b hnn
wild-type
Arl13b hnn
wild-type
Arl13b hnn
untransfected
cilia localized
non-cilia localized

Figure 4.2. Arl13b regulates cilia length. A) Quantification of the percent of ciliated cells in wild-type and *Arl13b*^{hnn} MEFs ($p<0.0001$). B) Schematic of the Arl13b constructs that were transfected into MEFs. C-D) Immunofluorescence for acetylated α-tubulin in wild-type and *Arl13b*^{hnn} MEFs shows shortened cilia in *Arl13b*^{hnn} MEFs. E-L) Immunofluorescence for GFP and acetylated α-tubulin in wild-type and *Arl13b*^{hnn} MEFs expressing GFP-tagged Arl13b constructs. M) Quantification of cilia length in MEFs with and without transfection. The constructs are separated by those that localize to cilia and those that do not. Error bars are ± the standard deviation. Untransfected wild-type versus *Arl13b*^{hnn} MEFs $p<0.0001$. For wild-type and *Arl13b*^{hnn} MEFs versus wild-type and *Arl13b*^{hnn} MEFs expressing Arl13b-GFP or untagged Arl13b, respectively, $p<0.0001$. This figure was contributed by Gladys Gonzales-Aviles.

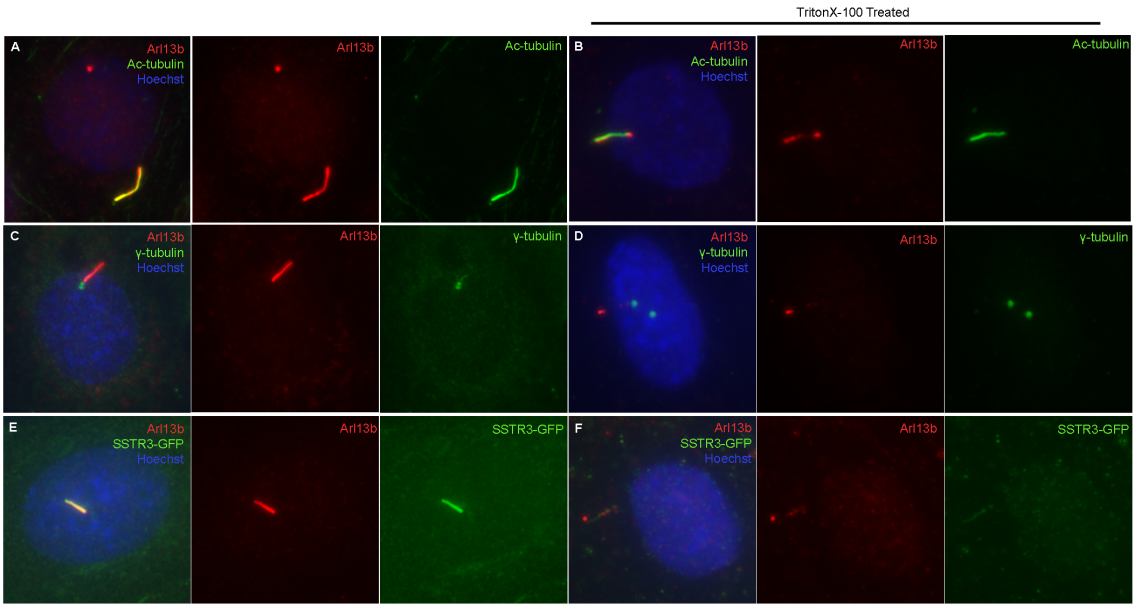

Figure 4.3. Ciliary Arl13b is TritonX-100 soluble. A, C) Immunofluorescence in IMCD3 cells shows Arl13b colocalizes with the cilia marker acetylated α-tubulin (A), and does not colocalize with the basal body marker γ-tubulin (C). B, D) Triton X-100 treatment results in the loss of a majority of Arl13b staining in the cilium, although axoneme staining with acetylated α-tubulin remains (B). E-F) The known cilia membrane protein SSTR3-GFP shows a similar loss of cilia staining with TritonX-100 treatment (F).

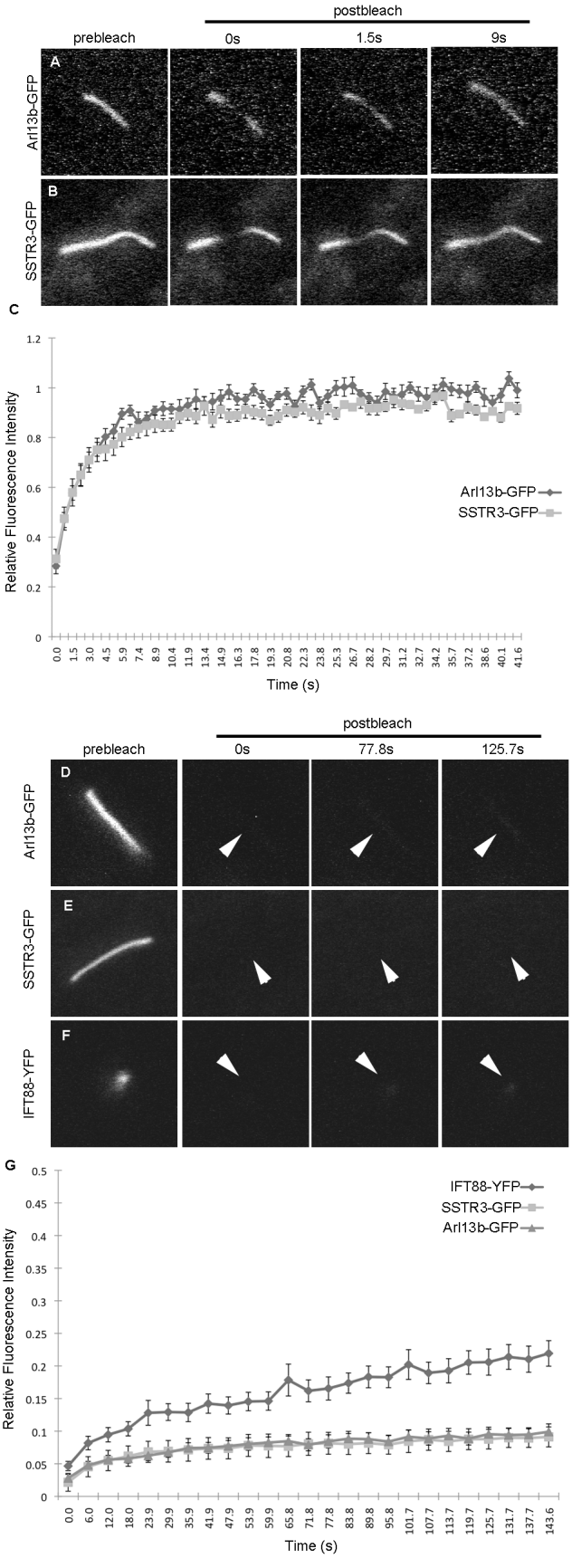
postbleach
prebleach
0s
1.5s
9s
A
Arl13b-GFP
B
SSTR3-GFP
C
Relative Fluorescence Intensity
Arl13b-GFP
SSTR3-GFP
Time (s)
postbleach
prebleach
0s
77.8s
125.7s
D
Arl13b-GFP
E
SSTR3-GFP
F
IFT88-YFP
G
Relative Fluorescence Intensity
IFT88-YFP
SSTR3-GFP
Arl13b-GFP
Time (s)

Figure 4.4. Arl13b-GFP dynamics reflect those of a cilia membrane protein. A-C) Photobleaching of a region of Arl13b-GFP (A) in the center of the cilium shows recovery dynamics within the cilium similar to SSTR3-GFP (B). This is quantified as fluorescence intensity within the bleached region relative to the whole cilium (C). J-M) Photobleaching Arl13b-GFP (D) and SSTR3-GFP (E) in the whole cilium does not result in recovery of fluorescence (G). IFT88-YFP has a faster recovery rate in the cilium (F, G). The arrowheads in D-F indicate the cilium. Error bars are ± the SEM (I, M).

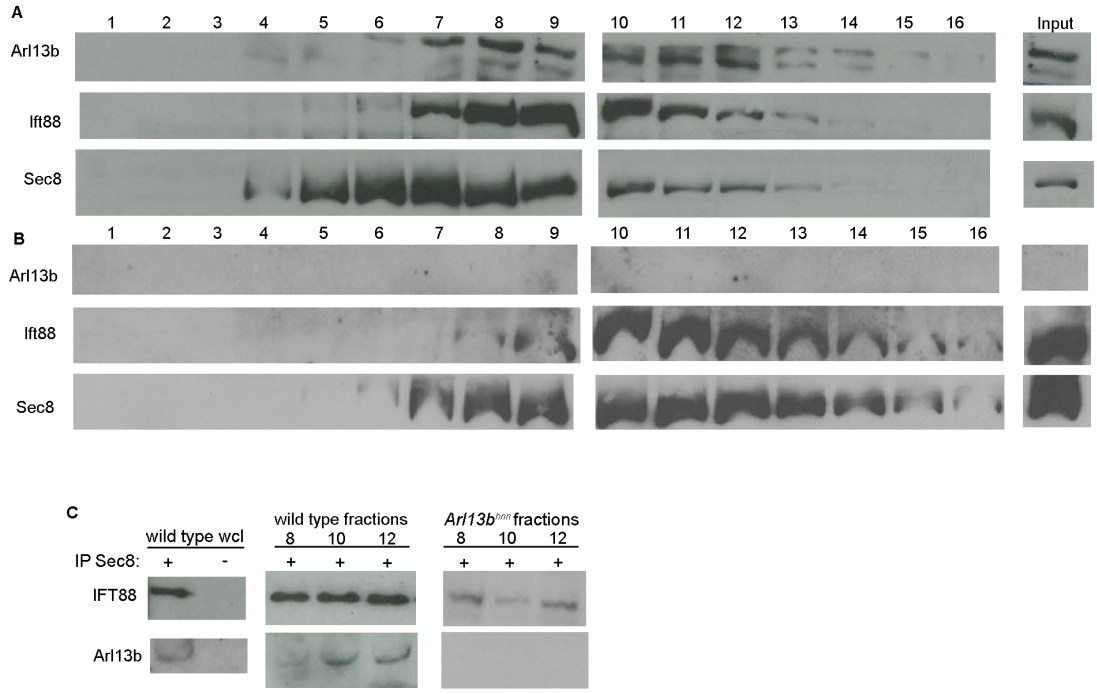

Figure 4.5. Arl13b is in a complex with IFT88 and Sec8. A) Western blot of gel filtration fractions from wild-type MEFs probed for Arl13b, Sec8, and IFT88. B) Western blot of gel filtration fractions of *Arl13b*^{hnn} MEFs probed for Arl13b, Sec8, and IFT88. C) Western blot for IFT88 and Arl13b from immunoprecipitations of Sec8 in whole cell lysates (wcl) from wild-type MEFs and from fractions 8 10 and 12 of the gel filtrations. The (-) lane was precipitated with beads only. All immunoprecipitations and their corresponding Western blots were performed simultaneously. This figure was contributed by Gladys Gonzales-Aviles.

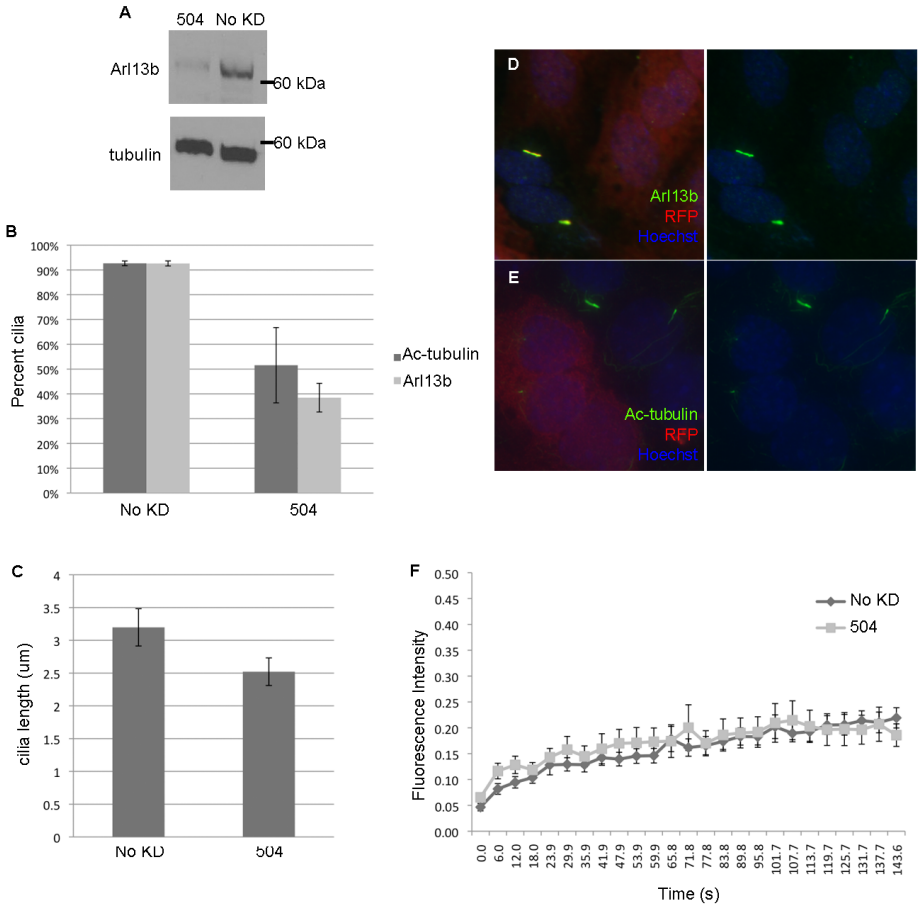

Figure 4.6. IFT88 recovery is intact in *Arl13b* mutant cells. A) Western blot showing knockdown of Arl13b in IMCD3 cells. B) Quantification of the percent of cells showing cilia stained with acetylated α-tubulin and Arl13b. C) Quantification of cilia length in knockdown cells compared to no knockdown, $p<0.03$. D,E) Immunofluorescence for Arl13b (D) and acetylated α-tubulin (E) costained with RFP in cells expressing the 504 knockdown construct. F) Recovery of IFT88-EYFP in IMCD3 cells with and without knockdown of Arl13b. Error bars are ± SEM (C, F) and ± standard deviation (B).

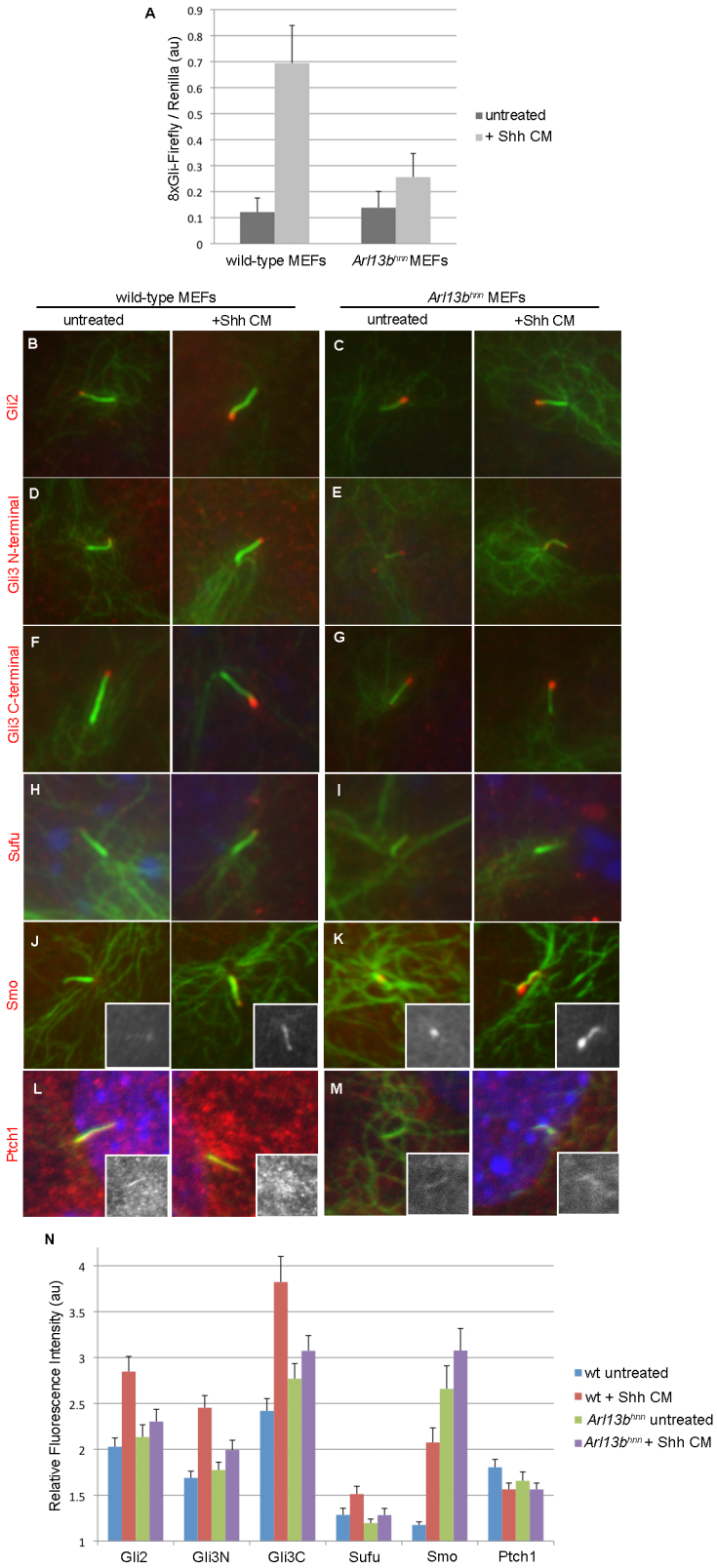
A
8xGli-Firefly / Renilla (au)
0.9
0.8
0.7
0.6
0.5
0.4
0.3
0.2
0.1
0
wild-type MEFs
Arl13b^hnn MEFs
untreated
+ Shh CM
wild-type MEFs
Arl13b^hnn MEFs
untreated
+Shh CM
untreated
+Shh CM
B
C
D
E
F
G
H
I
J
K
L
M
Gli2
Gli3 N-terminal
Gli3 C-terminal
Sufu
Smo
Ptch1
N
Relative Fluorescence Intensity (au)
4
3.5
3
2.5
2
1.5
1
Gli2
Gli3N
Gli3C
Sufu
Smo
Ptch1
wt untreated
wt + Shh CM
Arl13b^hnn untreated
Arl13b^hnn + Shh CM

Figure 4.7. Shh signaling component localization is disrupted in *Arl13b*^{hnn} MEFs. A) Quantification of Gli-luciferase activity relative to Renilla luciferase. B-M) Immunofluorescence for acetylated α-tubulin (green) and Gli2, Gli3, Sufu, Smo, and Ptch1 (red). In wild-type MEFs (B, D, F, H, J, L) Gli2, Gli3, and Sufu are enriched after Shh-conditioned media treatment, while Ptch1 levels are reduced. *Arl13b*^{hnn} MEFs (C, E, G, I, K, M) do not show significant enrichment of Gli2, Gli3, Sufu, or Smo, and Ptch1 staining is not significantly reduced after Shh-conditioned media treatment. Insets in J-M are showing Ptch1 and Smo staining alone in grayscale. N) Quantification of average fluorescence intensity in the tip of the cilium (Gli2, Gli3, and Sufu) or the entire cilium (Ptch1 and Smo) relative to cell body staining. Error Bars are ± SEM. $p<0.0001$ for wild-type MEFs with conditioned media versus wild-type MEFs untreated using the Gli and Smo antibodies, and $p<0.03$ using the Ptch1 and Sufu antibodies. $p>0.05$ for *Arl13b*^{hnn} MEFS with conditioned media versus *Arl13b*^{hnn} MEFS untreated for all antibodies.

CHAPTER 5

MODELS OF ARL13B FUNCTION

5.1 Arl13b in Nodal signaling

The results presented in chapter three, *The Cilia Protein Arl13b is Required for Efficient Nodal Signaling During Left-Right Axis Specification in Mouse,* describe the left-right axis defects in *Arl13b*^{hnn} mutant embryos, which have shortened cilia. We found that *Arl13b*^{hnn} mutants have a quite complex pattern of *Nodal* expression: it is severely delayed in the LPM, followed by expression is in the left, right, or both sides of the LPM, and at late stages of *Nodal* expression, the expression is most often bilateral. We also found that *Nodal* enrichment in the node of our mutants is not maintained. Because of the importance of cilia in establishing the LR axis, it was not surprising that these mutants have LR axis defects. However, we were surprised to see that these mutants have such a unique pattern of *Nodal* expression, one that has not been found in any other mutants with cilia defects. Other cilia mutants show spatial misexpression of *Nodal* in the LPM, however the *Arl13b*^{hnn} mutant is the first to show a severe temporal delay of *Nodal* expression. My results indicate that the delayed *Nodal* expression and defects in *Nodal* enrichment are due to a genetic interaction between *Arl13b* and *Nodal*.

Nodal is a secreted TGFβ signaling molecule that induces its own expression as well as the expression of its secreted inhibitors *Lefty1* and *Lefty2 (Yamamoto et al., 2003)*. The balance between the expression and diffusion of Nodal and the expression and diffusion of Lefty1 and Lefty2 leads to highly regulated patterning of the mouse embryo, and disruption of the levels of either Nodal or its inhibitors can be detrimental to patterning (Meno et al., 1998; Meno et al., 2001; Nakamura et al., 2006; Schier, 2009). In the node, the initial expression and enrichment of Nodal is ligand independent, and Nodal enhances and maintains its enrichment through autoregulation. Nodal then diffuses to the

left LPM to induce its own expression there as well as that of its inhibitors (Oki et al., 2007). In *Arl13b*^{hnn} mutants, my data supports a model where the levels of Nodal signaling activity are slightly reduced, which leads to an inability to maintain *Nodal* enrichment in the node and causes delayed expression in the LPM.

Other cilia mutants have not shown a genetic interaction with *Nodal*, and the Nodal signaling pathway has not been shown to require intact cilia for function (Collignon et al., 1996; Huangfu et al., 2003). Therefore, we propose that Arl13b has a cilia independent function in regulating Nodal signaling activity. To test this, we generated *Arl13b*^{hnn} mutants that lack cilia, *Arl13b*^{hnn}*;IFT172*^{wim} mutants, however our results were difficult to interpret because lack of cilia in the entire embryo leads to loss of the Nodal inhibitor *Lefty1* in the midline (Nakamura et al., 2006). Because *Lefty1* is a secreted proteins and can diffuse over long distances to inhibit Nodal, removing cilia and therefore *Lefty1* would allow increased Nodal signaling activity in the LPM (Nakamura et al., 2006; Tabin, 2006). In fact, the expression of *Nodal* that we saw in *Arl13b*^{hnn}*;IFT172*^{wim} mutants was an intermediate phenotype: there was no longer a severe delay in *Nodal* expression, but the expression that we saw was not as robust as in *IFT172*^{wim} mutants, supporting a cilia independent role for Arl13b in Nodal signaling.

How then could Arl13b affect Nodal signaling activity? Nodal signaling occurs through the secretion of a proprotein whose N-terminus is cleaved to generate the mature Nodal ligand. The Nodal ligand binds its co-receptors, the EGF-CFC proteins Cryptic and Cripto (Yeo and Whitman, 2001; Yan et al., 2002), and its receptors, the serine/threonine kinase receptors Alk4 and ActRIIA/B (Reissmann et al., 2001). Receptor binding causes the phosphorylation of the transcription factors Smad2 and Smad3 allowing them to

interact with Smad4 and enter the nucleus to activate target genes, such as the *Nodal* gene itself. Because our results as well as others show that Arl13b is a membrane associated GTPase (Cevik et al., 2010), we predict that Arl13b may function at the level of membrane localization or internalization of Nodal signaling components to regulate the Nodal signaling pathway. Membrane localization and intracellular trafficking play an important role in Nodal signaling (Constam, 2009; Schier, 2009). One of the mammalian co-receptors for Nodal, Cripto, is required for efficient Nodal signaling, and localizes to lipid rafts to recruit Nodal to these membrane microdomains where it can be processed to its mature active form (Blanchet et al., 2008b). Upon Nodal binding to Cripto and being processed, the complex is internalized through clathrin and caveolin independent endocytosis where it is targeted to early endosomes for pathway activation through the Alk4 and ActRIIA/B receptors (Blanchet et al., 2008b; Blanchet et al., 2008a). Drugs that inhibit lipid raft internalization block the endocytosis of Nodal and diminish pathway activation (Blanchet et al., 2008b). It is not clear why Nodal signaling occurs through an endosomal signaling complex as opposed to the plasma membrane, but it may be important for Nodal signal intensity and duration (Constam, 2009). Therefore, based on our data showing a reduction in Nodal signaling activity in *Arl13b*^{hnn} mutants, it is easy to imagine a role for Arl13b in maintaining lipid raft integrity or recruitment of proteins to lipids rafts, which is required for the internalization of Nodal signaling complexes. In support of our model, the cilium shares identity with lipid rafts. For example, some of the lipids that are found in rafts, such as the gangliosides GM1 and GM3 are also found in cilia (Janich and Corbeil, 2007), and the SNARE protein SNAP-25 localizes to cilia as well as lipid rafts (Low et al., 1998; Salaun et al., 2005). It will be interesting to

determine if Arl13b functions outside of the cilium at the plasma membrane, perhaps regulating lipid raft organization or internalization of endocytic vesicles. A function for Arl13b in membrane trafficking and/or endocytosis could be vital for Nodal signaling activity as well as other cellular processes.

4.2 The Function of Arl13b in Cilia and Shh Signaling

Chapter four, *Arl13b Regulates Ciliogenesis and the Dynamic Localization of Shh Signaling Proteins*, presents the importance of Arl13b in regulating cilia length, ciliary tubulin modifications, and the localization of the Shh signaling components to the cilium. We found that Arl13b may interact with the exocyst complex protein Sec8 and the anterograde complex IFT protein IFT88, which likely contributes to the roles of Arl13b in protein localization to cilia and ciliogenesis.

The overexpression of Arl13b leads to significantly longer cilia in mouse embryonic fibroblasts (MEFs) while cells that lack or have significantly less Arl13b, *Arl13b*^{hnn} MEFs and *Arl13b* knock-down IMCD3 cells, respectively, have much fewer cilia and the cilia are shorter than wild-type. This phenotype is similar to what was found for Rab8 and Sec10 knockdown and overexpression (Nachury et al., 2007; Zuo et al., 2009). Sec10 is a component of the exocyst complex and Rab8 is a small GTPase that is a homolog of yeast Sec4p which is involved in regulating the exocyst complex (Guo et al., 1999). The importance of the exocyst complex in ciliogenesis is only beginning to be appreciated, but given the parallels between ciliogenesis and exocytosis (Baldari and Rosenbaum, 2010), it is intriguing to imagine that the exocyst complex is required for the delivery and/or fusion of vesicles at the cilium. Because we found that Arl13b interacts

with the exocyst protein Sec8 in MEFs, we propose that Arl13b regulates the exocyst complex at the cilium, perhaps through regulating the exocyst at the cilium. Therefore, when there is excess Arl13b, delivery of vesicles with associated ciliary proteins to the cilium is enhanced, leading to longer cilia while in the absence of Arl13b, vesicle delivery is reduced causing complete loss of cilia in most cells and shortened cilia in other cells.

Because of the requirement of IFT in building cilia, we expect that exocyst vesicles being targeted to the cilium will have IFT proteins associated. This is supported by findings that IFT proteins share homology to coat proteins and that they function in exocytosis in unciliated cells (Jekely and Arendt, 2006; Finetti et al., 2009), and by our results showing that IFT88 immunoprecipitates with Sec8. It has also been proposed that for proper localization of even soluble ciliary proteins, associations with vesicles may be required (Baldari and Rosenbaum, 2010). Therefore, if Arl13b is required for exocyst regulation at the cilium, having excess Arl13b would increase in exocyst targeting to cilia as well as cause excess IFT protein localization to cilia leading to longer cilia. Likewise loss of Arl13b and therefore reduced exocyst targeting to cilia would result in fewer IFT particles in cilia and therefore shortened or absent cilia. Concordantly, results from Zuo et al. showed that IFT88 protein levels are reduced in cells with significantly reduced levels of the exocyst protein Sec10, suggesting that IFT88 is stabilized by the exocyst.

Supporting a fundamental role for Arl13b in regulation of proteins targeting at the cilium, we found that the levels of many components of Shh signaling pathway were defective in *Arl13b*^{hnn} cilia, and there was a defect in shifting their localization in response to the Shh ligand. Most interesting, we saw that Smo levels were increased in

Arl13b^{hnn} cilia, although it was improperly distributed within the cilium. If Arl13b regulates the exocyst complex at the cilium, one possibility is that vesicles are unable to fuse at the cilia membrane, and the staining pattern of Smo is supportive of the hypothesis.

These results have major implications for the function of Arl13b in cilia, as well as for the impact that Arl13b has on Shh signaling. We know that there is a defect in Shh signaling in *Arl13b*^{hnn} mutant embryos, where the highest levels of Shh signaling activity are not reached and that activity is expanded dorsally in a ligand independent way (Caspary et al., 2007). Because the localization of Shh components to the cilium is required for Shh pathway activation (Haycraft et al., 2005; Rohatgi et al., 2007; Kovacs et al., 2008), the defect in Shh signaling that we see in our mutants is two-fold. First, there was an inability to correctly enrich the Gli proteins, which could lead to the inability to reach the highest levels of Shh signaling activity in the *Arl13b*^{hnn} neural tube. Second, Smo was improperly enriched in *Arl13b*^{hnn} cilia, which could cause the expanded ligand independent Shh signaling activity in the neural tube. It is still not clear why GliR formation is intact in *Arl13b*^{hnn} mutants and only GliA function is affected, however a differential requirement of cilia for GliA and GliR formation is one possibility. In mouse mutants that lack cilia, GliA is abolished while low levels of GliR are still present (Haycraft et al., 2005). GliR formation requires proteosomes found at the base of cilia; therefore, loss of cilia could still allows proteosomal processing of GliR, although it may be less efficient. Therefore in our *Arl13b*^{hnn} mutants, because cilia are still present albeit shortened, the defects in localization of proteins to the cilium may lead to a more severe disruption of GliA formation while GliR formation would be unaffected.

In summary, the results presented in this dissertation add to our understanding of the recently uncharacterized GTPase Arl13b, and through our studies of Arl13b, we have added knowledge to the regulation of ciliogenesis, deepened our understanding of LR axis specification, found a potential regulator of Nodal signaling, and emphasized the importance of the levels of Shh signaling components in cilia for pathway activation.

REFERENCES:

Afzelius, B. A. (1976). A human syndrome caused by immotile cilia. *Science* **193**, 317-319.

Anderson, R. G. (1972). The three-dimensional structure of the basal body from the rhesus monkey oviduct. *J Cell Biol* **54**, 246-265.

Babbey, C. M., Bacallao, R. L. and Dunn, K. W. (2010). Rab10 associates with primary cilia and the exocyst complex in renal epithelial cells. *Am J Physiol Renal Physiol* **299**, F495-506.

Baker, S. A., Freeman, K., Luby-Phelps, K., Pazour, G. J. and Besharse, J. C. (2003). IFT20 links kinesin II with a mammalian intraflagellar transport complex that is conserved in motile flagella and sensory cilia. *J Biol Chem* **278**, 34211-34218.

Baldari, C. T. and Rosenbaum, J. (2010). Intraflagellar transport: it's not just for cilia anymore. *Curr Opin Cell Biol* **22**, 75-80.

Basu, B. and Brueckner, M. (2008). Cilia multifunctional organelles at the center of vertebrate left-right asymmetry. *Curr Top Dev Biol* **85**, 151-174.

Berbari, N. F., O'Connor, A. K., Haycraft, C. J. and Yoder, B. K. (2009). The primary cilium as a complex signaling center. *Curr Biol* **19**, R526-535.

Berbari, N. F., Johnson, A. D., Lewis, J. S., Askwith, C. C. and Mykytyn, K. (2008). Identification of ciliary localization sequences within the third intracellular loop of G protein-coupled receptors. *Mol Biol Cell* **19**, 1540-1547.

Bhowmick, R., Li, M., Sun, J., Baker, S. A., Insinna, C. and Besharse, J. C. (2009). Photoreceptor IFT complexes containing chaperones, guanylyl cyclase 1 and rhodopsin. *Traffic* **10**, 648-663.

Bisgrove, B. W. and Yost, H. J. (2006). The roles of cilia in developmental disorders and disease. *Development* **133**, 4131-4143.

Bisgrove, B. W., Morelli, S. H. and Yost, H. J. (2003). Genetics of human laterality disorders: insights from vertebrate model systems. *Annu Rev Genomics Hum Genet* **4**, 1-32.

Blanchet, M. H., Le Good, J. A., Oorschot, V., Baflast, S., Minchiotti, G., Klumperman, J. and Constam, D. B. (2008a). Cripto localizes Nodal at the limiting membrane of early endosomes. *Sci Signal* **1**, ra13.

Blanchet, M. H., Le Good, J. A., Mesnard, D., Oorschot, V., Baflast, S., Minchiotti, G., Klumperman, J. and Constam, D. B. (2008b). Cripto recruits Furin and PACE4 and controls Nodal trafficking during proteolytic maturation. *Embo J* **27**, 2580-2591.

Boehlke, C., Bashkurov, M., Buescher, A., Krick, T., John, A. K., Nitschke, R., Walz, G. and Kuehn, E. W. (2010). Differential role of Rab proteins in ciliary trafficking: Rab23 regulates smoothened levels. *J Cell Sci* **123**, 1460-1467.

Bonnafe, E., Touka, M., AitLounis, A., Baas, D., Barras, E., Ucla, C., Moreau, A., Flamant, F., Dubruille, R., Couble, P. et al. (2004). The transcription factor RFX3 directs nodal cilium development and left-right asymmetry specification. *Mol Cell Biol* **24**, 4417-4427.

Brennan, J., Norris, D. P. and Robertson, E. J. (2002). Nodal activity in the node governs left-right asymmetry. *Genes Dev* **16**, 2339-2344.

Brown, N. A. and Wolpert, L. (1990). The development of handedness in left/right asymmetry. *Development* **109**, 1-9.

Campione, M., Steinbeisser, H., Schweickert, A., Deissler, K., van Bebber, F., Lowe, L. A., Nowotschin, S., Viebahn, C., Haffter, P., Kuehn, M. R. et al. (1999). The homeobox gene Pitx2: mediator of asymmetric left-right signaling in vertebrate heart and gut looping. *Development* **126**, 1225-1234.

Cantagrel, V., Silhavy, J. L., Bielas, S. L., Swistun, D., Marsh, S. E., Bertrand, J. Y., Audollent, S., Attie-Bitach, T., Holden, K. R., Dobyns, W. B. et al. (2008). Mutations in the cilia gene ARL13B lead to the classical form of Joubert syndrome. *Am J Hum Genet* **83**, 170-179.

Caspary, T., Larkins, C. E. and Anderson, K. V. (2007). The graded response to Sonic Hedgehog depends on cilia architecture. *Dev Cell* **12**, 767-778.

Caspary, T., C.E. Larkins, and K.V. Anderson. (2007). The graded response to Sonic Hedgehog depends on cilia architecture. *Developmental Cell*, 767-778.

Cevik, S., Hori, Y., Kaplan, O. I., Kida, K., Toivenon, T., Foley-Fisher, C., Cottell, D., Katada, T., Kontani, K. and Blacque, O. E. (2010). Joubert syndrome Arl13b functions at ciliary membranes and stabilizes protein transport in Caenorhabditis elegans. *J Cell Biol* **188**, 953-969.

Chen, C. and Shen, M. M. (2004). Two modes by which Lefty proteins inhibit nodal signaling. *Curr Biol* **14**, 618-624.

Chen, J., Knowles, H. J., Hebert, J. L. and Hackett, B. P. (1998). Mutation of the mouse hepatocyte nuclear factor/forkhead homologue 4 gene results in an absence of cilia and random left-right asymmetry. *J Clin Invest* **102**, 1077-1082.

Chen, M. H., Wilson, C. W., Li, Y. J., Law, K. K., Lu, C. S., Gacayan, R., Zhang, X., Hui, C. C. and Chuang, P. T. (2009). Cilium-independent regulation of Gli protein

function by Sufu in Hedgehog signaling is evolutionarily conserved. *Genes Dev* **23**, 1910-1928.

Chiang, C., Litingtung, Y., Lee, E., Young, K. E., Corden, J. L., Westphal, H. and Beachy, P. A. (1996). Cyclopia and defective axial patterning in mice lacking Sonic hedgehog gene function. *Nature* **383**, 407-413.

Cole, D. G. and Snell, W. J. (2009). SnapShot: Intraflagellar transport. *Cell* **137**, 784-784.e781.

Collignon, J., Varlet, I. and Robertson, E. J. (1996). Relationship between asymmetric nodal expression and the direction of embryonic turning. *Nature* **381**, 155-158.

Constam, D. B. (2009). Riding shotgun: a dual role for the epidermal growth factor-Cripto/FRL-1/Cryptic protein Cripto in Nodal trafficking. *Traffic* **10**, 783-791.

Corbit, K. C., Aanstad, P., Singla, V., Norman, A. R., Stainier, D. Y. and Reiter, J. F. (2005). Vertebrate Smoothened functions at the primary cilium. *Nature* **437**, 1018-1021.

Corbit, K. C., Shyer, A. E., Dowdle, W. E., Gaulden, J., Singla, V. and Reiter, J. F. (2007). Kif3a constrains beta-catenin-dependent Wnt signalling through dual ciliary and non-ciliary mechanisms. *Nat Cell Biol* **0**, 0.

Cortellino, S., Wang, C., Wang, B., Bassi, M. R., Caretti, E., Champeval, D., Calmont, A., Jarnik, M., Burch, J., Zaret, K. S. et al. (2009). Defective ciliogenesis, embryonic lethality and severe impairment of the Sonic Hedgehog pathway caused by inactivation of the mouse complex A intraflagellar transport gene Ift122/Wdr10, partially overlapping with the DNA repair gene Med1/Mbd4. *Dev Biol* **325**, 225-237.

Cuvillier, A., Redon, F., Antoine, J. C., Chardin, P., DeVos, T. and Merlin, G. (2000). LdARL-3A, a Leishmania promastigote-specific ADP-ribosylation factor-like protein, is essential for flagellum integrity. *J Cell Sci* **113 (Pt 11)**, 2065-2074.

D'Souza-Schorey, C. and Chavrier, P. (2006). ARF proteins: roles in membrane traffic and beyond. *Nat Rev Mol Cell Biol* **7**, 347-358.

Dave, D., Wloga, D., Sharma, N. and Gaertig, J. (2009). DYF-1 Is required for assembly of the axoneme in Tetrahymena thermophila. *Eukaryot Cell* **8**, 1397-1406.

Dawe, H. R., Farr, H. and Gull, K. (2007). Centriole/basal body morphogenesis and migration during ciliogenesis in animal cells. *J Cell Sci* **120**, 7-15.

Deane, J. A., Cole, D. G., Seeley, E. S., Diener, D. R. and Rosenbaum, J. L. (2001). Localization of intraflagellar transport protein IFT52 identifies basal body transitional fibers as the docking site for IFT particles. *Curr Biol* **11**, 1586-1590.

Deretic, D., Williams, A. H., Ransom, N., Morel, V., Hargrave, P. A. and Arendt, A. (2005). Rhodopsin C terminus, the site of mutations causing retinal disease, regulates trafficking by binding to ADP-ribosylation factor 4 (ARF4). *Proc Natl Acad Sci U S A* **102**, 3301-3306.

Dishinger, J. F., Kee, H. L., Jenkins, P. M., Fan, S., Hurd, T. W., Hammond, J. W., Truong, Y. N., Margolis, B., Martens, J. R. and Verhey, K. J. (2010). Ciliary entry of the kinesin-2 motor KIF17 is regulated by importin-beta2 and RanGTP. *Nat Cell Biol* **12**, 703-710.

Duldulao, N. A., Lee, S. and Sun, Z. (2009). Cilia localization is essential for in vivo functions of the Joubert syndrome protein Arl13b/Scorpion. *Development* **136**, 4033-4042.

Dwyer, N. D., Adler, C. E., Crump, J. G., L'Etoile, N. D. and Bargmann, C. I. (2001). Polarized dendritic transport and the AP-1 mu1 clathrin adaptor UNC-101 localize odorant receptors to olfactory cilia. *Neuron* **31**, 277-287.

Echelard, Y., Epstein, D. J., St-Jacques, B., Shen, L., Mohler, J., McMahon, J. A. and McMahon, A. P. (1993). Sonic hedgehog, a member of a family of putative signaling molecules, is implicated in the regulation of CNS polarity. *Cell* **75**, 1417-1430.

Eggenschwiler, J. T. and Anderson, K. V. (2007). Cilia and developmental signaling. *Annu Rev Cell Dev Biol* **23**, 345-373.

Eggenschwiler, J. T., Espinoza, E. and Anderson, K. V. (2001). Rab23 is an essential negative regulator of the mouse Sonic hedgehog signalling pathway. *Nature* **412**, 194-198.

Ericson, J., Briscoe, J., Rashbass, P., van Heyningen, V. and Jessell, T. M. (1997). Graded sonic hedgehog signaling and the specification of cell fate in the ventral neural tube. *Cold Spring Harb Symp Quant Biol* **62**, 451-466.

Essner, J. J., Amack, J. D., Nyholm, M. K., Harris, E. B. and Yost, H. J. (2005). Kupffer's vesicle is a ciliated organ of asymmetry in the zebrafish embryo that initiates left-right development of the brain, heart and gut. *Development* **132**, 1247-1260.

Fan, S., Fogg, V., Wang, Q., Chen, X. W., Liu, C. J. and Margolis, B. (2007). A novel Crumbs3 isoform regulates cell division and ciliogenesis via importin beta interactions. *J Cell Biol* **178**, 387-398.

Fan, Z. C., Behal, R. H., Geimer, S., Wang, Z., Williamson, S. M., Zhang, H., Cole, D. G. and Qin, H. (2010). Chlamydomonas IFT70/CrDYF-1 is a core component of IFT particle complex B and is required for flagellar assembly. *Mol Biol Cell* **21**, 2696-2706.

Feistel, K. and Blum, M. (2006). Three types of cilia including a novel 9+4 axoneme on the notochordal plate of the rabbit embryo. *Dev Dyn* **235**, 3348-3358.

Ferrante, M. I., Zullo, A., Barra, A., Bimonte, S., Messaddeq, N., Studer, M., Dolle, P. and Franco, B. (2006). Oral-facial-digital type I protein is required for primary cilia formation and left-right axis specification. *Nat Genet* **38**, 112-117.

Finetti, F., Paccani, S. R., Riparbelli, M. G., Giacomello, E., Perinetti, G., Pazour, G. J., Rosenbaum, J. L. and Baldari, C. T. (2009). Intraflagellar transport is required for polarized recycling of the TCR/CD3 complex to the immune synapse. *Nat Cell Biol* **11**, 1332-1339.

Follit, J. A., Tuft, R. A., Fogarty, K. E. and Pazour, G. J. (2006). The intraflagellar transport protein IFT20 is associated with the Golgi complex and is required for cilia assembly. *Mol Biol Cell* **17**, 3781-3792.

Garcia-Garcia, M. J., Eggenschwiler, J. T., Caspary, T., Alcorn, H. L., Wyler, M. R., Huangfu, D., Rakeman, A. S., Lee, J. D., Feinberg, E. H., Timmer, J. R. et al. (2005). Analysis of mouse embryonic patterning and morphogenesis by forward genetics. *Proc Natl Acad Sci U S A* **102**, 5913-5919.

Geng, L., Okuhara, D., Yu, Z., Tian, X., Cai, Y., Shibazaki, S. and Somlo, S. (2006). Polycystin-2 traffics to cilia independently of polycystin-1 by using an N-terminal RVxP motif. *J Cell Sci* **119**, 1383-1395.

Germino, G. G. (2005). Linking cilia to Wnts. *Nat Genet* **37**, 455-457.

Gherman, A., Davis, E. E. and Katsanis, N. (2006). The ciliary proteome database: an integrated community resource for the genetic and functional dissection of cilia. *Nat Genet* **38**, 961-962.

Goodrich, L. V., Milenkovic, L., Higgins, K. M. and Scott, M. P. (1997). Altered neural cell fates and medulloblastoma in mouse patched mutants. *Science* **277**, 1109-1113.

Grande, C. and Patel, N. H. (2009). Nodal signalling is involved in left-right asymmetry in snails. *Nature* **457**, 1007-1011.

Griffis, E. R., Altan, N., Lippincott-Schwartz, J. and Powers, M. A. (2002). Nup98 is a mobile nucleoporin with transcription-dependent dynamics. *Mol Biol Cell* **13**, 1282-1297.

Grindstaff, K. K., Yeaman, C., Anandasabapathy, N., Hsu, S. C., Rodriguez-Boulan, E., Scheller, R. H. and Nelson, W. J. (1998). Sec6/8 complex is recruited to cell-cell contacts and specifies transport vesicle delivery to the basal-lateral membrane in epithelial cells. *Cell* **93**, 731-740.

Guo, W., Roth, D., Walch-Solimena, C. and Novick, P. (1999). The exocyst is an effector for Sec4p, targeting secretory vesicles to sites of exocytosis. *Embo J* **18**, 1071-1080.

Han, Y. G., Kwok, B. H. and Kernan, M. J. (2003). Intraflagellar transport is required in Drosophila to differentiate sensory cilia but not sperm. *Curr Biol* **13**, 1679-1686.

Haycraft, C. J., Banizs, B., Aydin-Son, Y., Zhang, Q., Michaud, E. J. and Yoder, B. K. (2005). Gli2 and Gli3 localize to cilia and require the intraflagellar transport protein polaris for processing and function. *PLoS Genet* **1**, e53.

He, B. and Guo, W. (2009). The exocyst complex in polarized exocytosis. *Curr Opin Cell Biol* **21**, 537-542.

Hirokawa, N., Tanaka, Y. and Okada, Y. (2009). Left-right determination: involvement of molecular motor KIF3, cilia, and nodal flow. *Cold Spring Harb Perspect Biol* **1**, a000802.

Hori, Y., Kobayashi, T., Kikko, Y., Kontani, K. and Katada, T. (2008). Domain architecture of the atypical Arf-family GTPase Arl13b involved in cilia formation. *Biochem Biophys Res Commun* **373**, 119-124.

Houde, C., Dickinson, R. J., Houtzager, V. M., Cullum, R., Montpetit, R., Metzler, M., Simpson, E. M., Roy, S., Hayden, M. R., Hoodless, P. A. et al. (2006). Hippi is essential for node cilia assembly and Sonic hedgehog signaling. *Dev Biol* **300**, 523-533.

Hu, Q., Milenkovic, L., Jin, H., Scott, M. P., Nachury, M. V., Spiliotis, E. T. and Nelson, W. J. (2010). A septin diffusion barrier at the base of the primary cilium maintains ciliary membrane protein distribution. *Science* **329**, 436-439.

Huangfu, D. and Anderson, K. V. (2005). Cilia and Hedgehog responsiveness in the mouse. *Proc Natl Acad Sci U S A* **102**, 11325-11330.

Huangfu, D., Liu, A., Rakeman, A. S., Murcia, N. S., Niswander, L. and Anderson, K. V. (2003). Hedgehog signalling in the mouse requires intraflagellar transport proteins. *Nature* **426**, 83-87.

Humke, E. W., Dorn, K. V., Milenkovic, L., Scott, M. P. and Rohatgi, R. (2010). The output of Hedgehog signaling is controlled by the dynamic association between Suppressor of Fused and the Gli proteins. *Genes Dev* **24**, 670-682.

Insinna, C. and Besharse, J. C. (2008). Intraflagellar transport and the sensory outer segment of vertebrate photoreceptors. *Dev Dyn* **237**, 1982-1992.

Insinna, C., Pathak, N., Perkins, B., Drummond, I. and Besharse, J. C. (2008). The homodimeric kinesin, Kif17, is essential for vertebrate photoreceptor sensory outer segment development. *Dev Biol* **316**, 160-170.

Insinna, C., Humby, M., Sedmak, T., Wolfrum, U. and Besharse, J. C. (2009). Different roles for KIF17 and kinesin II in photoreceptor development and maintenance. *Dev Dyn* **238**, 2211-2222.

Janich, P. and Corbeil, D. (2007). GM1 and GM3 gangliosides highlight distinct lipid microdomains within the apical domain of epithelial cells. *FEBS Lett* **581**, 1783-1787.

Jekely, G. and Arendt, D. (2006). Evolution of intraflagellar transport from coated vesicles and autogenous origin of the eukaryotic cilium. *Bioessays* **28**, 191-198.

Jenkins, P. M., Hurd, T. W., Zhang, L., McEwen, D. P., Brown, R. L., Margolis, B., Verhey, K. J. and Martens, J. R. (2006). Ciliary targeting of olfactory CNG channels requires the CNGB1b subunit and the kinesin-2 motor protein, KIF17. *Curr Biol* **16**, 1211-1216.

Jia, J., Kolterud, A., Zeng, H., Hoover, A., Teglund, S., Toftgard, R. and Liu, A. (2009). Suppressor of Fused inhibits mammalian Hedgehog signaling in the absence of cilia. *Dev Biol* **330**, 452-460.

Jian, X., Cavenagh, M., Gruschus, J. M., Randazzo, P. A. and Kahn, R. A. (2010). Modifications to the C-terminus of Arf1 alter cell functions and protein interactions. *Traffic* **11**, 732-742.

Jin, H., White, S. R., Shida, T., Schulz, S., Aguiar, M., Gygi, S. P., Bazan, J. F. and Nachury, M. V. (2010). The conserved Bardet-Biedl syndrome proteins assemble a coat that traffics membrane proteins to cilia. *Cell* **141**, 1208-1219.

Kahn, R. A., Volpicelli-Daley, L., Bowzard, B., Shrivastava-Ranjan, P., Li, Y., Zhou, C. and Cunningham, L. (2005). Arf family GTPases: roles in membrane traffic and microtubule dynamics. *Biochem Soc Trans* **33**, 1269-1272.

Knodler, A., Feng, S., Zhang, J., Zhang, X., Das, A., Peranen, J. and Guo, W. (2010). Coordination of Rab8 and Rab11 in primary ciliogenesis. *Proc Natl Acad Sci U S A* **107**, 6346-6351.

Kovacs, J. J., Whalen, E. J., Liu, R., Xiao, K., Kim, J., Chen, M., Wang, J., Chen, W. and Lefkowitz, R. J. (2008). Beta-arrestin-mediated localization of smoothened to the primary cilium. *Science* **320**, 1777-1781.

Kozminski, K. G., Beech, P. L. and Rosenbaum, J. L. (1995). The Chlamydomonas kinesin-like protein FLA10 is involved in motility associated with the flagellar membrane. *J Cell Biol* **131**, 1517-1527.

Kozminski, K. G., Johnson, K. A., Forscher, P. and Rosenbaum, J. L. (1993). A motility in the eukaryotic flagellum unrelated to flagellar beating. *Proc Natl Acad Sci U S A* **90**, 5519-5523.

Krebs, L. T., Iwai, N., Nonaka, S., Welsh, I. C., Lan, Y., Jiang, R., Saijoh, Y., O'Brien, T. P., Hamada, H. and Gridley, T. (2003). Notch signaling regulates left-right asymmetry determination by inducing Nodal expression. *Genes Dev* **17**, 1207-1212.

Leroux, M. R. (2007). Taking vesicular transport to the cilium. *Cell* **129**, 1041-1043.

Li, Y., Wei, Q., Zhang, Y., Ling, K. and Hu, J. (2010). The small GTPases ARL-13 and ARL-3 coordinate intraflagellar transport and ciliogenesis. *J Cell Biol* **189**, 1039-1051.

Lin, C. R., Kioussi, C., O'Connell, S., Briata, P., Szeto, D., Liu, F., Izpisua-Belmonte, J. C. and Rosenfeld, M. G. (1999). Pitx2 regulates lung asymmetry, cardiac positioning and pituitary and tooth morphogenesis. *Nature* **401**, 279-282.

Liu, A., Wang, B. and Niswander, L. A. (2005). Mouse intraflagellar transport proteins regulate both the activator and repressor functions of Gli transcription factors. *Development* **132**, 3103-3111.

Liu, C., Liu, W., Lu, M. F., Brown, N. A. and Martin, J. F. (2001). Regulation of left-right asymmetry by thresholds of Pitx2c activity. *Development* **128**, 2039-2048.

Low, S. H., Roche, P. A., Anderson, H. A., van Ijzendoorn, S. C., Zhang, M., Mostov, K. E. and Weimbs, T. (1998). Targeting of SNAP-23 and SNAP-25 in polarized epithelial cells. *J Biol Chem* **273**, 3422-3430.

Lowe, L. A., Yamada, S. and Kuehn, M. R. (2001). Genetic dissection of nodal function in patterning the mouse embryo. *Development* **128**, 1831-1843.

Lowe, L. A., Supp, D. M., Sampath, K., Yokoyama, T., Wright, C. V., Potter, S. S., Overbeek, P. and Kuehn, M. R. (1996). Conserved left-right asymmetry of nodal expression and alterations in murine situs inversus. *Nature* **381**, 158-161.

Maretto, S., Cordenonsi, M., Dupont, S., Braghetta, P., Broccoli, V., Hassan, A. B., Volpin, D., Bressan, G. M. and Piccolo, S. (2003). Mapping Wnt/beta-catenin signaling during mouse development and in colorectal tumors. *Proc Natl Acad Sci U S A* **100**, 3299-3304.

Marques, S., Borges, A. C., Silva, A. C., Freitas, S., Cordenonsi, M. and Belo, J. A. (2004). The activity of the Nodal antagonist Cerl-2 in the mouse node is required for correct L/R body axis. *Genes Dev* **18**, 2342-2347.

Marshall, W. F. and Rosenbaum, J. L. (2001). Intraflagellar transport balances continuous turnover of outer doublet microtubules: implications for flagellar length control. *J Cell Biol* **155**, 405-414.

Marszalek, J. R., Ruiz-Lozano, P., Roberts, E., Chien, K. R. and Goldstein, L. S. (1999). Situs inversus and embryonic ciliary morphogenesis defects in mouse mutants lacking the KIF3A subunit of kinesin-II. *Proc Natl Acad Sci U S A* **96**, 5043-5048.

Masa-aki Nakaya, K. B., Tadasuke Tsukiyama, Shaulan Jaime, J. Alan Rawls and and Yamaguchi, T. P. (2005). Wnt3a links left-right determination with segmentation and anteroposterior axis elongation. *Development* **132**, 5425-5436.

Matsuura, K., Lefebvre, P. A., Kamiya, R. and Hirono, M. (2002). Kinesin-II is not essential for mitosis and cell growth in Chlamydomonas. *Cell Motil Cytoskeleton* **52**, 195-201.

May, S. R., Ashique, A. M., Karlen, M., Wang, B., Shen, Y., Zarbalis, K., Reiter, J., Ericson, J. and Peterson, A. S. (2005). Loss of the retrograde motor for IFT disrupts localization of Smo to cilia and prevents the expression of both activator and repressor functions of Gli. *Dev Biol* **287**, 378-389.

Mazelova, J., Astuto-Gribble, L., Inoue, H., Tam, B. M., Schonteich, E., Prekeris, R., Moritz, O. L., Randazzo, P. A. and Deretic, D. (2009). Ciliary targeting motif VxPx directs assembly of a trafficking module through Arf4. *Embo J* **28**, 183-192.

McGrath, J., Somlo, S., Makova, S., Tian, X. and Brueckner, M. (2003). Two populations of node monocilia initiate left-right asymmetry in the mouse. *Cell* **114**, 61-73.

McMahon, A. P., Ingham, P. W. and Tabin, C. J. (2003). Developmental roles and clinical significance of hedgehog signaling. *Curr Top Dev Biol* **53**, 1-114.

Meno, C., Shimono, A., Saijoh, Y., Yashiro, K., Mochida, K., Ohishi, S., Noji, S., Kondoh, H. and Hamada, H. (1998). lefty-1 is required for left-right determination as a regulator of lefty-2 and nodal. *Cell* **94**, 287-297.

Meno, C., Takeuchi, J., Sakuma, R., Koshiba-Takeuchi, K., Ohishi, S., Saijoh, Y., Miyazaki, J., ten Dijke, P., Ogura, T. and Hamada, H. (2001). Diffusion of nodal signaling activity in the absence of the feedback inhibitor Lefty2. *Dev Cell* **1**, 127-138.

Merrill, A. E., Merriman, B., Farrington-Rock, C., Camacho, N., Sebald, E. T., Funari, V. A., Schibler, M. J., Firestein, M. H., Cohn, Z. A., Priore, M. A. et al. (2009). Ciliary abnormalities due to defects in the retrograde transport protein DYNC2H1 in short-rib polydactyly syndrome. *Am J Hum Genet* **84**, 542-549.

Meyer, N. P. and Roelink, H. (2003). The amino-terminal region of Gli3 antagonizes the Shh response and acts in dorsoventral fate specification in the developing spinal cord. *Dev Biol* **257**, 343-355.

Milenkovic, L., Scott, M. P. and Rohatgi, R. (2009). Lateral transport of Smoothened from the plasma membrane to the membrane of the cilium. *J Cell Biol* **187**, 365-374.

Nachury, M. V., Loktev, A. V., Zhang, Q., Westlake, C. J., Peranen, J., Merdes, A., Slusarski, D. C., Scheller, R. H., Bazan, J. F., Sheffield, V. C. et al. (2007). A core complex of BBS proteins cooperates with the GTPase Rab8 to promote ciliary membrane biogenesis. *Cell* **129**, 1201-1213.

Nakamura, T., Mine, N., Nakaguchi, E., Mochizuki, A., Yamamoto, M., Yashiro, K., Meno, C. and Hamada, H. (2006). Generation of robust left-right asymmetry in the

mouse embryo requires a self-enhancement and lateral-inhibition system. *Dev Cell* **11**, 495-504.

Nonaka, S., Shiratori, H., Saijoh, Y. and Hamada, H. (2002). Determination of left-right patterning of the mouse embryo by artificial nodal flow. *Nature* **418**, 96-99.

Nonaka, S., Yoshiba, S., Watanabe, D., Ikeuchi, S., Goto, T., Marshall, W. F. and Hamada, H. (2005). De novo formation of left-right asymmetry by posterior tilt of nodal cilia. *PLoS Biol* **3**, e268.

Nonaka, S., Tanaka, Y., Okada, Y., Takeda, S., Harada, A., Kanai, Y., Kido, M. and Hirokawa, N. (1998). Randomization of left-right asymmetry due to loss of nodal cilia generating leftward flow of extraembryonic fluid in mice lacking KIF3B motor protein. *Cell* **95**, 829-837.

Norman, R. X., Ko, H. W., Huang, V., Eun, C. M., Abler, L. L., Zhang, Z., Sun, X. and Eggenschwiler, J. T. (2009). Tubby-like protein 3 (TULP3) regulates patterning in the mouse embryo through inhibition of Hedgehog signaling. *Hum Mol Genet* **18**, 1740-1754.

Norris, D. P., Brennan, J., Bikoff, E. K. and Robertson, E. J. (2002). The Foxh1-dependent autoregulatory enhancer controls the level of Nodal signals in the mouse embryo. *Development* **129**, 3455-3468.

Novick, P., Field, C. and Schekman, R. (1980). Identification of 23 complementation groups required for post-translational events in the yeast secretory pathway. *Cell* **21**, 205-215.

Ocbina, P. J. and Anderson, K. V. (2008). Intraflagellar transport, cilia, and mammalian Hedgehog signaling: analysis in mouse embryonic fibroblasts. *Dev Dyn* **237**, 2030-2038.

Okabe, N., Xu, B. and Burdine, R. D. (2008). Fluid dynamics in zebrafish Kupffer's vesicle. *Dev Dyn* **237**, 3602-3612.

Okada, Y., Nonaka, S., Tanaka, Y., Saijoh, Y., Hamada, H. and Hirokawa, N. (1999). Abnormal nodal flow precedes situs inversus in iv and inv mice. *Mol Cell* **4**, 459-468.

Oki, S., Hashimoto, R., Okui, Y., Shen, M. M., Mekada, E., Otani, H., Saijoh, Y. and Hamada, H. (2007). Sulfated glycosaminoglycans are necessary for Nodal signal transmission from the node to the left lateral plate in the mouse embryo. *Development* **134**, 3893-3904.

Oztan, A., Silvis, M., Weisz, O. A., Bradbury, N. A., Hsu, S. C., Goldenring, J. R., Yeaman, C. and Apodaca, G. (2007). Exocyst requirement for endocytic traffic directed toward the apical and basolateral poles of polarized MDCK cells. *Mol Biol Cell* **18**, 3978-3992.

Pan, Y., Bai, C. B., Joyner, A. L. and Wang, B. (2006). Sonic hedgehog signaling regulates Gli2 transcriptional activity by suppressing its processing and degradation. *Mol Cell Biol* **26**, 3365-3377.

Papermaster, D. S., Schneider, B. G. and Besharse, J. C. (1985). Vesicular transport of newly synthesized opsin from the Golgi apparatus toward the rod outer segment. Ultrastructural immunocytochemical and autoradiographic evidence in Xenopus retinas. *Invest Ophthalmol Vis Sci* **26**, 1386-1404.

Pathak, N., Obara, T., Mangos, S., Liu, Y. and Drummond, I. A. (2007). The zebrafish fleer gene encodes an essential regulator of cilia tubulin polyglutamylation. *Mol Biol Cell* **18**, 4353-4364.

Patterson, V. L., Damrau, C., Paudyal, A., Reeve, B., Grimes, D. T., Stewart, M. E., Williams, D. J., Siggers, P., Greenfield, A. and Murdoch, J. N. (2009). Mouse hitchhiker mutants have spina bifida, dorso-ventral patterning defects and polydactyly: identification of Tulp3 as a novel negative regulator of the Sonic hedgehog pathway. *Hum Mol Genet* **18**, 1719-1739.

Pazour, G. J., Dickert, B. L. and Witman, G. B. (1999). The DHC1b (DHC2) isoform of cytoplasmic dynein is required for flagellar assembly. *J Cell Biol* **144**, 473-481.

Pazour, G. J., San Agustin, J. T., Follit, J. A., Rosenbaum, J. L. and Witman, G. B. (2002). Polycystin-2 localizes to kidney cilia and the ciliary level is elevated in orpk mice with polycystic kidney disease. *Curr Biol* **12**, R378-380.

Pedersen, L. B., Veland, I. R., Schroder, J. M. and Christensen, S. T. (2008). Assembly of primary cilia. *Dev Dyn* **237**, 1993-2006.

Peeters, H. and Devriendt, K. (2006). Human laterality disorders. *Eur J Med Genet* **49**, 349-362.

Perdiz, D., Mackeh, R., Pous, C. and Baillet, A. (2010). The ins and outs of tubulin acetylation: More than just a post-translational modification? *Cell Signal*.

Pigino, G., Geimer, S., Lanzavecchia, S., Paccagnini, E., Cantele, F., Diener, D. R., Rosenbaum, J. L. and Lupetti, P. (2009). Electron-tomographic analysis of intraflagellar transport particle trains in situ. *J Cell Biol* **187**, 135-148.

Praetorius, H. A. and Spring, K. R. (2001). Bending the MDCK cell primary cilium increases intracellular calcium. *J Membr Biol* **184**, 71-79.

Praetorius, H. A. and Spring, K. R. (2003). Removal of the MDCK cell primary cilium abolishes flow sensing. *J Membr Biol* **191**, 69-76.

Prigent, M., Dubois, T., Raposo, G., Derrien, V., Tenza, D., Rosse, C., Camonis, J. and Chavrier, P. (2003). ARF6 controls post-endocytic recycling through its downstream exocyst complex effector. *J Cell Biol* **163**, 1111-1121.

Pugacheva, E. N., Jablonski, S. A., Hartman, T. R., Henske, E. P. and Golemis, E. A. (2007). HEF1-dependent Aurora A activation induces disassembly of the primary cilium. *Cell* **129**, 1351-1363.

Raya, A. and Belmonte, J. C. (2006). Left-right asymmetry in the vertebrate embryo: from early information to higher-level integration. *Nat Rev Genet* **7**, 283-293.

Raya, A. and Izpisua Belmonte, J. C. (2008). Insights into the establishment of left-right asymmetries in vertebrates. *Birth Defects Res C Embryo Today* **84**, 81-94.

Raya, A., Kawakami, Y., Rodriguez-Esteban, C., Buscher, D., Koth, C. M., Itoh, T., Morita, M., Raya, R. M., Dubova, I., Bessa, J. G. et al. (2003). Notch activity induces Nodal expression and mediates the establishment of left-right asymmetry in vertebrate embryos. *Genes Dev* **17**, 1213-1218.

Redeker, V., Levilliers, N., Vinolo, E., Rossier, J., Jaillard, D., Burnette, D., Gaertig, J. and Bre, M. H. (2005). Mutations of tubulin glycylation sites reveal cross-talk between the C termini of alpha- and beta-tubulin and affect the ciliary matrix in Tetrahymena. *J Biol Chem* **280**, 596-606.

Reissmann, E., Jornvall, H., Blokzijl, A., Andersson, O., Chang, C., Minchiotti, G., Persico, M. G., Ibanez, C. F. and Brivanlou, A. H. (2001). The orphan receptor ALK7 and the Activin receptor ALK4 mediate signaling by Nodal proteins during vertebrate development. *Genes Dev* **15**, 2010-2022.

Rieder, C. L., Jensen, C. G. and Jensen, L. C. (1979). The resorption of primary cilia during mitosis in a vertebrate (PtK1) cell line. *J Ultrastruct Res* **68**, 173-185.

Rogers, K. K., Wilson, P. D., Snyder, R. W., Zhang, X., Guo, W., Burrow, C. R. and Lipschutz, J. H. (2004). The exocyst localizes to the primary cilium in MDCK cells. *Biochem Biophys Res Commun* **319**, 138-143.

Rohatgi, R. and Snell, W. J. (2010). The ciliary membrane. *Curr Opin Cell Biol* **22**, 541-546.

Rohatgi, R., Milenkovic, L. and Scott, M. P. (2007). Patched1 regulates hedgehog signaling at the primary cilium. *Science* **317**, 372-376.

Rosenbaum, J. L. and Witman, G. B. (2002). Intraflagellar transport. *Nat Rev Mol Cell Biol* **3**, 813-825.

Ryan, A. K., Blumberg, B., Rodriguez-Esteban, C., Yonei-Tamura, S., Tamura, K., Tsukui, T., de la Pena, J., Sabbagh, W., Greenwald, J., Choe, S. et al. (1998). Pitx2 determines left-right asymmetry of internal organs in vertebrates. *Nature* **394**, 545-551.

Sakuma, R., Ohnishi Yi, Y., Meno, C., Fujii, H., Juan, H., Takeuchi, J., Ogura, T., Li, E., Miyazono, K. and Hamada, H. (2002). Inhibition of Nodal signalling by Lefty mediated through interaction with common receptors and efficient diffusion. *Genes Cells* **7**, 401-412.

Salaun, C., Gould, G. W. and Chamberlain, L. H. (2005). The SNARE proteins SNAP-25 and SNAP-23 display different affinities for lipid rafts in PC12 cells. Regulation by distinct cysteine-rich domains. *J Biol Chem* **280**, 1236-1240.

Sarpal, R., Todi, S. V., Sivan-Loukianova, E., Shirolikar, S., Subramanian, N., Raff, E. C., Erickson, J. W., Ray, K. and Eberl, D. F. (2003). Drosophila KAP interacts with the kinesin II motor subunit KLP64D to assemble chordotonal sensory cilia, but not sperm tails. *Curr Biol* **13**, 1687-1696.

Sasaki, H., Hui, C., Nakafuku, M. and Kondoh, H. (1997). A binding site for Gli proteins is essential for HNF-3beta floor plate enhancer activity in transgenics and can respond to Shh in vitro. *Development* **124**, 1313-1322.

Sasaki, H., Nishizaki, Y., Hui, C., Nakafuku, M. and Kondoh, H. (1999). Regulation of Gli2 and Gli3 activities by an amino-terminal repression domain: implication of Gli2 and Gli3 as primary mediators of Shh signaling. *Development* **126**, 3915-3924.

Satir, P. and Christensen, S. T. (2006). Overview of Structure and Function of Mammalian Cilia. *Annu Rev Physiol*.

Satir, P. and Christensen, S. T. (2007). Overview of structure and function of mammalian cilia. *Annu Rev Physiol* **69**, 377-400.

Schier, A. F. (2009). Nodal morphogens. *Cold Spring Harb Perspect Biol* **1**, a003459.

Schneider, L., Clement, C. A., Teilmann, S. C., Pazour, G. J., Hoffmann, E. K., Satir, P. and Christensen, S. T. (2005). PDGFRalphaalpha signaling is regulated through the primary cilium in fibroblasts. *Curr Biol* **15**, 1861-1866.

Schrick, J. J., Vogel, P., Abuin, A., Hampton, B. and Rice, D. S. (2006). ADP-ribosylation factor-like 3 is involved in kidney and photoreceptor development. *Am J Pathol* **168**, 1288-1298.

Schweickert, A., Weber, T., Beyer, T., Vick, P., Bogusch, S., Feistel, K. and Blum, M. (2007). Cilia-driven leftward flow determines laterality in Xenopus. *Curr Biol* **17**, 60-66.

Seeley, E. S. and Nachury, M. V. (2010). The perennial organelle: assembly and disassembly of the primary cilium. *J Cell Sci* **123**, 511-518.

Shen, M. M., Wang, H. and Leder, P. (1997). A differential display strategy identifies Cryptic, a novel EGF-related gene expressed in the axial and lateral mesoderm during mouse gastrulation. *Development* **124**, 429-442.

Shiratori, H. and Hamada, H. (2006). The left-right axis in the mouse: from origin to morphology. *Development* **133**, 2095-2104.

Signor, D., Wedaman, K. P., Orozco, J. T., Dwyer, N. D., Bargmann, C. I., Rose, L. S. and Scholey, J. M. (1999). Role of a class DHC1b dynein in retrograde transport of IFT motors and IFT raft particles along cilia, but not dendrites, in chemosensory neurons of living Caenorhabditis elegans. *J Cell Biol* **147**, 519-530.

Simons, M., Gloy, J., Ganner, A., Bullerkotte, A., Bashkurov, M., Kronig, C., Schermer, B., Benzing, T., Cabello, O. A., Jenny, A. et al. (2005). Inversin, the gene product mutated in nephronophthisis type II, functions as a molecular switch between Wnt signaling pathways. *Nat Genet* **37**, 537-543.

Singla, V. and Reiter, J. F. (2006). The primary cilium as the cell's antenna: Signaling at a sensory organelle. *Science* **313**, 629-633.

Snow, J. J., Ou, G., Gunnarson, A. L., Walker, M. R., Zhou, H. M., Brust-Mascher, I. and Scholey, J. M. (2004). Two anterograde intraflagellar transport motors cooperate to build sensory cilia on C. elegans neurons. *Nat Cell Biol* **6**, 1109-1113.

Sorokin, S. (1962). Centrioles and the formation of rudimentary cilia by fibroblasts and smooth muscle cells. *J Cell Biol* **15**, 363-377.

Speder, P., Petzoldt, A., Suzanne, M. and Noselli, S. (2007). Strategies to establish left/right asymmetry in vertebrates and invertebrates. *Curr Opin Genet Dev* **17**, 351-358.

Spektor, A., Tsang, W. Y., Khoo, D. and Dynlacht, B. D. (2007). Cep97 and CP110 suppress a cilia assembly program. *Cell* **130**, 678-690.

Stamataki, D., Ulloa, F., Tsoni, S. V., Mynett, A. and Briscoe, J. (2005). A gradient of Gli activity mediates graded Sonic Hedgehog signaling in the neural tube. *Genes Dev* **19**, 626-641.

Sun, Z., Amsterdam, A., Pazour, G. J., Cole, D. G., Miller, M. S. and Hopkins, N. (2004). A genetic screen in zebrafish identifies cilia genes as a principal cause of cystic kidney. *Development* **131**, 4085-4093.

Supp, D. M., Witte, D. P., Potter, S. S. and Brueckner, M. (1997). Mutation of an axonemal dynein affects left-right asymmetry in inversus viscerum mice. *Nature* **389**, 963-966.

Sutherland, M. J. and Ware, S. M. (2009). Disorders of left-right asymmetry: heterotaxy and situs inversus. *Am J Med Genet C Semin Med Genet* **151C**, 307-317.

Tabin, C. (2005). Do we know anything about how left-right asymmetry is first established in the vertebrate embryo? *J Mol Histol* **36**, 317-323.

Tabin, C. J. (2006). The key to left-right asymmetry. *Cell* **127**, 27-32.

Taipale, J., Chen, J. K., Cooper, M. K., Wang, B., Mann, R. K., Milenkovic, L., Scott, M. P. and Beachy, P. A. (2000). Effects of oncogenic mutations in Smoothened and Patched can be reversed by cyclopamine. *Nature* **406**, 1005-1009.

Tanaka, C., Sakuma, R., Nakamura, T., Hamada, H. and Saijoh, Y. (2007). Long-range action of Nodal requires interaction with GDF1. *Genes Dev* **21**, 3272-3282.

Tanaka, Y., Okada, Y. and Hirokawa, N. (2005). FGF-induced vesicular release of Sonic hedgehog and retinoic acid in leftward nodal flow is critical for left-right determination. *Nature* **435**, 172-177.

TerBush, D. R., Maurice, T., Roth, D. and Novick, P. (1996). The Exocyst is a multiprotein complex required for exocytosis in Saccharomyces cerevisiae. *Embo J* **15**, 6483-6494.

Tobin, J. L. and Beales, P. L. (2009). The nonmotile ciliopathies. *Genet Med* **11**, 386-402.

Tran, P. V., Haycraft, C. J., Besschetnova, T. Y., Turbe-Doan, A., Stottmann, R. W., Herron, B. J., Chesebro, A. L., Qiu, H., Scherz, P. J., Shah, J. V. et al. (2008). THM1 negatively modulates mouse sonic hedgehog signal transduction and affects retrograde intraflagellar transport in cilia. *Nat Genet* **40**, 403-410.

Tsiairis, C. D. and McMahon, A. P. (2009). An Hh-dependent pathway in lateral plate mesoderm enables the generation of left/right asymmetry. *Curr Biol* **19**, 1912-1917.

Tucker, R. W., Pardee, A. B. and Fujiwara, K. (1979). Centriole ciliation is related to quiescence and DNA synthesis in 3T3 cells. *Cell* **17**, 527-535.

Vandenberg, L. N. and Levin, M. (2009). Perspectives and open problems in the early phases of left-right patterning. *Semin Cell Dev Biol* **20**, 456-463.

Veland, I. R., Awan, A., Pedersen, L. B., Yoder, B. K. and Christensen, S. T. (2009). Primary cilia and signaling pathways in mammalian development, health and disease. *Nephron Physiol* **111**, p39-53.

Vieira, O. V., Gaus, K., Verkade, P., Fullekrug, J., Vaz, W. L. and Simons, K. (2006). FAPP2, cilium formation, and compartmentalization of the apical membrane in polarized Madin-Darby canine kidney (MDCK) cells. *Proc Natl Acad Sci U S A* **103**, 18556-18561.

Vierkotten, J., Dildrop, R., Peters, T., Wang, B. and Ruther, U. (2007). Ftm is a novel basal body protein of cilia involved in Shh signalling. *Development* **134**, 2569-2577.

Vorobjev, I. A. and Chentsov Yu, S. (1982). Centrioles in the cell cycle. I. Epithelial cells. *J Cell Biol* **93**, 938-949.

Wang, B., Fallon, J. F. and Beachy, P. A. (2000). Hedgehog-regulated processing of Gli3 produces an anterior/posterior repressor gradient in the developing vertebrate limb. *Cell* **100**, 423-434.

Wang, Y., Zhou, Z., Walsh, C. T. and McMahon, A. P. (2009). Selective translocation of intracellular Smoothened to the primary cilium in response to Hedgehog pathway modulation. *Proc Natl Acad Sci U S A* **106**, 2623-2628.

Webber, W. A. and Lee, J. (1975). Fine structure of mammalian renal cilia. *Anat Rec* **182**, 339-343.

Wen, X., Lai, C. K., Evangelista, M., Hongo, J. A., de Sauvage, F. J. and Scales, S. J. (2010). Kinetics of hedgehog-dependent full-length Gli3 accumulation in primary cilia and subsequent degradation. *Mol Cell Biol* **30**, 1910-1922.

Wheatley, D. N., Wang, A. M. and Strugnell, G. E. (1996). Expression of primary cilia in mammalian cells. *Cell Biol Int* **20**, 73-81.

Wiens, C. J., Tong, Y., Esmail, M. A., Oh, E., Gerdes, J. M., Wang, J., Tempel, W., Rattner, J. B., Katsanis, N., Park, H. W. et al. (2010). Bardet-Biedl syndrome-associated small GTPase ARL6 (BBS3) functions at or near the ciliary gate and modulates Wnt signaling. *J Biol Chem* **285**, 16218-16230.

Wong, S. Y. and Reiter, J. F. (2008). The primary cilium at the crossroads of mammalian hedgehog signaling. *Curr Top Dev Biol* **85**, 225-260.

Wu, H., Rossi, G. and Brennwald, P. (2008). The ghost in the machine: small GTPases as spatial regulators of exocytosis. *Trends Cell Biol* **18**, 397-404.

Yamamoto, M., Mine, N., Mochida, K., Sakai, Y., Saijoh, Y., Meno, C. and Hamada, H. (2003). Nodal signaling induces the midline barrier by activating Nodal expression in the lateral plate. *Development* **130**, 1795-1804.

Yan, Y. T., Liu, J. J., Luo, Y., E, C., Haltiwanger, R. S., Abate-Shen, C. and Shen, M. M. (2002). Dual roles of Cripto as a ligand and coreceptor in the nodal signaling pathway. *Mol Cell Biol* **22**, 4439-4449.

Yeo, C. and Whitman, M. (2001). Nodal signals to Smads through Cripto-dependent and Cripto-independent mechanisms. *Mol Cell* **7**, 949-957.

Yoshida, K. and Saiga, H. (2008). Left-right asymmetric expression of Pitx is regulated by the asymmetric Nodal signaling through an intronic enhancer in Ciona intestinalis. *Dev Genes Evol* **218**, 353-360.

Zhang, X. M., Ramalho-Santos, M. and McMahon, A. P. (2001). Smoothened mutants reveal redundant roles for Shh and Ihh signaling including regulation of L/R asymmetry by the mouse node. *Cell* **105**, 781-792.

Zhang, X. M., Ellis, S., Sriratana, A., Mitchell, C. A. and Rowe, T. (2004). Sec15 is an effector for the Rab11 GTPase in mammalian cells. *J Biol Chem* **279**, 43027-43034.

Zhou, C., Cunningham, L., Marcus, A. I., Li, Y. and Kahn, R. A. (2006). Arl2 and Arl3 regulate different microtubule-dependent processes. *Mol Biol Cell* **17**, 2476-2487.

Zuo, X., Guo, W. and Lipschutz, J. H. (2009). The exocyst protein Sec10 is necessary for primary ciliogenesis and cystogenesis in vitro. *Mol Biol Cell* **20**, 2522-2529.